

Universität  
Rostock



Traditio et Innovatio

# Etherification of glycerol with alcohols to sustainable synthetic fuel over green acidic clinoptilolite

## Dissertation

zur Erlangung des akademischen Grades  
*Doctor rerum naturalium (Dr. rer. nat.)*  
der Mathematisch-Naturwissenschaftlichen Fakultät  
der Universität Rostock

vorgelegt von Hieu Trung Do, geboren am 27.01.1990 in Hanam

Rostock, 15.06.2021

[https://doi.org/10.18453/rosdok\\_id00003123](https://doi.org/10.18453/rosdok_id00003123)



Dieses Werk ist lizenziert unter einer  
Creative Commons Namensnennung 4.0 International Lizenz.

Die vorliegende Arbeit wurde in der Zeit von Januar 2018 bis March 2021 am Institut für Chemie der Universität Rostock am Lehrstuhl für Anorganische Chemie in der Arbeitsgruppe von Prof. Dr. Axel Schulz angefertigt.

1. Gutachter: Prof. Dr. Axel Schulz, Universität Rostock, Institut für Chemie
2. Gutachter: Prof. Dr. Evgeni Kondratenko, Rostock, Leibniz-Institut für Katalyse
3. Gutachter: Prof. Dr. Le Thanh Son, Hanoi Universität der Wissenschaften, VNU

Jahr der Einreichung: 2021

Jahr der Verteidigung: 2021

## **ERKLÄRUNG**

Ich versichere hiermit an Eides statt, dass ich die vorliegende Arbeit selbstständig angefertigt und ohne fremde Hilfe verfasst habe. Dazu habe ich keine außer den von mir angegebenen Hilfsmitteln und Quellen verwendet und die den benutzten Werken inhaltlich und wörtlich entnommenen Stellen habe ich als solche kenntlich gemacht.

Rostock, 15.06.2021

.....

Do Trung Hieu

# Acknowledgements

This thesis was prepared in the Department of Inorganic Chemistry, Institute of Chemistry, at the University of Rostock, Germany.

I would like to thank my supervisor Prof. Dr. Axel Schulz - Head of the Inorganic Department, for giving me an opportunity to work in his group and for all the support that I received. Especially, I would like to express my thanks to my supervisor Dr. Hendrik Kosslick for his patient and continuously support until my thesis was finished. I would like to thank also Prof. Le Thanh Son, Vice Director of the Hanoi University of Science (VNU) who supported my chemistry education and scientific carrier. I would like to thank the Analysis department of the Institute of Chemistry and the Leibniz-Institute for Catalysis at the University of Rostock (LIKAT) for excellent assistance in catalyst characterization and testing analysis in three years of my PhD stay. I am specifically very grateful to Ms. Dr. Christine Fischer, Ms. Susann Buchholz, Ms. Susanne Schareina, and Ms. Katrin Fiedler (LIKAT) for GC and MS analysis, MS. Dr. Ulrike Schümann (LKV-Rostock) for oxygenate fuel additive analytics, Dr. Dirk Michalik for NMR measurements, Prof. Dr. Marcus Frank and Mr. Dr. Armin Springer (EMZ) for SEM, TEM and EDX investigations, and Ms. Dr. Astrid Lehmann for AAS measurements. I am also gratefully to Mr. Dr. Alexander Villinger for XRD measurement as well as Mr. Dipl.-Chem. Reinhard Eckelt for BET measurements and helpful discussions.

I would like to express my deep gratitude to all the leaders and members of RoHan project, for the courses and essential scientific advice that allowed me to know to approach the research subject and finish my Ph.D. research. Especially I thank Prof. Udo Kragl, Mr. Dr. Dirk Hollmann (UR), Dr. Esteban Mejia (LIKAT), Prof. Le Thanh Son (HUS-VNU), and Prof. Le Minh Thang (HUST) for their efforts to bring this project to success.

I would also like to thank Dr. Jörg Harlorf, Dr. Ronald Wustrack, Dr. Jonas Bresien, Ms. Regina Brosin, Ms. Kerstin Bohn, Mr. Torsten Rathsach, and all members of the group for the advice, encouragement, patience, and kindness they have shown throughout my work and laboratory experiment.

Finally, I would like to thank my family, my friends for their support and encouragement in my life.

# Danksagungen

Diese Arbeit wurde am Institut für Chemie, Anorganische Chemie, der Universität Rostock angefertigt. Insbesondere möchte ich meinem Betreuer, Herrn Prof. Dr. Axel Schulz für die Aufnahme in seinem Arbeitskreis und für die Betreuung meiner Doktorarbeit danken. Auch möchte ich meinem unmittelbaren Betreuer Dr. Hendrik Kosslick für seine geduldige und kontinuierliche Unterstützung bis zum Abschluss meiner Doktorarbeit danken. Herrn Prof. Dr. Le Thanh Son möchte ich meinen Dank aussprechen für die Motivation und seine gezeigte Unterstützung. Ich möchte den Mitarbeitern und Mitarbeiterinnen der Bereiche Analytik des Instituts für Chemie und des Leibniz-Institutes für Katalyse an der Universität Rostock (LIKAT) für die ausgezeichnete Unterstützung bei der Charakterisierung der Katalysatoren und deren katalytischer Testung danken. Ich danke allen für die freundliche Aufnahme und die konstruktive Arbeitsatmosphäre. Mein besonderer Dank gilt Frau Dr. Christine Fischer, Frau Dr. Susanne Schareina (LIKAT) für die GC-Analysen, MS. Dr. Ulrike Schümann (LKV-Rostock) für Kraftstoffadditivanalytik. Sehr dankbar bin ich auch Herrn Dr. Dirk Michalik für NMR-Messungen, Herrn Dr. Alexander Villingner für die XRD-Messungen, Herrn Dr. Reinhard Eckelt für die Stickstoff Ad- und Desorptionsmessungen und deren Diskussion. Herrn Dr. Armin Springer (EMZ) und Prof. Dr. Marcus Frank für SEM- und TEM-Messungen, und Frau Dr. Astrid Lehmann für AAS-Messungen.

Ich möchte allen Leitern und Mitgliedern des Rohan-Projekts meinen tiefen Dank für Kurse und wichtige wissenschaftliche Ratschläge aussprechen, die es mir ermöglichten, mich dem Forschungsthema zu nähern und meine Promotion abzuschließen. Insbesondere danke ich auch Prof. Dr. Udo Kragl, Dr. Dirk Hollmann (University of Rostock), Dr. Esteban Mejia (LIKAT), Prof. Dr. Le Thanh Son (Hanoi University of Science, HUS-VNU, Vietnam), und Prof. Dr. Le Minh Thang (Hanoi University of Science and Technology, HUST, Vietnam) für die gegebene erfolgreiche Unterstützung im Rahmen des RoHan-Projektes.

Ich möchte auch Herrn Dr. Jörg Harlorf, Herrn Dr. Ronald Wustrack, Dr. Jonas Bresien, Ms. Regina Brosin, Ms. Kerstin Bohn, Herrn. Torsten Rathsack, und allen Mitgliedern der Gruppe für den Rat, die Ermutigung, die Geduld und die Freundlichkeit danken, die sie während meiner Arbeit gezeigt haben.

Abschließend möchte ich meiner Familie, meinen Freunden und insbesondere meinen Eltern für ihre Unterstützung und Ermutigung in meinem Leben danken.

# Summary

Acidic natural zeolite clinoptilolite (HCLIN) was prepared by ammonium-ion exchange of the natural zeolite precursor (CLIN), followed by calcination of the obtained ammonium-exchanged clinoptilolite (NH<sub>4</sub>CLIN). Obtained zeolite materials were characterized regarding composition, structure, morphology, acidity using AAS, XRD, SEM, TEM, EDX, FTIR, BET, and NH<sub>3</sub>-TPD. The catalytic properties of the prepared catalysts were tested in the etherification of glycerol with *tert*-butanol to the corresponding mono-, di-, and tri-ethers (M, D, T). The results show that the starting material natural zeolite and the obtained HCLIN catalysts are thermally stable until 600 °C. The zeolitic NH<sub>4</sub><sup>+</sup> ions decompose over a wide temperature range of *ca.* 250 °C to 550 °C to weak, medium-strong (350-450 °C), and strong H<sup>+</sup> Brønsted acid sites (BS) in HCLINs. Different acidic HCLIN catalysts were prepared by calcination of NH<sub>4</sub>CLIN at temperatures were called HCLIN300, HCLIN400, HCLIN500, and HCLIN600. In the catalyst HCLIN300 the micropores are still blocked by the cations. Hence, catalysis can take place only at or near the external catalyst surface. After heating to 400-500 °C, micropores are available and high specific surface areas and micropore volumes were observed. Micropores are declined due to partial thermal destruction of the framework structure. Interestingly, highest conversions of glycerol are observed with HCLIN300, which contains lower amount of BS, as the pore system is still closed, it is concluded that the catalytic reaction takes place at or near the catalyst surface. A markedly decline of activity in terms of conversion is found with the catalysts HCLIN400 and HCLIN500 although the internal micropores is available and consequently, a maximum number of BS are formed. The finding points to the loss of weak BS by dehydroxylation and the low accessibility of Gly to BS in the micropores. The damaged HCLIN600 shows very low activity. Additionally, the influence of reaction conditions as reaction time, reaction temperature, catalyst loading, and the glycerol to butanol ratio as well as different alcohols were tested. The improved catalytic performance found with tertiary alcohols is assigned to the stabilization of the intermediate formed carbocation by the tertiary alkyl groups and to its hydrophobic properties, which keep off water from the reaction site. The presence of water is a critical parameter. The acid natural zeolite clinoptilolite is an active sustainable catalyst in the etherification of glycerol with tertiary butanol to di-ether. It is of potential for the replacement of so far used mineral acids or bases. The formed di-ether is a *sustainable synthetic fuel* additive for biodiesel transportation fuel and, therefore, for the CO<sub>2</sub> cycling.

# Zusammenfassung

Modifizierter saurer Clinoptilolith wurde als wirtschaftlicher umweltfreundlicher Katalysator bei der Veretherungsreaktion zwischen dem nachwachsenden Rohstoff Glycerin (Gly) und *tert*-Butanol (TBA) zu Ethern (mono-, di- und tri-*tert*-butylglycerol ether) verwendet. Di-, tri-ether könnte besser in Diesel oder Biodiesel als Oxygenat-Kraftstoffadditiv gelöst werden. Diese Arbeit trug zu den Zielen der nachhaltigen Entwicklung (SDGs) bei. Natürlicher Zeolith, Clinoptilolith, kann einfach durch Ionenaustausch mit 0,2 M  $\text{NH}_4\text{NO}_3$ -Lösung und anschließende  $\text{NH}_4$  -Zersetzung (Kalzinierungsprozess) protoniert werden. Das gebildete  $\text{H}^+$  an der Sauerstoffbrücke  $\text{Si-O(H)-Al}$  ist die Brønsted-Säurestelle (BS). Der optimierte Säurekatalysator hatte eine hohe Aktivität bei der Glycerinumwandlung, die 80% erreichte, und die Selektivität von di- und tri-ether betrug 28 bis 30% nach 4 Stunden Reaktion bei 140 °C mit 5% Katalysatorbeladung.

Die Kalzinierungsbedingungen bei 300 °C in kurzer Zeit, die viel niedriger als im anderen Bericht sind, ergaben die höchste Veretherung von Gly und TBA. Obwohl Zersetzung von  $\text{NH}_4^+$  zu  $\text{H}^+$  in einem weiten Bereich von 250-550 °C (wie durch IR, TGA,  $\text{NH}_3$ -TPD gezeigt). Bei 400 °C öffnet sich die Pore des Katalysators, die spezifische Oberfläche nahm zu, wenn die meisten  $\text{NH}_4^+$  innerhalb und nahe des Fensters der Pore zersetzt wurden. Die katalytischen Aktivitäten von HCLIN400 nahmen jedoch ab, was durch die thermische Stabilität der externen BS erklärt werden konnte. Die anderen gebildeten Säurestellen sind nicht zugänglich und leicht zu gefüllt. Ihre Porositäten weisen zu Beginn der Reaktion den höchsten Einfluss auf Umwandlung und Selektivität gegenüber HCLIN400 auf, wenn die Adsorptionseigenschaft des Katalysators stärker ausgeprägt ist als die Säurestellen.

Die XRD, SEM, TEM, AAS, TGA, BET, IR und  $\text{NH}_3$ -TPD Methoden wurden verwendet, um die erhaltenen Acidity Clinoptilolite (HCLIN) -Proben zu charakterisieren. Daher wurden ihre Eigenschaften wie Kristallin, Morphologie, Porosität, Säuregehalt geklärt. Diese Eigenschaften standen im Zusammenhang mit der Wasserentfernung als Dehydratisierung, Dehydroxylierung und Zersetzung von  $\text{NH}_4^+$ . Zweck, dass die Geschwindigkeit der Dehydroxylierung niedriger als die Geschwindigkeit der  $\text{H}^+$  -Bildung gehalten wurde, um das Ausbleichen des schwachen BS zu vermeiden. Die Aktivität nahm ab, wenn es bei höherer Temperatur oder über einen längeren Zeitraum kalziniert wurde. Das Gerüst wurde bei 500-600 °C beschädigt.

# Table of contents

1	Main Goals .....	1
2	Introduction .....	2
2.1	General .....	2
2.2	Background .....	10
2.2.1	Biodiesel production and by-product glycerol .....	10
2.2.2	Etherification of glycerol .....	11
2.2.3	Zeolite catalysts .....	14
2.3	State-of-Art .....	20
2.3.1	Glycerol conversion .....	20
2.3.2	Etherification of glycerol with <i>tert</i> -butanol .....	23
2.4	Motivation .....	28
3	Experimental .....	29
3.1	Materials .....	29
3.2	Catalyst preparation .....	30
3.3	Characterization .....	31
3.4	Catalysis .....	34
3.4.1	Apparatus and equipment .....	34
3.4.2	Catalytic testing .....	35
3.4.3	Analysis .....	37
4	Results and discussion .....	39
4.1	Characterization .....	39
4.1.1	X-ray diffraction analysis (XRD) .....	39
4.1.2	Chemical analysis (AAS) .....	42
4.1.3	Scanning electron microscopy (SEM) .....	43
4.1.4	Transmission electron microscopy (TEM) .....	46



4.1.5	Energy dispersive x-ray analysis (EDX)	47
4.1.6	Nitrogen adsorption and desorption measurements	50
4.1.7	Fourier transform infrared spectroscopy (FTIR)	52
4.1.8	Thermogravimetric analysis (TGA)	54
4.1.9	Temperature-programed desorption of ammonia (TPD)	55
4.1.10	Summary	57
4.2	Catalysis	59
4.2.1	Assessment of catalyst preparation and testing	59
4.2.1.1	Influence of the activation temperature	60
4.2.1.2	Influence of the activation temperature on the BET specific surface area	62
4.2.1.3	Influence of ammonium ion exchange conditions	62
4.2.1.4	Conclusion of assessment	64
4.2.2	Catalytic performance	65
4.2.2.1	Influence of catalyst activation on the activity and selectivity	65
4.2.2.2	Influence of reaction conditions on the activity and selectivity	70
4.2.2.3	Catalyst reuse	74
4.2.2.4	Summary of catalytic performance	77
4.3	Different alcohols	79
5	Conclusions	82
6	Reference	84
7	Appendix	89

# List of Figures

**Figure 1.** The global CO<sub>2</sub> emission from 1850 until 2017 and the contribution of different regions and countries. Source of data: Carbon Dioxide Information Analysis Centre (CDIAC) and drawn by origin software. .... 5

**Figure 2.** The CO<sub>2</sub> emission by the different sectors. Source: Carbon Dioxide Information Analysis Center (CDIAC) 2017 and drawn by origin software. .... 6

**Figure 3.** Photosynthesis in chloroplast of leaf, solar energy is converted to ATP and NADPH, which is necessary in Calvin cycle. Whereas CO<sub>2</sub> and H<sub>2</sub>O are converted to sugar (80–85%, mainly as glucose, fructose, sucrose, and starch) and storing light energy as chemical energy.<sup>[7,8]</sup> ..... 7

**Figure 4.** The cycle of CO<sub>2</sub> from transportations. .... 9

**Figure 5.** The surface of heterogeneous catalyst with a reaction on its active sites. .... 14

**Figure 6.** Oxygen rings occurring in zeolites formed TOT bridges (T=Si,Al) forming secondary building units of zeolites (SBUs).<sup>[40]</sup> ..... 16

**Figure 7.** Clinoptilolite structure: **(a)** from HEU framework edited by using Diamond software, at c axis viewer TO<sub>4</sub> structure 10 and 8 oxygen ring openings, **(b)** Columnar model of 2-dimensional channel arrangement of HEU framework. The clinoptilolite structure according to Yamanaka et al.<sup>[46]</sup> ..... 17

**Figure 8.** Clinoptilolite structure in a unit cell at a, b c axis direction to see the location of cation and free water in 8 and 10 oxygen ring windows (Framework type HEU) edited by using Diamond software. .... 18

**Figure 9.** Etherification of glycerol in a reflux system. .... 36

**Figure 10.** High-pressure autoclave reactor. .... 36

**Figure 11.** Construction of the autoclave reactor: High-pressure reactor with 150 mL volume capacity 5500 Parr autoclave with controller Parr 4848 used in catalyst testing. .... 38

**Figure 12.** Powder XRD patterns of a) starting clinoptilolite CLIN, b) ammonium exchanged NH<sub>4</sub>CLIN, and the acidic forms: c) HCLIN250, d) HCLIN300, e)

HCLIN400, f) HCLIN450, g) HCLIN500, h) HCLIN600 calcined at corresponding temperatures (250 °C to 600 °C): "CL"- the typical peak of CLIN pattern, "CR"-Cristobalite, "Mor"- Mordenite, "Q"-Quartz, "Fel"-Feldspar..<sup>[64]</sup> 39

**Figure 13.** Influence of the calcination temperature on the crystallite size of clinoptilolite. Starting material CLIN, ammonium form NH<sub>4</sub>CLIN (ion-exchange with 0.2M solution NH<sub>4</sub>NO<sub>3</sub>, 80 °C, 2h two times), calcination temperatures C250, C300, C400, C500, C600, samples named as HCLIN250, HCLIN300, HCLIN400, HCLIN500, HCLIN600. .... 42

**Figure 14.** SEM images of (a) CLIN, (b) NH<sub>4</sub>CLIN, (c) HCLIN200, (d) HCLIN300, (e) HCLIN400, (f) HCLIN500, (g) HCLIN600 with 1 k of magnification. .... 44

**Figure 15.** High resolution SEM images of (a) CLIN, (b) NH<sub>4</sub>CLIN, (c)-(d) HCLIN200, (e) HCLIN300, (f) HCLIN500, (g) HCLIN600 with 100 k of magnification. .... 45

**Figure 16.** TEM images of 4 samples NH<sub>4</sub>CLIN, HCLIN300, HCLIN500, HCLIN600 sample at 50-100 nm scales. .... 46

**Figure 17.** Energy dispersive X-ray (EDX) mapping analysis for aluminum element distribution in two samples NH<sub>4</sub>CLIN (right) and HCLIN300 (left). .... 47

**Figure 18.** Energy dispersive X-ray (EDX) mapping analysis of oxygen element distribution in two sample CLIN (left), HCLIN500 (right). .... 47

**Figure 19.** Element mapping based on energy dispersive X-ray (EDX) analysis of N distribution of two samples NH<sub>4</sub>HCLIN and HCLIN300. .... 48

**Figure 20.** Energy dispersive X-ray (EDX) element mapping analysis of the K (pink) and Na (blue) distribution for two samples HCLIN300 (right) and NH<sub>4</sub>CLIN (left): blue colored dots represent Na and pink colored dots belong to K. .... 48

**Figure 21.** Energy dispersive X-ray (EDX) mapping analysis for nitrogen (green), and potassium (pink) element distribution in two sample NH<sub>4</sub>CLIN (left), HCLIN500 (right). .... 49

**Figure 22.** Energy dispersive X-ray (EDX) mapping analysis for sodium element distribution in two samples CLIN (left), HCLIN500 (right). .... 49

**Figure 23.** Energy dispersive X-ray (EDX) mapping analysis for calcium element in two samples CLIN (left), HCLIN500 (right). .... 50

<b>Figure 24.</b> Nitrogen adsorption/desorption isotherms of a) HCLIN400, HCLIN500, HCLIN600, NH <sub>4</sub> CLIN100, e) NH <sub>4</sub> CLIN200, HCLIN300. ....	50
<b>Figure 25.</b> The IUPAC classification of adsorption isotherms of different porous systems showing both the adsorption and desorption pathways. Note the differences observed between internal micro pores and inter particle macro pores (type I and type II isotherms). <sup>[79]</sup> .....	51
<b>Figure 26.</b> FTIR lattice vibration spectra of clinoptilolite CLIN after different treatment: a) starting material CLIN, b) ammonium exchanged NH <sub>4</sub> CLIN, and c) calcined HCLIN200, d) HCLIN300, e) HCLIN400, f) HCLIN500, g) HCLIN600. ....	53
<b>Figure 27.</b> Combined TG-DSC curves of an ammonium exchanged NH <sub>4</sub> CLIN with 5 weight loss steps. a) from 50 to 150 °C, b) from 150 to 280 °C, c) from 280 to 450 °C, d) from 450 to 570 °C, e) above 600 °C. ....	54
<b>Figure 28.</b> Temperature programmed ammonia desorption curves of NH <sub>4</sub> CLIN (exchange condition: 0.2M NH <sub>4</sub> NO <sub>3</sub> at 80 °C for 2 hour two times; calcination at 300 °C and 400 °C in 30 minute) with NH <sub>3</sub> flow treatment for NH <sub>4</sub> HCLIN (a), HCLIN300 (b), HCLIN400 (c) (Pre-treatment of samples at 180 °C, NH <sub>3</sub> gas loading at 100 °C). Without NH <sub>3</sub> loading NH <sub>4</sub> CLIN (d) and HCLIN300 (e).....	56
<b>Figure 29.</b> Decrease of the ammonium ion content of HCLIN compared to NH <sub>4</sub> CLIN after thermal activation at 300 °C to 500 °C, recreation by ammonium re-exchange, and the corresponding loss of BS by thermal dehydroxylation obtained from FTIR measurements. ....	59
<b>Figure 30.</b> Influence of the activation temperature on the conversion of glycerol over HCLIN catalysts: NH <sub>4</sub> CLIN200, HCLIN300, HCLIN600 calcined for 30 min at 230, 320, 420, 520, and 620 °C. Reaction conditions: 110 °C in autoclave, Gly/TBA = 1/4, 5 % catalyst per mass of glycerol. (NH <sub>4</sub> CLIN prepared with two times exchange with 0.2 M NH <sub>4</sub> NO <sub>3</sub> solution 80 °C for 2 hours each).....	60
<b>Figure 31.</b> Glycerol conversion vs. calcination temperature: HCLIN200, HCLIN300, HCLIN600 catalysts, calcined in 1 min at 200, 300, 400, 500, and 600 °C (achieved oven temperatures). Reaction condition: 86 °C under reflux, Gly/TBA =1/4, catalyst/Gly mass = 7.5 %. Catalyst preparation was used NH <sub>4</sub> NO <sub>3</sub> 0.5M. ....	61

- Figure 32.** Glycerol conversion Vs. reaction time  $t$  over HCLIN300 catalysts, calcined 320 °C in 1 min. Condition: 110 °C in autoclave, reaction time: 1 min, 1 h, 2 h, and 3 h, Gly/TBA =1/4, catalyst/Gly mass = 5 %. Ion exchange with different concentration of  $\text{NH}_4\text{NO}_3$  solution (a) 0.05 M, (b) 0.1 M, (c) 0.4 M, (d) 0.2 M, and two times ion exchange with 0.2 M solution (e), (f) calcination at 300 °C in 1 min, 30 min, and (g) at 320 °C 1 min..... 63
- Figure 33.** Influence of the catalyst activation temperature on the glycerol conversion to M1, M2, D1, D2 ethers over different catalysts. Reaction condition: 110 °C, 1 min (just after reaching the reaction temperature in the autoclave), Gly/TBA =1/4, catalyst/Gly mass = 5 %, reaction time: Using catalyst is HCLIN300 short time activated for 1 min at 300 °C. .... 66
- Figure 34.** Influence of the catalyst activation temperature on the glycerol conversion to M1, M2, D1, D2 ethers after 4h of reaction over different catalysts HCLIN300 to HCLIN600 (short-time activation of 1min). Reaction condition: 110 °C, in autoclave, Gly/TBA =1/4, catalyst/Gly mass = 5 % in reaction time: 4h. .... 66
- Figure 35.** IR spectra of ammonium exchanged  $\text{NH}_4\text{CLIN}$ , HCLINs obtained after calcination at 300, 400, and 500 °C and corresponding ammonium re-exchanged samples Re-HCLIN. The deformation vibration band at  $1440\text{ cm}^{-1}$  corresponds to the vibration of the ammonium ion  $\text{NH}_4^+$ . .... 68
- Figure 36.** Influence of the calcination time of HCLIN300 catalyst on the conversion of glycerol with TBA after (a) 60 min and (b) 120 min of etherification reaction, c) influence on acidity of catalyst (Table 16). Reaction condition: Gly/TBA =1/4, catalyst/Gly mass = 5 %, 110 °C in autoclave). .... 69
- Figure 37.** Glycerol conversion vs. reaction time over HCLIN300, catalyst (30 min calcination) - change of the composition of the reaction solution. Condition: 110 °C in autoclave, Gly/TBA =1/4, catalyst 5 % per mass of glycerol, after reaction time: 30 min, 2h, 6h 20h, HCLIN400 (30min, 2h, 8h, 24h), HCLIN500 (30min, 2h, 6h, 24h). .... 71
- Figure 38.** Influence of the Gly/TBA ratio on the content of M1, M2, D1, D2, T, Gly of the reaction solution with time: 1min, 2h, 6h 20h 30 min, 2h, 6h, 20h. Gly/TBA ratio=1/5 (left) and 1/8 (right), reaction temperature: 110 °C..... 72

- Figure 39.** Influence of the reaction temperature on the conversion of glycerol to M1, M2, D1, D2 ethers and on the selectivity over different catalysts. Conditions: in an autoclave, Gly/TBA =1/4, catalyst content 5% per mass Gly, HCLIN300, reaction time 4h, reaction temperature 110 °C 140 and 160 °C..... 73
- Figure 40.** Influence of the catalyst loading on glycerol conversion to mono-ether M, di-ethers D, and tri-ether T (rare to see <1%) over HCLIN300. Catalyst loading: 2.5, 5, 7.5, 10 % per mass of glycerol. Reaction conditions: 110 °C, 4h reaction time, in an autoclave, Gly/TBA=1/4. The catalyst obtained by 30 min calcination HCLIN300..... 74
- Figure 41.** Influence of the re-use of HCLIN300 on the selectivity to mono-, di, and tri-ether (M, D, T) in the etherification of glycerol and t-butanol. Catalyst: HCLIN300 (NH<sub>4</sub>CLIN ion-exchanged solution 0.2 M, 30 min calcination reaction condition: 110 °C in autoclave for 2h, Gly/TBA =1/4, catalyst/Gly mass ratio = 0.3. .... 75
- Figure 42.** The conversion of glycerol reaction using HCLIN300 with a catalyst loading of (A) 30% and (B) 5%with respect to the glycerol content: (a) NH<sub>4</sub>CLIN - ion-exchanged with 0.2M NH<sub>4</sub>NO<sub>3</sub> solution, 30 min. calcination), (b) first, (c) second, and (d) third reuse. Reaction condition: 110 °C in autoclave 2h, Gly/TBA =1/4. .... 76
- Figure 43.** DSC (left) and TG curve (right) of the used catalyst and the reactivated catalyst: (a) Used catalyst HCLIN300 without washing (—), (b) separated catalyst washed with water (— ), (c) separated catalyst washed with ethanol (—). .... 76
- Figure 44.** Comparison of the conversion achieved of different alcohol reactants (C1-C5) in the etherification with glycerol over HCLIN300.. The difference of their isomers n, iso, sec, tert (noticed as n, i, s, t) was compared. All the samples were taken after 2 hours of reaction at 140 °C, 5% catalyst loading, and ratio with glycerol 1:4, in an autoclave..... 79
- Figure 45.** Composition of M1, M2, D1, D2, T, Gly of the products in the etherification reaction of glycerol with t-amyl alcohol after different reaction times: 30 min, 2h, 6h, 1 day, 2 days. Reaction conditions: autoclave, autogeneous pressure, 140 °C, 5wt% catalyst, 1:4 Gly/t-amyl ratio (left), With t-butanol after 30min, 1h30, 2h, 4h, and 6h of reaction. 1:4 Gly/t-butanol ratio (right)..... 80

**Figure 46.** FTIR lattice vibration spectra of clinoptilolite CLIN after different treatment: a) starting material CLIN, b) ammonium exchanged  $\text{NH}_4\text{CLIN}$ , and c) calcined HCLIN200, d) HCLIN300, e) HCLIN400, f) HCLIN500, g) HCLIN600. .... 89

**Figure 47.** GC-FID result of samples of reaction between glycerol and t-butanol. The peaks of, T, D1, D2, M1, M2, and Gly were noted with their retention time. .... 89

## List of Schemes

- Scheme 1:** Photosynthetic product is from the light and carbon reactions of photosynthesis. In the vast majority of photosynthetic systems, carbon partitioning is primarily directed toward fatty acid (~10%).<sup>[9]</sup> ..... 7
- Scheme 2:** Conversion of pyruvate to acetyl-CoA, which is continuous as a component in the mechanism of fatty acids and vegetable oils in leaves with coenzyme A support.<sup>[10]</sup> ..... 8
- Scheme 3:** Trans-esterification reaction between vegetable oil and animal fat (triglyceride) with short chain alcohol in bio-diesel production. .... 10
- Scheme 4:** Catalytic etherification between short chain alcohol and glycerol. .... 11
- Scheme 5:** Etherification between glycerol (Gly) and *t*-butanol to form mono-ether (M1): *tert*-butoxypropane-2,3-diol, (M2): *tert*-butoxypropane-1,3-diol, di-ether (D1): 1,3-di-*tert*-butoxypropanol, (D2): 1,2-di-*tert*-butoxypropanol and tri-ether (T): tri-*tert*-butoxypropanol as oxygenate fuel additive as sustainable renewable energy. .... 12
- Scheme 6:** Brønsted and Lewis acid sites exist on the zeolite catalyst, and the related dehydroxylation.<sup>[32][33]</sup> ..... 14
- Scheme 7:** Ion exchange process and decomposition of ammonium ions of NH<sub>4</sub>CLIN to the protonated form of clinoptilolite HCLIN as green synthesis. M<sup>+</sup> is represents cations Na<sup>+</sup>, K<sup>+</sup>, and M<sup>2+</sup> is as Ca<sup>2+</sup>, and Mg<sup>2+</sup> cation in the clinoptilolite..... 19



# List of Tables

<b>Table 1:</b> Sustainable development goals (SDGs).....	2
<b>Table 2:</b> Contributions of Green Chemistry.....	3
<b>Table 3:</b> Free diameter of difference Oxygen ring types in clinoptilolite framework.....	17
<b>Table 4:</b> Textural and acidity properties of organic resin amberlyst A-15 and USY, H-Beta, HZSM-5 and zeolites and catalytic activity, conversion (C) and selectivity (S) in etherification of glycerol (Gly) with tertiary butanol (TBA) to the corresponding mono, di and tri-ethers (M,D,T).....	22
<b>Table 5:</b> Properties of alcohols.....	29
<b>Table 6:</b> Observed XRD reflections and peak intensities of natural clinoptilolite sample CLIN, ammonium exchanged clinoptilolite NH <sub>4</sub> CLIN and acidic forms HCLIN obtained after calcination at different temperatures (250 °C to 600 °C). Reflection angle $2\theta$ (°): peak I to IX are (CL) 9.9°, (CL) 11.2°, (CL) 13.1°, (CL) 17.4°, (CR) 21.9°, (CL) 22.5°, (CL) 26.1°, (CL) 30.2°, (CL) 31.1° (CL- clinoptilolite, CR- cristobalite).....	40
<b>Table 7:</b> Crystallite sizes of clinoptilolite, ammonium exchanged clinoptilolite NH <sub>4</sub> CLIN and its acidic forms HCLIN obtained after calcination at different temperatures (250 °C to 600 °C) determined by the Scherrer formulae from the width of the XRD reflection at a $2\theta = 9.9^\circ$ .....	41
<b>Table 8:</b> Chemical composition (wt%) of elements Ca, K, Fe, Mg, Na, N, and H of four samples: Starting material CLIN, ammonium form NH <sub>4</sub> CLIN, calcined samples at 300 °C HCLIN300, and 500 °C named as HCLIN500.....	42
<b>Table 9:</b> Classification of pores by the pore size.....	52
<b>Table 10:</b> Specific surface areas and specific microspore volumes of ammonium exchanged and thermally activated HCLINs.....	52
<b>Table 11:</b> Wavenumbers of typical zeolite lattice vibrations and vibrations of functional groups of clinoptilolite CLIN, ammonium exchanged NH <sub>4</sub> CLIN, and different calcined HCLIN samples.....	53
<b>Table 12:</b> Amounts of ammonia released from NH <sub>4</sub> CLIN, and from remaining ammonium ions of thermal activated catalysts HCLIN300, HCLIN400, and HCLIN500, and calculated acidity measured by TPD of ammonia.....	57

<b>Table 13:</b> Specific surface area of clinoptilolite catalysts calcined at different temperatures: 200, 300, 400, 500, 600 °C. ....	62
<b>Table 14:</b> Conditions of catalyst preparation by ion exchange and calcination, amount of starting material in NH <sub>4</sub> NO <sub>3</sub> concentration solution, the temperature of ion exchange, calcination condition. ....	64
<b>Table 15:</b> Influence of the calcination temperature of HCLIN catalysts on the degree of ammonium re- exchange determined by IR spectroscopy from the change of the intensity of ammonium NH <sub>4</sub> <sup>+</sup> deformation band. The intensity of the asym TOT vibration band used as internal standard. ....	68
<b>Table 16:</b> Influence of calcination time to the composition of ammonium ion to BS using the formation of HCLIN300 by activation of NH <sub>4</sub> CLIN at 300 °C. ....	69
<b>Table 17:</b> Comparison of the catalytic performance of the natural zeolite catalyst HCLIN with synthetic zeolite catalysts and the acidic organic resin A-15. ....	78

# List of Abbreviations

---

<b>Ads.</b>	Adsorption	<b>HCLIN</b>	Protonated CLIN, acid form
<b>BET.</b>	Brunauer–Emmett–Teller	<b>IR</b>	Infrared spectroscopy
<b>BJH</b>	Barrett, Joyner, Halenda	<b>LS</b>	Lewis acid sites
<b>BS</b>	Brønsted acid sites	<b>MTBE</b>	Methyl <i>tert</i> -butyl ether
<b>ca.</b>	Approximately Cation	<b>M1</b>	1- <i>tert</i> -butoxypropane-2,3-diol
<b>Cat.</b>	Catalyst	<b>M2</b>	2- <i>tert</i> -butoxypropane-1,2-diol
<b>CLIN</b>	Starting Clinoptilolite	<b>NH<sub>4</sub>CLIN</b>	NH <sub>4</sub> <sup>+</sup> exchanged CLIN
<b>conc.</b>	Concentration	<b>SEM</b>	Scanning electron microscopy
<b>DSC</b>	Differential scanning calorimetry	<b>SRC</b>	Standard reaction condition
<b>D1</b>	1,3- <i>tert</i> -butoxypropane-2-ol	<b>T</b>	tri- <i>tert</i> -butoxypropan
<b>D2</b>	1,2- <i>tert</i> -butoxypropane-2-ol	<b>TAME</b>	Tertiary amyl methyl ether
<b>EDX</b>	Energy dispersive X-Ray	<b>TBA</b>	<i>tert</i> -butanol or <i>t</i> -butanol
<b>ETBE</b>	Ethyl tertiary butyl ether	<b>TEM</b>	Transmission electron microscopy
<b>et al.</b>	And others	<b>TGA</b>	Thermogravimetry analysis
<b>etc.</b>	And other similar things	<b>TPD</b>	Temperature programmed desorption
<b>e.g.</b>	For example	<b>V</b>	Volume
<b>GC</b>	Gas chromatography	<b>Vs.</b>	Versus
<b>Gly</b>	Glycerol	<b>XRD</b>	X-ray diffraction
		<b>wt%</b>	Weight percent

---

# Used units

Quantity	Symbol	Name	Conversion
Length	Å	Angstrom	1 Å = $10^{-10}$ m
	µm	Micrometer	1 µm = $10^{-6}$ m
	nm	Nanometer	1 nm = $10^{-9}$ m
Weigh	Mt	Megaton	1 Mt = $10^6$ ton
Temperature	°C	Degree Celsius	x °C = (x + 273.15) K
Volume	mL	Milliliter	1 ml = 1 cm <sup>3</sup> = $10^{-6}$ m <sup>3</sup>
	ppm	Parts-per-million	1ppm = 1µL/L
wavenumber	cm <sup>-1</sup>	Reciprocal centimeter	1 cm <sup>-1</sup> = 100 m <sup>-1</sup>
Wavelength	nm	Nanometer	1 nm = $10^{-9}$ m
Time	h	Hour	1h = 60 min = 3600 s
	min	Minute	1 min = 60 s
Pressure	Bar	Bar	1 bar = 100000 Pa = 0.98 atm = 1.02 kgf/cm <sup>2</sup> = 14.5 Psi
Energy	eV	Electron volt	1 eV = $1.6 \times 10^{-19}$ J
	TWh	Terawatt-hour	1 TWh = $3.6 \times 10^{15}$ J

# 1 Main Goals

## ***Goals***

Firstly, this work is contribution to the climate change activities by limiting the CO<sub>2</sub> release into the atmosphere. Therefore, the fossil transportation fuel is replaced by a sustainable synthetic fuel (*SSF*) based on renewable feedstock using heterogeneous catalysis as a key technology.

It aims the development of a sustainable green acid catalyst based on natural zeolite clinoptilolite and the testing in the catalytic etherification of the renewable feedstock glycerol, a by-product of the biodiesel production, with tertiary butanol to glycerol di-ether for use as a fuel additive. This way the carbon dioxide will be cycled.

Additionally, this work aims to contribute to the collaborative education and research program RoHan of the University of Rostock/LIKAT, Hanoi University of Science - VNU, and Hanoi University of Science and Technology, dedicated to sustainability using heterogeneous catalysis as a key technology, which was funded by the DAAD.

## ***Objectives***

- Preparation and characterization of an acidic solid catalyst based on natural zeolite clinoptilolite
- Assessment of catalyst preparation (ammonium ion exchange, thermal activation) and testing conditions (temperature, catalyst loading, reaction time, concentration)
- Investigation of catalyst properties in the etherification of glycerol
- Acidity, morphology, and textural properties
- Study of the catalytic performance in the etherification of glycerol with *t*-butanol
- Comparison of the performance with other alcohols like short-chain and amyl alcohol

Bench test of the obtained di-ether product aims to a reliable fuel additive.

## 2 Introduction

### 2.1 General

#### 2.1.1 Sustainable development goals

The situation all over the world is characterized by climate change, environmental pollution, economic inequality, and social life problems in many countries. The required activities in order to solve these problems were summarized by the United Nations, the European Union and other institutions in sustainable development goals (SDGs) (Table 1). At the Earth Summit in Rio, 1992, more than 178 countries accepted the Agenda 21. These goals aim to bring people together in peace and prosperity, with a partnership plan to improve human lives and protect the environment.

**Table 1:** Sustainable development goals (SDGs).

---

1) Climate Action	10) Gender Equality
2) Clean Water and Sanitation	11) No Poverty
3) Affordable and clean Energy	12) Zero Hunger
4) Life below Water	13) Good Health & Well-being
5) Life on Land	14) Quality Education
6) Responsible Consumption and Production	15) Peace, Justice and strong Institutions
7) Decent Work and Economic Growth	16) Sustainable Cities and Communities
8) Industry, Innovation and Infrastructure	17) Partnerships for the Goals
9) Reduced Inequalities	

---

Remarkably, the energy and the environment situation are the most important issues for the countries, especially for the developing countries faced with limited fossil resources and quickly increase of the population and consumption. In 2019, the total world energy consumption was 140,000 TWh/y. About 85% came from fossil fuels, only 4% from biodiesel

or other renewable fuels, 4 % from nuclear, and 4% from renewables (hydro, wind, solar, geothermal). About 18% of the used energy was electricity and the other energy was used for heat and transportation. The high and boosting energy demand is a reason for the global warming and environmental problems. Moreover, CO<sub>2</sub> emission from fuel consumption for heating and transportation considering 3,5E10 tons in 2017 is the main source of air pollution and causes the Glass House effect. The goal, given by IEA 2012 (International Energy Agency), to limit the increase of global temperature on earth, to less than 2 °C becomes more and more difficult to achieve.<sup>[1,2]</sup>

**Green chemistry** (Table 2) has the potential to make significant contributions for the achievement of the sustainability development in the following fields:

- ✓ Climate Action e.g. by reduction of CO<sub>2</sub> emission
- ✓ Sustainable and Clean Energy
- ✓ Clean Water
- ✓ Responsible Consumption and Production
- ✓ Industry and Innovation.

The development of green synthesis processes of materials and the sustainable use of feedstock are extremely important to reduce the global warming and to prevent the climate change. Catalysts play a key role in environmental protection by green processes. Catalysts could improve the process efficiency such as reducing the reaction time and reaction temperature. They can also diminish the formation of by-products and enhance the productivity and selectivity of chemical processes. Moreover, many catalysts play a superior, important, or indispensable part in separation,<sup>[3]</sup> conversion, or cycling of the glasshouse gas CO<sub>2</sub><sup>[2,4,5]</sup> as a renewable source. They are included in the contributions of green chemistry.

**Table 2:** Contributions of Green Chemistry.

1) Use of Renewable Feedstock's	7) Safer Solvents and Auxiliaries
2) Atom Economy	8) Reduce Derivatives
3) Less Hazardous Synthesis	9) Design Safer Chemicals
4) Catalysis	10) Design for Biological Degradable Materials
5) Prevention of Waste	11) Real-time Analysis for Pollution Prevention
6) Improve Energy Efficiency	12) Safer Chemistry for Accident Prevention

## 2.1.2 Climate change by global warming - CO<sub>2</sub> emission from human activities in different regions

The climate change was recently identified to be a main subject of concern. The increase of carbon dioxide concentration in the air is expected to be responsible for the temperature increase causing the climate change. CO<sub>2</sub> emission is increasing throughout the world. Therefore, not only the limited available fossil oil requires use of renewable resources but also the reduction of the CO<sub>2</sub> emission.

For a long time during our development, the traditional energy sources that we use are fossil oils, coal, and gas. The energy and heat are produced by material combustion. Currently, the oil production rate reaches approximately 12 Mt/day and its demand is predicted to rise to 16 Mt/day by 2030.

However, these resources are limited on the Earth because oil and coal need millions of years for transformation from hydrocarbon agglomeration in trees (by photosynthesis process) and in animal bodies as organic compounds. Severe conditions like high pressure, temperature and long-time are required for the transformation to fossil resources.<sup>[6]</sup> These fuels have a high-energy capacity, high energy density, are easy to handle, to store and to transfer because the energy is saved as chemical energy. For these reasons, they are very important for the human development. Therefore, we have to find a way to prolong the availability this limited natural energy resource e.g. by using renewable sources for transportation fuel production. This way allows reducing the CO<sub>2</sub> emission into the atmosphere. Every year more than 36 billion tons of CO<sub>2</sub> were released from human activities. The CO<sub>2</sub> concentration in the atmosphere is over 400 ppm, the highest in the last 800,000 years. Figure 1 shows the global carbon dioxide emission of different countries and regions starting from the year 1845 until 2017. It shows a boosting of the CO<sub>2</sub> emission with the beginning of the industrial revolution. A 7-fold, increase of the CO<sub>2</sub> emission is observed since the year 1950 until today. In parallel the global temperature increased from 1901 to 2000 by 2 °C, with markedly rising tendency. At the same time, markedly climate changes are observed as storms, heavy rains, and prolonged dry seasons.



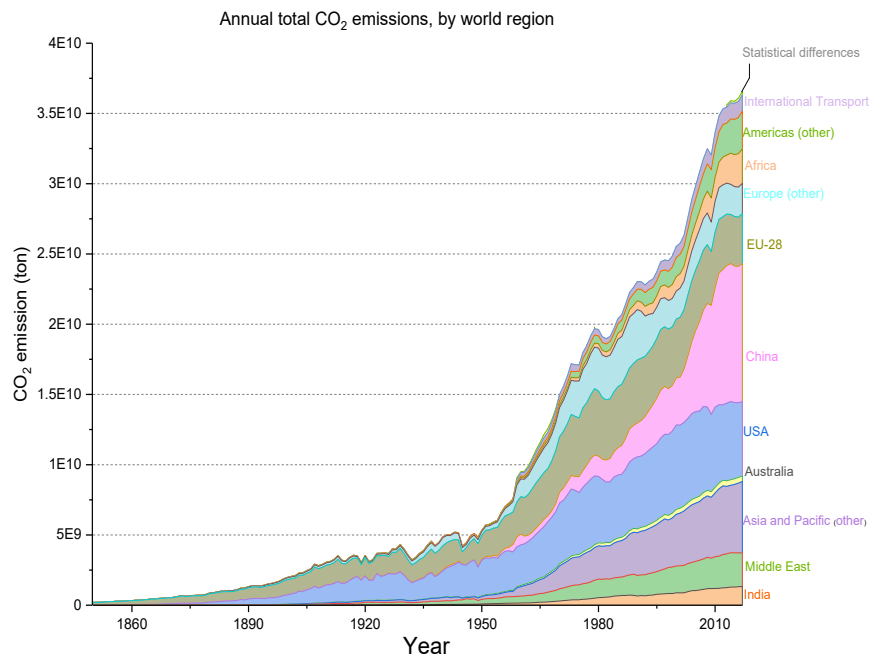


**Figure 1.** The global CO<sub>2</sub> emission from 1850 until 2017 and the contribution of different regions and countries. Source of data: Carbon Dioxide Information Analysis Centre (CDIAC) and drawn by origin software.

The USA (one of the most developed country) is the country with the highest CO<sub>2</sub> emission. With 399 billion tones, the USA contributes 25 % of the cumulative emission to date, followed by EU (22 %); China (13 %); Russia (6 %), and Japan (4 %). In the future, the developing countries with a high population will need more energy, especially from combustion. In 2017, China has released 9.8 billion tones CO<sub>2</sub> into the environment that amounts to 27% of global emissions, while the USA contributed 15 %, the EU 9.8 %, and Russia 4.7 %. The CO<sub>2</sub> emission will be further boosted by the progress of the developing countries.

### 2.1.3 Carbon dioxide emission from different human activity

The contribution of different areas of human activities to the emission of CO<sub>2</sub> is shown in Figure 2. Indeed, the electricity and heat production contribute with 49% most to the overall carbon dioxide release into the atmosphere.

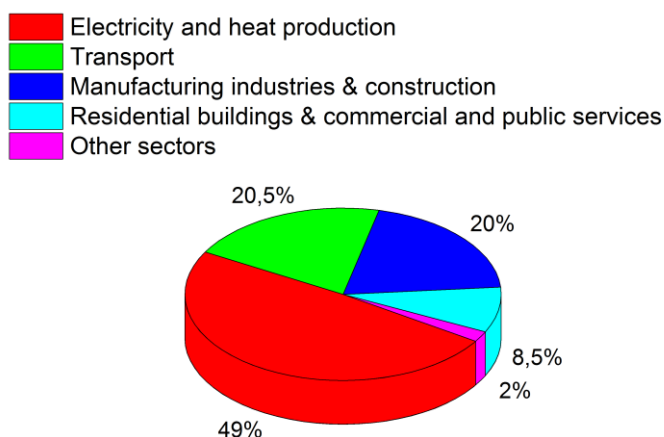


**Figure 2.** The CO<sub>2</sub> emission by the different sectors. Source: Carbon Dioxide Information Analysis Center (CDIAC) 2017 and drawn by origin software.

Besides electricity and heat production, the use of transportation fuels (Fig. 2) causes a major part of carbon dioxide emission of *ca.* 20.5%. This contribution is rapidly growing due to increasing urbanization and economic growth. The CO<sub>2</sub> emissions are also dangerous because it is so close with human activities. Therefore, the replacement of fossil transportation fuels by the renewable synthetic fuel could make a significant contribution to the reduction of the CO<sub>2</sub> emission in relative short time.

#### 2.1.4 Role of chemistry

The development and use of renewable transportation fuels is a potential approach to reduce the CO<sub>2</sub> emissions into the atmosphere. The nature provides renewable resources that can be used as starting materials for synthesis of transportation fuels as cellulose, sugar, or vegetable oil. In nature, these materials are produced by photosynthesis carbon dioxide and water using sunlight energy. Photosynthesis is a process occurring in chloroplasts of the plants, algae and others (Fig. 3).

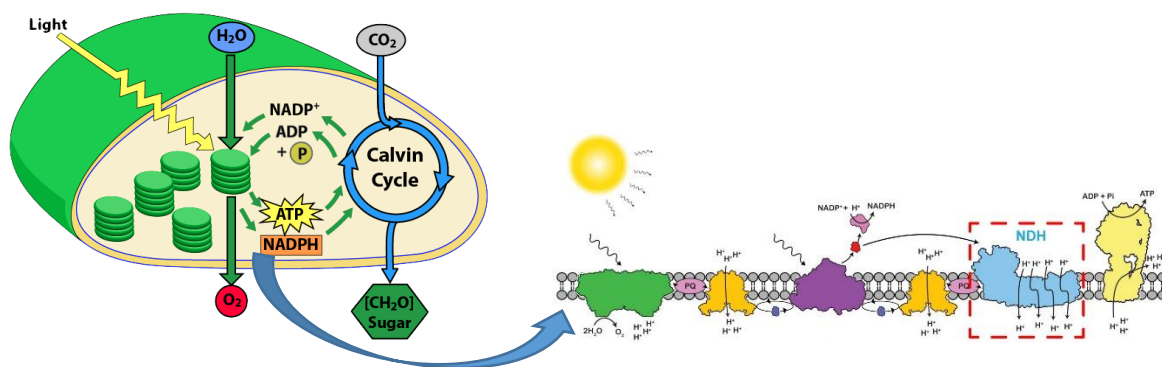
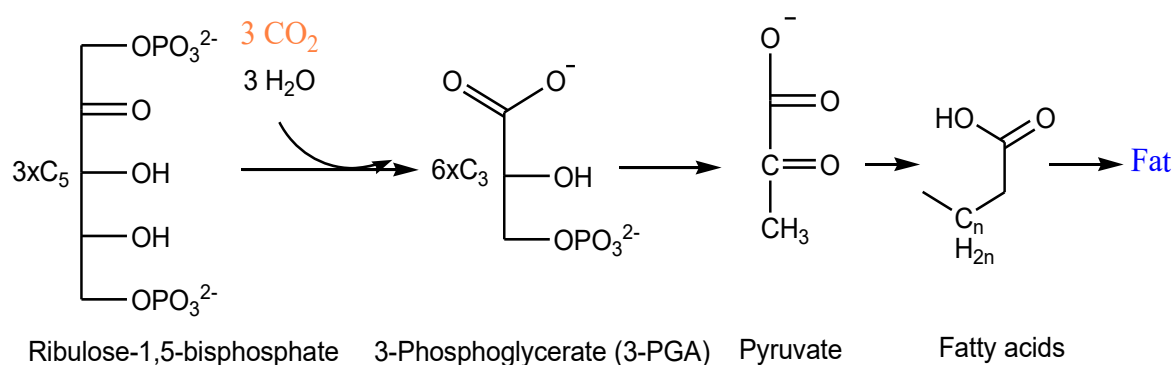


**Figure 3.** Photosynthesis in chloroplast of leaf, solar energy is converted to ATP and NADPH, which is necessary in Calvin cycle. Whereas CO<sub>2</sub> and H<sub>2</sub>O are converted to sugar (80–85%), fatty acids 10%), bio-oil and terpenoids 5%) storing light energy as chemical energy.<sup>[7,8]</sup>

Figure 3 shows two main steps of the photosynthesis in the chloroplasts:

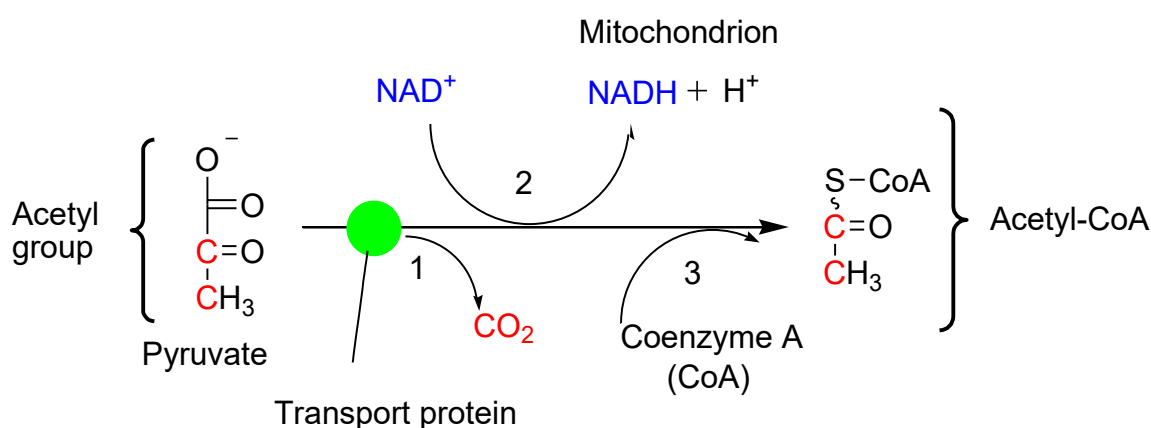
1. The light reactions: Powered by energy from light, the chloroplast oxidizes water, reduces the electron carrier NADP<sup>+</sup> to NADPH, and combines adenosine diphosphate (ADP) and one inorganic phosphate group (P<sub>i</sub>) to form ATP. Having lost electrons and protons, water is converted to oxygen, which is released from the chloroplast into the atmosphere.
2. The Calvin cycle: The chloroplast uses energy from ATP and reducing and the reductant NADPH to reduce carbon dioxide to the three-carbon sugar G3P (glyceraldehyde phosphate), the key reaction product of the photosynthesis process. While carbon dioxide is reduced, NADPH is oxidized to HADP<sup>+</sup>. ATP functions as energy carrier. Its energy is released by the transformation ADP and P<sub>i</sub>.

The formation of fatty acids in the Calvin cycle is shown in Scheme 1.



**Scheme 1:** Photosynthetic product is from the light and carbon reactions of photosynthesis. In the vast majority of photosynthetic systems, carbon partitioning is primarily directed toward fatty acid (~10%).<sup>[9]</sup>

A branch from Calvin cycle of the photosynthesis is shown: isoprene, oil, and sugars are formed naturally in trees by using  $\text{CO}_2$  and  $\text{H}_2\text{O}$  as starting materials. Whereas, in the dark reaction three ribulose-1,5-bisphosphate ( $\text{C}_5$ ) molecules are combined with three  $\text{CO}_2$  and three  $\text{H}_2\text{O}$  molecules to form six 3-Phosphoglycerate ( $\text{C}_3$  or 3-PGA) molecules. The required energy is provided by the chemical energy of the ATP generated by photosynthesis. One 3-PGA molecule will be involved in formation of the pyruvates ( $\text{C}_3$ ). Then acetyl-CoA enzyme assists the conversion of pyruvates to fatty acids and finally to e.g. vegetable oil and fat. The other 3-PGA molecules will be converted to G3P (glyceraldehyde phosphate) for cycling of RuBP ( $\text{C}_5$  ribulose-1,5-bisphosphate) in the Calvin cycle and for the glucose ( $\text{C}_6$ ) synthesis.<sup>[9]</sup>



**Scheme 2:** Conversion of pyruvate to acetyl-CoA, which is continuous as a component in the mechanism of fatty acids and vegetable oils in leaves with coenzyme A support.<sup>[10]</sup>

The sugar and vegetable oils can be used for the (chemical) synthesis of alcohols, ether, and fatty acid ester used as biodiesel. Fatty acid esters of polyol like glycerol are used already in various applications such as food processing.<sup>[11]</sup> The requirement to convert glycerol to other valuable products as a transportation fuel is still a necessary demand in order to cycle significant amounts of carbon dioxide to reduce the further increase of the  $\text{CO}_2$  concentration in air and to stop climate change. These “green” fuels are all sustainable synthetic fuels e.g. SAF – sustainable airplane fuel.

## 2.1.5 Biodiesel

Biodiesel, as sustainable synthetic fuel, has recently been considered as the best alternative candidate for diesel fuel substitution by renewable ones. In 2009 about 9 million tons of biodiesel were produced in Europe.<sup>[12]</sup> The diesel derivative B20 with 20% biodiesel blended into normal diesel could be used without any engineering modification.<sup>[13–15]</sup> The biodiesel is

an important transportation fuel received from vegetable oil by transesterification with methanol or other alcohols (Scheme 3 below).

However, the biodiesel production yields also *ca.* 10 wt% of glycerol as a by-product. The use of glycerol from natural sources for the synthesis of high-value transportation fuel is an interesting option.<sup>[12–25]</sup> The use as a fuel additive will reduce the emission of CO<sub>2</sub> from fossil fuel and the released CO<sub>2</sub> will be cycled in photosynthesis processes where solar energy is stored in the sugar, oils, and others (Fig. 3-4).<sup>[2,16]</sup> Green chemistry and catalysis can be used for the synthesis of renewable fuels via the etherification of glycerol to glycerol *t*-butyl ether as high-value fuel additive (Scheme 5). Especially the di- and tri-ether are target products for use as *Sustainable Synthetic Fuel*. “The glycerol ether synthesis is a bench test for green chemistry”. Specially, catalysis an ontribute to master this challenge. The transesterification and etherification<sup>[17–26]</sup> are catalyzed by mineral acids, basis as homogeneous catalysts. It is a target to replace so far the environmental non-friendly corrosive mineral acids like H<sub>2</sub>SO<sub>4</sub> by heterogeneous catalysts as zeolites. Because this process uses renewable feedstock, it is more environmentally friendly and can reduce the CO<sub>2</sub> emission markedly, while the CO<sub>2</sub> will be cycled (Fig. 4).

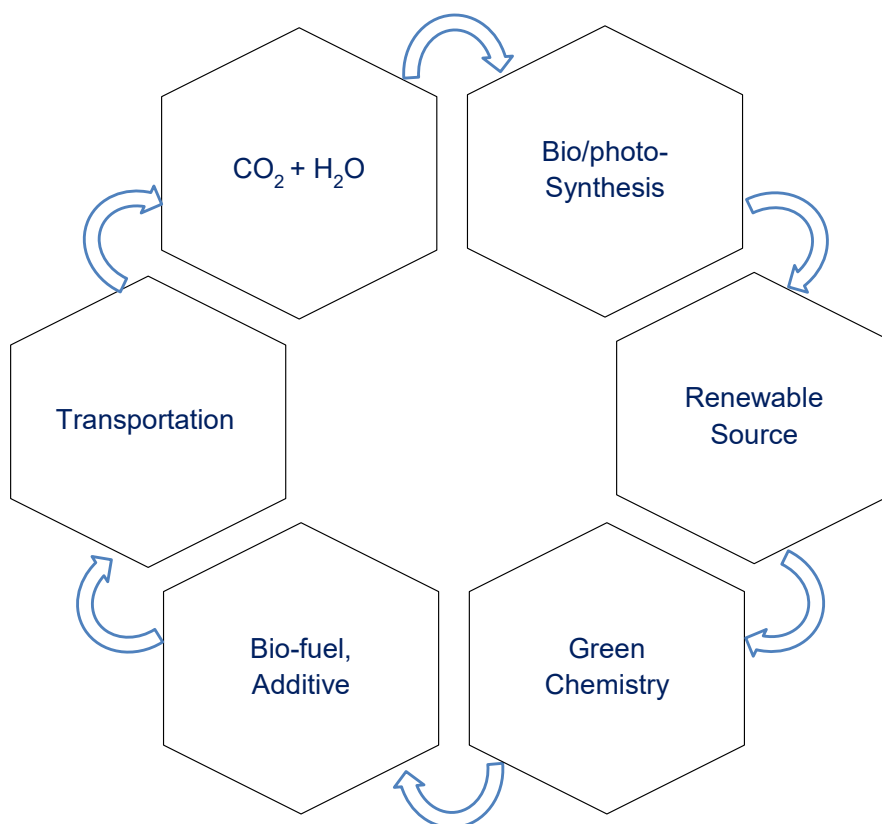


**Figure 4.** The cycle of CO<sub>2</sub> from transportations.

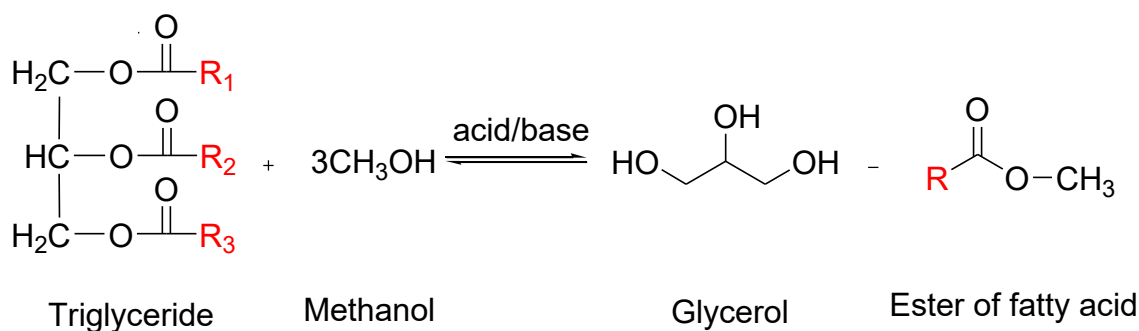
Fuel additives from glycerol could represent a promising way of enhancing the combustion efficiency in internal combustion engines with a significant reduction of pollutant emissions. Among several oxygenated additives proposed to blend with diesel such as MTBE, ETBE, TAME, the ethers of glycerol are attracted because it has a higher Octane number and Cetane number.<sup>[27]</sup>

- *The present project aims to synthesize fuel additives from the etherification of glycerol with the short-chain alcohol t-butanol over a heterogeneous zeolite catalyst. In addition, natural zeolite like clinoptilolite instead of a synthetic one has been focusing regularly.*

## 2.2 Background

### 2.2.1 Biodiesel production and by-product glycerol

In Scheme 3, biodiesel is the ester of fatty acid of trans-esterification reaction wherein triglyceride reactants are renewable source: vegetable oil, animal fat, or abundant chemicals as waste cooking oil. Besides, glycerol is the main by-product in biodiesel industrial, about 10 wt% of product in each batch.



**Scheme 3:** Trans-esterification reaction between vegetable oil and animal fat (triglyceride) with short chain alcohol in bio-diesel production.

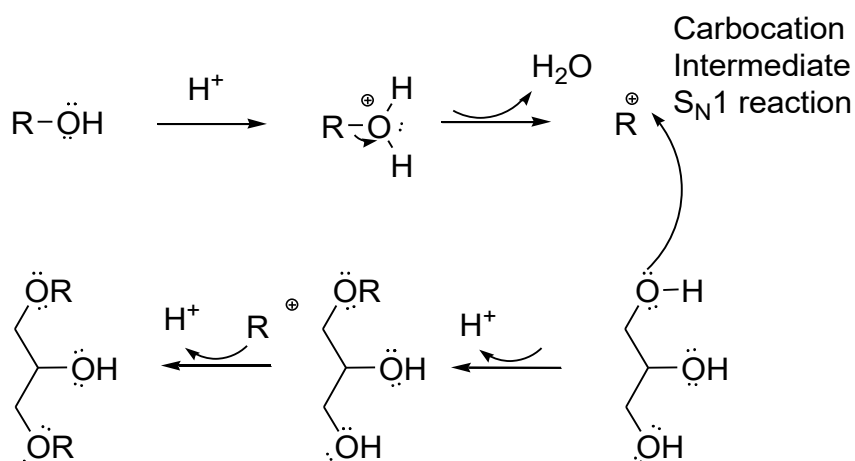
The improvement of the biodiesel process by the etherification of Gly by-product with TBA is of importance. The high demand of transportation fuel and the necessary action against the climate change by reduction of the carbon dioxide release into the atmosphere require the development of sustainable fuels and fuel production technologies. This way the biodiesel

process would be completed by the use of the glycerol by-product for the synthesis of sustainable fuel additives (SSF).

## 2.2.2 Etherification of glycerol

In Scheme 4, etherification reaction, which was used to convert glycerol, is an important basic reaction between two hydroxyl groups to form one ether compound and release one water molecular. Acid is a general catalyst for the etherification reaction. Normally, a homogeneous catalyst can be used like  $\text{H}_2\text{SO}_4$ .

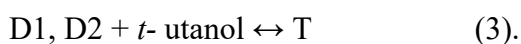
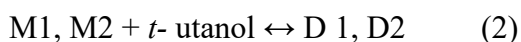
Besides, the main etherification while the ether is formed, dehydration reaction also occurs to form alkene.

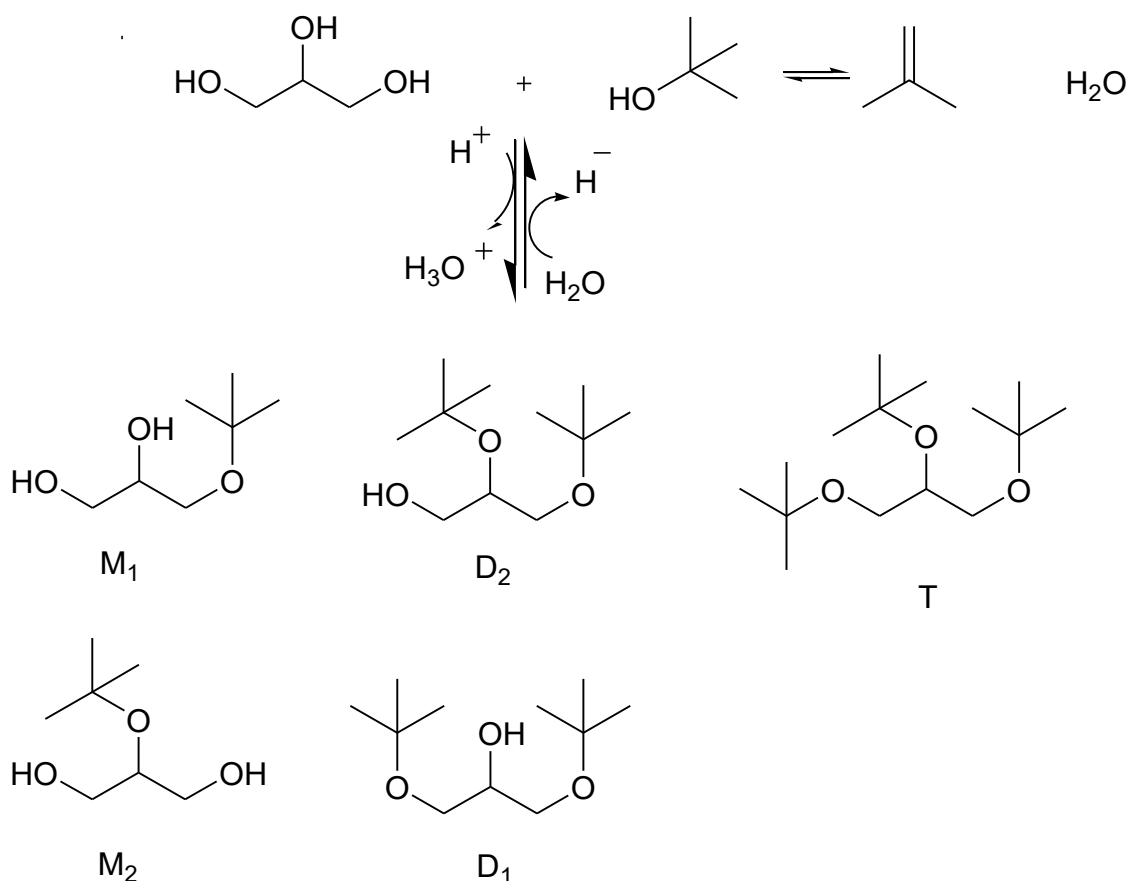


**Scheme 4:** Catalytic etherification between short chain alcohol and glycerol.

This etherification of glycerol with light alcohol special with *t*-butanol proceeds according to the nucleophilic  $\text{S}_{\text{N}}1$  substitution mechanism because of steric hindrance and the formation of stabilized carbon tertiary alkyl cations from tertiary alkyl alcohols. However, they could be reversibly converted to an alkene in the presence of protons. Firstly, alcohol is protonated by a hydronium ion, followed by cleavage of a water molecule leaving the carbocation, which nucleophilic attacks the glycerol, and forms the ether (Scheme 4 and 5).

Three reversible steps in the range can consider this process:





**Scheme 5:** Etherification between glycerol (Gly) and *t*-butanol to form mono-ether (M1): *tert*-butoxypropane-2,3-diol, (M2): *tert*-butoxypropane-1,3-diol, di-ether (D1): 1,3-di-*tert*-butoxypropanol, (D2): 1,2-di-*tert*-butoxypropanol and tri-ether (T): tri-*tert*-butoxypropanol as oxygenate fuel additive as sustainable renewable energy.

In this etherification reaction, the conversion and the selectivity of (high) ethers *t*-butyl of glycerol D1, D2, and T are still low as many report shown recently, because of steric hindrance and competition between 3 hydroxyl groups of the glycerol with tertiary alkyl hydroxyl.<sup>[28]</sup> The selectivity to mono-ether is the highest in the etherification and the selectivity of di-ether was very low,<sup>[28,29]</sup> whereas the di-ether and tri-ether are the desired products as mentioned before. Therefore, the evaluation of catalytic activity and the optimization condition of the reaction was studied in detail. To my best knowledge, the etherification of glycerol with TBA over natural zeolite was not reported so far in the literature.

In this context, an industrially relevant route for the conversion of glycerol into oxygenate chemicals involves the etherification with *t*-butanol.<sup>[18,21,29,30]</sup> It is well known that the oxygenated additives can be directly blended into biodiesel. However, mono *t*-butyl ethers of



glycerol have a low solubility in diesel fuel. Therefore, to avoid an additional separation step, the etherification of glycerol should be selectively convert to di- and tri-ethers.<sup>[17,18,21–23,30]</sup>

However, the selectivity to di and tri-ether is still lower than expected. The enhancement of di- and tri-ether is the most challenging for scientists. Besides, the corrosion caused by acidic reaction conditions and the pollution by a high amount of wastewater from the washing process, product loss by separation by distillation, and product upgrading for use as a fuel are **drawbacks** of the homogeneous mineral acid-catalyzed etherification of glycerol. Substitution of homogeneous acid and base catalysis (NaOH, H<sub>2</sub>SO<sub>4</sub>) by heterogeneous catalysts is the solution.

### **Benefits of heterogeneous catalysts**

The heterogeneous catalysts its use application show the following benefits: Heterogeneous catalysts in generally are solid catalysts reactions where the reactants or products are in different phases e.g. gas/solid or liquid-solid/systems (Fig. 5). The heterogeneously catalyzed reaction involves a couple of steps as:

- Mass transfer of the reactants and products,
- Adsorption of a reactant at the catalyst surface,
- Diffusion to the active site e.g. in the pores of the zeolite,
- Catalytic chemical reaction at the active sites,
- Diffusion/ desorption of reaction products from the catalyst.

Therefore, mass transfer, adsorption, and accessibility of sites are importing (limiting) factors with heterogeneous catalysis.

Benefits of the use of heterogeneous catalysts are:

- Non-hazardous, avoid equipment corrosion
- Material saving by the high surface area catalyst support
- Reusable, stable in the reaction
- Use as fixed beds especially in the gas phase
- Easy separation from gas or liquid of reaction.

Heterogeneous catalysts can be easier separated from the reaction mixture and reused in the catalytic process (catalyst cycling).

Heterogeneous catalysts are stable and recyclable after the catalytic reactions on the surface of the catalyst (Fig. 5).

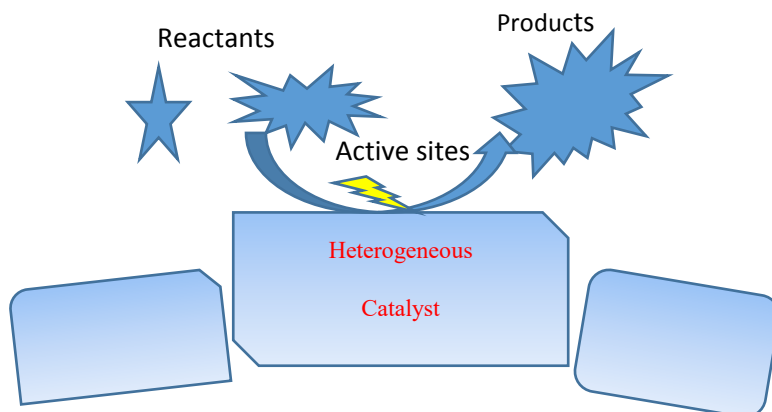
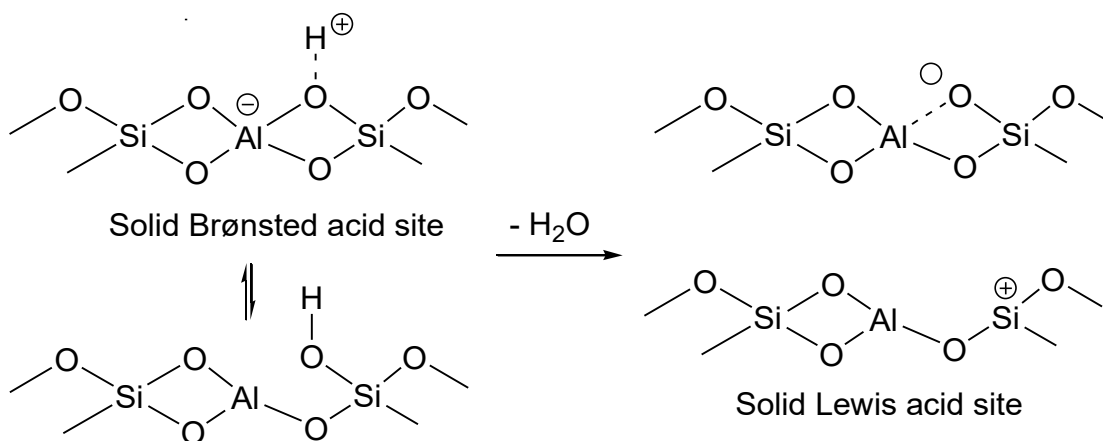


**Figure 5.** The surface of heterogeneous catalyst with a reaction on its active sites.

### 2.2.3 Zeolite catalysts

Zeolites are porous crystalline aluminosilicates. They show ion-exchange properties like resins.<sup>[31]</sup> The cations can be exchanged by protons yielding Brønsted acid sites BS (Scheme 6). Calcination at very high temperature leads to the dehydroxylation of catalytic active Brønsted acid bridging OH-groups.



**Scheme 6:** Brønsted and Lewis acid sites exist on the zeolite catalyst, and the related dehydroxylation.<sup>[32][33]</sup>

Zeolite frameworks can be modified in several ways: Desilication<sup>[34,35]</sup>, dealumination, or dehydroxylation. E.g., the dehydroxylation of dealuminated mordenite starts at 447 °C (Scheme 6). These processes occur under acid and base treatment or calcination at high temperature. Some synthesized zeolite was prepared at high temperature where the

dehydroxylation occurred. Such as H-ZSM5, H-BEA (the Brønsted acid sites (Si-O(H)-Al) in their framework are easy to dehydrogenate and turn into Lewis acid sites when heated above 500 °C.<sup>[36]</sup> A side effect of dehydration would reduce their crystalline and activities in the acid-catalyzed reaction such as cracking especially with the reaction used by Brønsted acid sites.

In zeolite catalysts, Brønsted acid sites located near the surface of catalysts, and a huge number of acid sites are located in the channels and windows of the zeolite pore system. The acidity depends on the Si/Al ratio framework, the BS accessibility on the porosity and its ion location in the zeolite structure.

### **Benefits of zeolite catalysts:**

- Non-hazardous crystalline material
- High specific surface area, acid site concentration, and adsorption ability
- Definite pore structure
- Shape and size selectivity
- Thermal and chemical stability
- Acidity can be defined

### **Zeolite structure and properties**

The term zeolite, which is a combination of the Greek words “to oil”, an “stone” as Greek language was constructed in 1756 by Axel Fredrik Cronstedt a Swedish mineralogist. This name could be stated for the material because water vapor is released from the pores during heating. Zeolites can be found in nature especially near volcanoes in the sea because they could be formed by the reaction of hot lava, water, and salts over thousands of years. More than 40 naturally occurring zeolite framework structures were discovered beside of over 240 synthetic zeolite structures. There are nine common natural zeolites available: analcime, chabazite, clinoptilolite, erionite, ferrierite, heulandite, laumontite, mordenite, and phillipsite.

They are microporous aluminosilicate framework minerals. They are used as ion exchanger and as commercial adsorbents. Zeolite is an ordered porous aluminosilicate crystalline. It is composed of  $\text{SiO}_4^{4-}$  and  $\text{AlO}_4^{5-}$  as tetrahedral  $\text{TO}_4$  linked at the corners by sharing all oxygen atoms to TOT. The negative charge around  $\text{AlO}_4^{5-}$  is compensated by the alkali cations  $\text{Na}^+$ ,  $\text{K}^+$  and/or earth-alkaline cations as  $\text{Mg}^{2+}$ ,  $\text{Ca}^{2+}$ , and free water molecules located in the confined environment in the microspore of the framework. These cations are loosely bound to

the framework and are easily exchangeable by other cations.<sup>[37]</sup> The tetrahedral  $\text{TO}_4$  is called primary building units. When these primary building units connect in different ways secondary building units, (SBUs) are formed (Fig. 6). Especially oxygen-8-, 10-, and 12-membered rings belong to the channels of the zeolite pore systems.

Main parameters of common used zeolites:

Synthesized zeolite **ZSM-5** (MFI type) has Si/Al ratio  $> 5$ , the framework contains two oxygen-10-membered ring channels: one is nearly circle-shaped (0.53 x 0.56 nm) and one of elliptical shape (0.51 x 0.55 nm). It has a quasi 3-dimensional pore system with y-shaped channel crosses.

Synthesized zeolite **Beta** (BEA type) has Si/Al ratio from 5-100. It exhibits a three-dimensional pore system formed by different 12-membered ring channels with different shapes and sizes : (0.67 x 0.66 nm) - (0.67 x 0.66 nm) - (0.55 x 0.56 nm).<sup>[38]</sup>

Synthesized zeolite **mordenite** (MOR type) has Si/Al ratio from 4 to 5.7 consists of oxygen-12-membered rings (O12R) the size of the window is (0.65 x 0.7 nm) and O8R pores (0.26 x 0.57 nm). The pore system is 2-dimensional.<sup>[38]</sup>

Synthesized zeolite **Y** (FAU type) has Si/Al ratio from 2.1 to 2.8, Y zeolite has a Si/Al ratio of ca. 2.2. It consists of 12- oxygen membered ring channels of 0.74 nm size and small-sized O6R forming a 3-dimensional pore system.<sup>[38]</sup>

In addition, a natural zeolite **clinoptilolite** (HEU type) has Si/Al ratio = 4-6. Clinoptilolite has 10-8-8 oxygen membered ring (O10R-O8R-O8R) channels, which have window sizes of (0.3 x 0.76 nm) - (0.26 x 0.47 nm) - (0.33 x 0.46 nm). The pore system is 2-dimensional.<sup>[39]</sup>

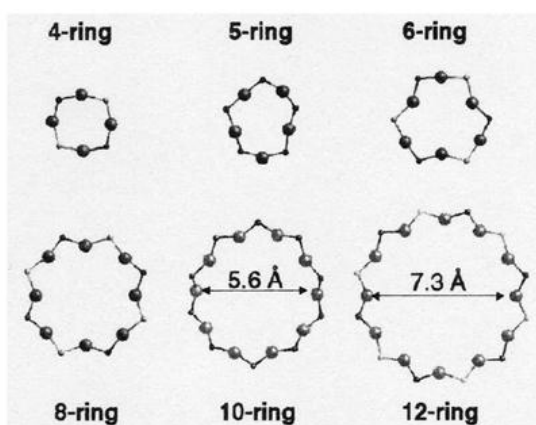


**Figure 6.** Oxygen rings occurring in zeolites formed TOT bridges (T=Si,Al) forming secondary building units of zeolites (SBUs).<sup>[40]</sup>

The free diameter of each ring approximates the distance of the adjacent oxygen atoms minus two times the radius of the oxygen atom (diameter: 1.2 Å) and depends on the hydration state of the zeolite as reported by Rabo et al. 8 ring in chabazite: hydrated (6.4 - 6.9 Å) dehydrated (5.8 - 7.3 Å).

### Natural zeolite Clinoptilolite

The natural zeolite clinoptilolite (HEU framework) (Fig. 7) is of special interest as a potential green catalyst, because of its abundance, medium pore size, and medium Si/Al ratio. Clinoptilolite and other zeolites have many potential applications: In petroleum as the catalyst for cracking and refining,<sup>[41-43]</sup> in food industry,<sup>[44]</sup> pharmacy, fertilize industry as absorbent and supplement, and in purification as absorbent.

**Table 3:** Free diameter of difference Oxygen ring types in clinoptilolite framework.

Oxygen ring type	Size (Å)	Oxygen ring type	Size (Å)
4-Oxygen ring	1.6-1.8	8-Oxygen ring	4.0- 5.5
5-Oxygen ring	1.8-2.7	10-Oxygen ring	4.1-7.4
6-Oxygen ring	2-3.4	12-Oxygen ring	7.4-9.4

The clinoptilolite contains an elliptical 10-membered (oxygen) ring of  $4.1 \times 7.5$  Å size, two types of 8-membered ring of  $4.1 \times 4.7$  Å, and  $4.0 \times 5.5$  Å size and oxygen-4, 5- membered rings (Table 3). For example, the term "10-ring" of the channel aperture in a zeolite (clinoptilolite) refers to a closed-loop that is built from eight tetrahedral coordinated silicon (or aluminum) atoms bridged with 10 oxygen atoms (Fig 7-b).<sup>[45]</sup> The channels A, B, and C are interconnected to a 2-dimensional pore system (Fig. 7).

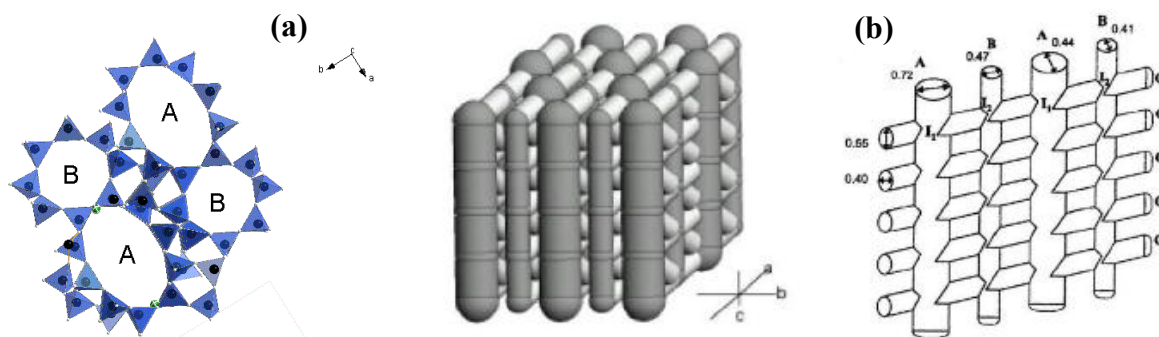


**Figure 7.** Clinoptilolite structure: (a) from HEU framework edited by using Diamond software, at c axis viewer TO<sub>4</sub> structure 10 and 8 oxygen ring openings, (b) Columnar model of 2-dimensional channel arrangement of HEU framework. The clinoptilolite structure according to Yamanaka et al.<sup>[46]</sup>

Clinoptilolite unit cell draw by Diamond software in Figure 8 has parameters:  $a = 17.66 \text{ \AA}$ ,  $b = 17.963 \text{ \AA}$ ,  $c = 7.400 \text{ \AA}$  and  $\beta = 116^\circ 47'$ . Along the a-axis and c-axis of the unit cell, the morphology of clinoptilolite crystals looks like plates. Especially, there are two channels running parallel to each other along the c axis. Channel A consists of 10-membered (tetrahedron) rings and channel B consists of the 8-membered rings. They are interconnected by the perpendicular channel C running along a-axis consisting of an 8-member ring with the size of 4.0–5.5  $\text{\AA}$  (Fig. 7).

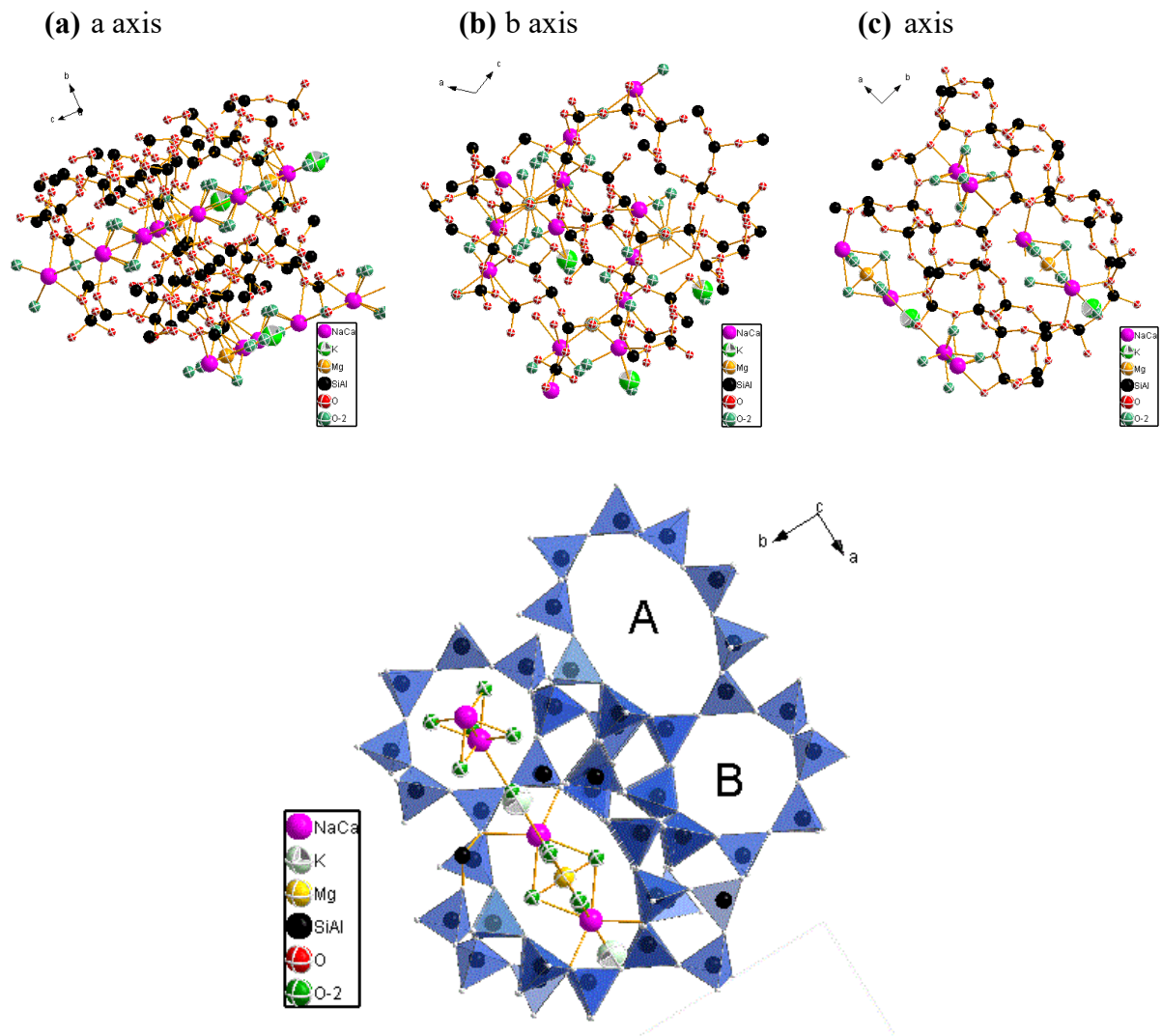


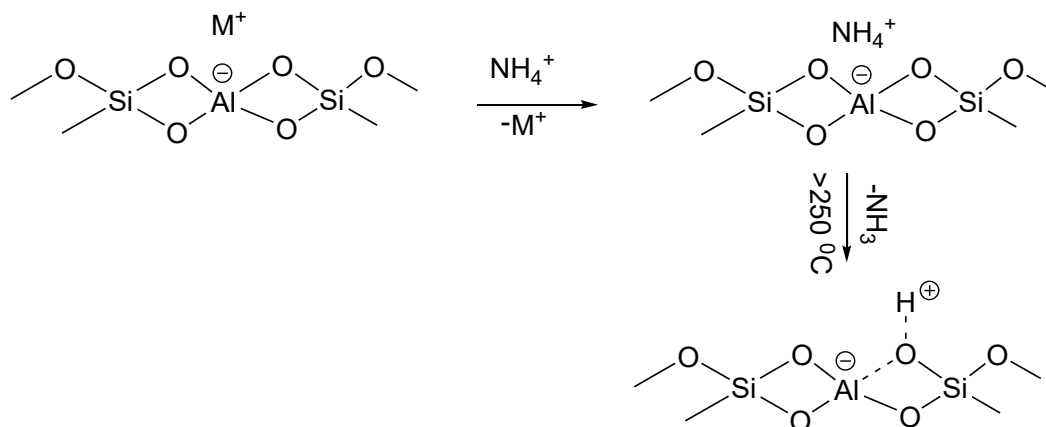
**Figure 8.** Clinoptilolite structure in a unit cell at a, b c axis direction to see the location of cation and free water in 8 and 10 oxygen ring windows (Framework type HEU) edited by using Diamond software.

The negative charge around the aluminum site in clinoptilolite is neutralized by crucial cations  $\text{K}^+$ ,  $\text{Ca}^{2+}$ ,  $\text{Na}^+$ , and  $\text{Mg}^{2+}$  depend on the initial environment of formation. Inside the pores, free water molecules are located. The stability increases and ion-exchange capacity decrease when the Si/Al ratio increases. Clinoptilolite natural zeolite has medium pore size

channels like ZSM-5 with Si/Al=5-6. The natural zeolite materials could be called live materials with a lot of advantage properties which are quickly become the most attractive topic for scientists.<sup>[46]</sup> Like the synthetic ones, natural zeolites show ion exchange properties, adsorption capability, size selectivity, acidity and following catalytic activity. Post-synthetic modifications improve the Brønsted acidity, and increase the glycerol conversion.<sup>[31,47]</sup>

Acidic modification is achieved after few following steps: ion exchange process<sup>[48]</sup> and calcination. This is a “green” process compare to a acidity modification by treatment with mineral acids.

### Acidic modification: ammonium ion exchange and calcination



**Scheme 7:** Ion exchange process and decomposition of ammonium ions of NH<sub>4</sub>CLIN to the protonated form of clinoptilolite HCLIN as green synthesis. M<sup>+</sup> is represents cations Na<sup>+</sup>, K<sup>+</sup>, and M<sup>2+</sup> Ca<sup>2+</sup>, and Mg<sup>2+</sup> cation in the clinoptilolite.

Based on this process shown in Scheme 7, the acid sites were created in a controlled manner by ammonium ion exchange and transformation to proton form by heating/calcination (from 250 °C to 550 °C). The acid site will be related to the known structure of clinoptilolite especially Si/Al ratio and crucial cation located around aluminum. Therefore, the obtained number and strength of acid sites can be tailored using the appropriate ion exchange<sup>[49]</sup> and calcination conditions.

However, the desired acid form BS of clinoptilolite in Scheme 7 could be influenced by overheating which causes dehydroxylation (Scheme 6). Synthesized zeolite such as H-ZSM5, H-BEA requiring high calcination temperature of activation and organic template removing usually beyond 450 °C.<sup>[50]</sup> Using natural zeolite, this higher calcination step could be saved to avoid the changing of the formed BS,<sup>[51–54]</sup> which is important for the catalyst.

Compare to synthetic zeolites, acid-modified natural zeolite clinoptilolite is not expensive, can be prepared without hazardous chemicals as mineral acids, bases, or organic templates, and reduced energy demand. It is considered a sustainable green catalyst.

The aims of this project are preparation, characterization of the acidic clinoptilolite catalyst, and testing of the catalyst performance in the etherification of glycerol with tertiary butanol to the corresponding ethers.

## 2.3 State-of-Art

Generally,  $H_2SO_4$ ,  $HCl$ ,  $H_3PO_4$ , and  $NaOH$  are known as highly homogeneous catalysts for condensation reaction as the etherification. They are/were preferentially used because of many advantages: they are cheap and available in many countries and are high activity. However, they suffer from severe disadvantages: they are hazardous, more difficult to handle, cause corrosion and environmental harmful and produce waste which disposal is expensive and difficult to handle. These catalysts cannot be cycled.

Therefore, heterogeneous zeolite catalysts were tested for the replacement of homogeneous catalyst in acid catalyzed condensation reactions as the etherification of glycerol. The investigations are summarized below.

### 2.3.1 Glycerol conversion

A useful heterogeneous catalyst has been applied such as synthesized zeolite<sup>[55,56]</sup> from coal ash,<sup>[57]</sup> Kaolin waste,<sup>[58]</sup> fly ash.<sup>[55,58]</sup> Their acidity and basicity characterization of protonic and cationic zeolites H-Y, HZSM-5, H-BEA, H $\beta$ ... are essential issues.<sup>[59-62]</sup> Addition, modified metal oxide,<sup>[63]</sup> natural zeolite,<sup>[64]</sup> ion exchange resin Amberlyst-15<sup>[26,65-67]</sup> etc. are used efficiently instead of homogenous catalyst like  $H_2SO_4$ ,  $HCl$ , ... because they are safer for equipment maintenance and can be easily separated to recycle many times without the activity reduction, ideally.<sup>[68]</sup>

Because of exposure developing of biodiesel, produce recent years, the conversion of glycerol to other valuable chemical are attracting such as oxidation or dehydration by using oxide catalysts.<sup>[69]</sup> Almost of reactions occur at high temperature 110-400 °C especially oxidation and dehydration of glycerol over oxide catalysts: Fe-MFI, Sn-MFI, Ag/ $Al_2O_3$ ,  $FePO_4$ .



Glycerol can also be reacted with other chemicals as acetone, aldehydes, alcohol, isobutene by using many acid catalysts.<sup>[27]</sup>

Among the fuel additive investigated from many reports, the etherification reaction of glycerol with alcohols to produce ether as fuel additive attracted research interest because the huge amount of glycerol could be converted with available alcohol to form a more valuable fuel additive; even glycerol by-product contains some impurities from biodiesel.

Etherification of glycerol and *tert*-butanol from literature shown in Table 4.

**Table 4:** Textural and acidity properties of organic resin amberlyst A-15 and USY, H-Beta, HZSM-5 and zeolites and catalytic activity, conversion (C) and selectivity (S) in etherification of glycerol (Gly) with tertiary butanol (TBA) to the corresponding mono, di and tri-ethers (M,D,T).

Catalyst	Properties of catalysts					Reaction condition (TBA/Gly Molar ratio, Reaction temperature, Time, Catalyst loading)	X <sub>Gly</sub> %	S <sub>M</sub> %	S <sub>D,T</sub> %	Ref
	Si/Al	Specific area (m <sup>2</sup> g <sup>-1</sup> )	External area (m <sup>2</sup> g <sup>-1</sup> )	Micropore volume (cm <sup>3</sup> g <sup>-1</sup> )	Acid site density (μmol NH <sub>3</sub> g <sup>-1</sup> )					
A-15					4700	4:1, 363 K, 3 h, 5 wt%	96	75	25	[17]
A-15					2370	4:1, 363 K, 10 h, 7.5 wt%	64	75	25	[47]
A-35						4:1, 353 K, 4 h, 8.5 wt%	80			[70]
H-Y	15	710	169	0,286	560	4:1, 363 K, 3 h, 5 wt%	78			[17]
USY-550	28	649	25	0.293	547	4:1, 365 K, 4h, 7.6 wt%	7			[62]
USY-550-L	3.4	628	66	0.263	739		11			[62]
USY-650	2.8	641	18	0.292	768		2			[62]
USY-650-L	3.9	614	57	0.260	983		30			
USY-650-L-2	11.2	741	64	0.321	794		75			
H-BEA	12.5	700	309	0,195	1030	4:1, 363 K, 3 h, 5 wt%	90	45	45	[17]
H-BEA	12.3	623	169	0.210	1155	4:1, 365 K, 4h, 7.6 wt%	77			[62]
BEA <sub>(MC)</sub>	15			0.22	752	4:1, 363 K, 10 h, 7.5 wt%	12	93	7	[47]
SC	9			0.25	470		61	74	26	
SC	10			0.25	798		57	81	19	
NC	12			0.22	487		54	70	30	
NC	15			0.24	354		57	71	29	
NSP	17			0.24	130		8	92	8	
FAU	2.6			0.34	403	4:1, 363 K, 10 h, 7.5 wt%	5	100	0	[47]
M	17			0.32	197		33	82	18	
M	40			0.29	100		23	82	18	
HZSM-5	12.3	337	4	0.156	1327	4:1, 365 K, 4h, 7.6 wt%	15			[62]
MOR <sub>(S)</sub>	10			0.2	1056	4:1, 363 K, 10 h, 7.5 wt%	9	97	3	[47]
MFI <sub>(MC)</sub>	40			0.17	304	4:1, 363 K, 10 h, 7.5 wt%	8	99	1	[47]
(NC)	45			0.18	332		20			
(NSH)	45			0.18	83		12			
(NSP)	20			0.18	151		6			
SiO <sub>2</sub>					0	4:1, 363 K, 10 h, 7.5 wt%	0		0	[47]
Al <sub>2</sub> O <sub>3</sub>					0		0		0	
SiO <sub>2</sub> -Al <sub>2</sub> O <sub>3</sub>	20			0.03	103		2		0	

where: USY-T-L (USY mean steaming treatment of NH<sub>4</sub>Y, T the temperature, L means submitted to acid leaching H<sub>2</sub>SO<sub>4</sub> 10 wt%, 2 mean the second cycle of treatment. C: commercial, S: synthesized, M: modified, N: nano

Table 4 shows that some heterogeneous catalysts were tested in the etherification of glycerol with TBA to the corresponding ether such as A-15, H-BEA, H-Y. The activity differs depending on the catalyst preparation and zeolite type: H-BEA, Y, HZSM-5, MFI, or MOR.

### 2.3.2 Etherification of glycerol with *tert*-butanol

K. Klepálová worked out etherification of glycerol with the highest conversion of 96% at the temperature 90 °C, molar ratio TBA/Gly= 4:1 after 180 min using A-15. H-BEA showed the highest selectivity and high conversion even has lower acidity than A-15 by TPDA results. It means that the acid sites, the external surface, and the hydrophobic of catalyst affected in this case.

In this research, the conversion with *iso*-butene (the possible considerable ratio) needs a higher temperature and the first increase of conversion was observed at 120 °C to 80% and next after the first 30 min decrease, which means that dealkylation of ethers with the formation of glycerol, mono-ether, and *iso*-butylene proceed as back reactions.<sup>[17]</sup>

M. Pilar Pico et al. reported kinetic model Amberlyst A-35 as a catalyst for etherification of glycerol and TBA. The conversion reaches 80% after 4h, with (7.5 wt% of catalyst) 50-80 °C, conversion of TBA and effect of Gly/TBA, RT, also discovered.<sup>[70]</sup>

#### **The conversion and selectivity increase by increasing of solubility and reactant diffusion**

Carmen M. Dominguez, Madrid improved etherification of Gly with TBA alcohol by the addition of di-butyl ether as a solvent.<sup>[71]</sup> The conversion of glycerol was the same 82 % by using 20 % A-15 as a catalyst at 70 °C, however the selectivity of di-ether increase from 26 to 44 % at 6h. Di-butyl ether is a good solvent to dissolve well the ether products and increase the selectivity of D, T ethers.

In other reports, the pressure was used to increase conversion of Gly and selectivity of di-ether when the hydrophobic reactant like isobutene was used or formed as a by-product.<sup>[66]</sup> Paula M. et al. investigated of increasing of hydrophobic of catalyst based on zeolites (USY, H-Beta, and H-ZSM5)<sup>[62]</sup> to avoid the self-reaction of Gly which was also mentioned by Sharmin Sultana Poly et al.<sup>[72]</sup>

### **The conversion and selectivity could be increased when demised back reaction**

N. Ozbay indicated the effects of sorption enhancement and isobutene formation on etherification of glycerol with *t*-butyl alcohol in a flow reactor by removing the water then significantly increase the yield of di-ether. However, while the glycerol conversion increase; *t*-butyl alcohol dehydration of TBA was enhanced due to the separation of reactants.

Recently, L. Aguado-Deblas used the microwave to assist the glycerol etherification over sulfonic acid catalysts and achieve higher conversion 93% of glycerol in 30 minutes and 25% selectivity of di-, tri-ether at T=130 °C, 5% catalyst.<sup>[73]</sup>

C. Cannilla et al. used A-15 catalyst in batch reactor coupled with water perm selective membrane; relevant glycerol conversion was reached with the membrane but at a reaction temperature higher than 140 °C. Unfortunately at such a temperature, the selective removal of water through the membrane also favors the dehydration and self- etherification of glycerol or alkyl alcohols by causing the formation of products that are difficult to separate from the reaction medium and also of products which, at moment, were hard to identify.<sup>[30]</sup>

In this strategy, the using of hydrophobic catalyst likes zeolite had some improvement as shown in reports.

### **Improve reaction products by catalyst investigation**

*Porosity, acidity, hydrophobic is a crucial parameter of catalyst in glycerol conversion and selectivity of the second or third reaction of 3 OH groups.*

Sh. Sultana Poly et al. used high silica H- $\beta$ , which has a high Si/Al ratio of 75 (H $\beta$ -75), and proton-exchanged BEA zeolite as a catalyst to convert glycerol.<sup>[72]</sup> This report demonstrated again the hydrophobicity help this catalyst had higher activity than typical homogeneous catalyst like H<sub>2</sub>SO<sub>4</sub> due to avoiding of self-reaction of glycerol to the dimerization product.

Besides the hydrophobicity, the accessibility of acid sites was investigated in presence of lab-made silica-supported acid catalysts such as A-15 (HSO<sub>3</sub>-SiO<sub>2</sub>), Cs-HPW (phosphor tungstic acid), HPW-17 (phosphor tungstic acid - SiO<sub>2</sub>) by F. Frusteri et al. with the range of 30-90 °C the highest activity catalyst A-15 shown 80% conversion of glycerol after 6h, 7,5 wt% catalyst loading.<sup>[18]</sup> Currently, these surface materials characterized by interconnected mesoporous and high accessibility of acid sites represent the best systems for the etherification reactions.

In-depth, C. Miranda indicated the role of porosity of zeolite in both gas and liquid phase

such as for zeolites featuring the biggest confining voids (i.e. the FAU super cage) successive etherification is favored, yet product desorption is hampered. Another hand, (their i.e. void volume, interconnection, size) has a crucial effect on confinement and shape selectivity and hence on catalytic key parameters (activity, selectivity, and stability) by comparing the performance of A-15, MOR, FAU, BEA and MFI.<sup>[47]</sup> A-15 has the highest acid sites (with macro pore easily to access) shown the highest conversion of glycerol at a short time but conversion is hampered by deactivation of the sulfonic resin, probably due to a product inhibition effect, e.g. by H<sub>2</sub>O. Large pore zeolite FAU and \*BEA shown lower conversion than A-15 because they have lower BS concentration (1.03 compared to 4.7 mmol/g from TPDA), but they have higher selectivity of di-, tri- ether because they are more stable and more hydrophobic than A-15. H-BEA showed better performance because its crystal size is smaller due to good diffusion and balance between hydrophobic/hydrophilic.

Besides, M. Chamack et al. compared two synthesized zirconium-modified mesoporous silica Zr-S (Zr salt was added to the sol-gel of SBA-15 as 4.9 wt% of zirconium) and immobilization of 8.7% of tungsten phosphoric acid (PW) species on Zr-S support)<sup>[74]</sup>. Acetylation of glycerol and acetic acid full conversion and > 60% selectivity of di-ether and 30% tri-ether with Zr-S and only 80% of glycerol conversion obtained with Zr-S/PW. Interestingly the acidity of Zr-S (0.185 mmol NH<sub>3</sub>/g; 0.35 mmol NH<sub>3</sub>/m<sup>2</sup>) was enhanced by introducing PW into its structure (0.47 mmol NH<sub>3</sub>/g; 1.30 mmol NH<sub>3</sub>/m<sup>2</sup>). After modification by impregnation in acid solution, the area surface area decreases, and the hydrophilic increases and less stable. This result agrees with Valter L.C. G. Higher hydrophobicity of Zr-S catalyst allowed the facile release of formed water from the silica channels, probably preserving the activity of catalytic sites during the reaction.<sup>[75]</sup> They also confirmed that a larger surface area of the catalyst strongly affects the catalytic activity in glycerol reaction, which comprises three consecutive reactions, special selectivity of di- or tri-ether or ester as M.S. Khayoon reported.<sup>[76,77]</sup>

Paula M. et al. investigated the influence of zeolites (USY, H-Beta, and HZSM-5) properties in the etherification of glycerol with ethyl alcohol at 200 °C. H-Beta and USY-650-L-2 (a USY sample steam treated and acid leached of NH<sub>4</sub>-Y) zeolites showed the best results for glycerol conversions, they enhance the conversion of glycerol. The hydrophobicity index of zeolites was measured and correlated with catalytic activity H-Beta > USY-650-L-2 > HZSM-5 > USY550 > USY650. They also contributed the mechanism of glycerol and ethyl alcohol etherification, Lewis and the Brønsted acid sites can be the active sites through glycerol or

ethanol adsorption.<sup>[62]</sup> The results show that the activity depends on two crucial parameters: acid sites and external surface area.

Subhash Magar reported the effect of the reaction time, temperature, catalyst to this reaction. Reaction conditions: glycerol/TBA (1:20), 110 °C, mont-KSF/O loading (0.250 g, 27.17 wt %), and 2–24 h. The BET surface area and surface acidity of various montmorillonite clay catalysts were shown. Among all of the catalysts, mont-A1 showed the highest surface area of 250 m<sup>2</sup>g<sup>-1</sup>, and the order of surface area values was found to be mont-A1 > mont-K10 > mont-KSF/O. The order of acidity was mont-A1 (0.005 mmol g<sup>-1</sup>) < mont-K10 (0.008 mmol g<sup>-1</sup>) < mont-KSF/O (0.015 mmol g<sup>-1</sup>).<sup>[28]</sup> This order of acidity played a more predominant role in their activity than the surface toward etherification, as discussed later.

In addition, Anna Dziejzicka et al. used an acidic modification of clinoptilolite for bigger molecule reaction of  $\alpha$ -pinene conversion. The crystallinity decreased with increasing of concentration of HCl treatment to protonate HEU (Clinoptilolite) or increasing calcination temperature. For comparison, NH<sub>4</sub>-HEU was prepared with a 10 wt% ammonium nitrate solution for 4 h at 80 °C and calcined. H-HEU-0.05HCl and H-HEU-300 showed the highest activity.<sup>[78]</sup> Jiangyin Lu investigated the recovering of BS for H-ZSM5 by calcination at high temperatures (500-800 °C). The lower calcination temperature left more acid sites on catalyst H-ZSM5.<sup>[42]</sup>

Information of clinoptilolite: There are two channels running parallel to the *c*-axis: (i) 10-membered rings (10-MR), type A channels with the dimension of 3.0 Å × 7.6 Å; and (ii) the smaller, 8 MR channels (3.3 Å × 4.6 Å). The third type C channels are also 8 MR and run parallel to the *a*-axis, with dimension (2.6 Å × 4.7 Å) comparable to the B type. Crystals of clinoptilolite are monoclinic, with the space group C2/m, however, sometimes the reported symmetry is lower.<sup>[39]</sup>

## Conclusion

The number of studies dealing with the etherification of glycerol with *tert*-butanol using heterogeneous catalysts is still very limited. Mostly the organic ion exchanger Amberlyst, a sulfonated resin, and a highly acidic zeolite beta, ZSM-5, mordenite, and different dealuminated Y-type zeolites were catalytically tested. To the best of my knowledge, natural zeolites as clinoptilolite were not investigated in the etherification of glycerol with *tert*-butanol.

The review of the available literature shows that so far used mineral acids can be replaced by acidic heterogeneous catalysts like zeolites or organic resins. The activity of acidic zeolites is sufficient, however, the selectivity to the wished di-ether or tri-ether is still low. Most efficient are acidic silica-rich zeolites of type BEA (zeolite beta) and MFI (ZSM-5). Natural zeolites as clinoptilolite were not investigated in the etherification of glycerol with *tert*-butanol. The influence of the acidity, hydrophobicity, and textural properties as specific surface area and pore volumes of used catalysts on the catalytic activity and selectivity was tested (Table 4). However, the obtained data are not consistent (confusing). The catalytic activity of reported catalysts is very different even with samples of similar structure and high acidity. e.g., the catalytic activity of a row of USY catalysts, showing similar acidity and specific surface area and pore volume, differs markedly. It is, therefore concluded, that besides these properties, other factors like the catalyst preparation procedure, the catalyst activation as well as testing conditions, e.g. the order of mixing of the reaction components are also important.

Therefore, this study focuses on the assessment of the preparation and activation of the commonly available natural zeolite clinoptilolite as an acid heterogeneous catalyst (HCLIN) and the investigation of its catalytic performance in the etherification of glycerol with *tert*-butanol and the comparison of the catalytic activity with other alcohols.

Natural zeolites are usually modified by direct treatment with mineral acid HCl or HNO<sub>3</sub> for preparation of the acidic catalytic H-form. However, this procedure is not sustainable and causes hazardous environmental problems e.g. by the release of wastewater, corrosion, catalytic material loss by destruction and dissolution of the zeolite, acid consumption by salt formation. Unfortunately, all catalysts could be poisoned and limited reuse times—specifically by using glycerol – acrolein polymerization.

The environmentally preferable route of acidification via ammonium ion exchange and thermal decomposition of the ammonium ions to protonated zeolites under the release of ammonia is rarely used.

## 2.4 Motivation

This work aims to contribute to the reduction of the greenhouse gas, carbon dioxide, released into the atmosphere. The increasing carbon dioxide emission is an important factor for the global warming and high responsibility for the observed climate change.

Catalysis is a key technology for a sustainable resource management. This project aims to develop a novel green heterogeneous catalyst based on natural zeolite in order to improve the sustainability of the biodiesel process. This will be achieved by the etherification of the glycerol by-product to di-*tert*-butyl-glycerol ether fuel additives. Thereby, the use of fossil carbon dioxide emitting fuels and fossil resources will be reduced. A part is replaced by the sustainable fuel additive, where the carbon dioxide is cycled.

Common industrial processes use hazardous and environmental less benign, corrosive, mineral acids and bases as catalysts. Its replacement by less hazardous and reusable heterogeneous zeolite catalysts is still a challenge.

So far tested synthetic zeolites will be replaced by a new natural zeolite based catalyst. This saves energy and reduces the use of chemicals required for the zeolite synthesis and production.

Additionally, the environmental pollution will be diminished by replacement of the usual mineral acid treatment of the natural zeolite by an ammonium ion exchange calcination process.

Process parameter for the catalyst preparation and etherification reaction will be investigated and provide the bases for the development of synthesis and process protocols to establish sustainable synthetic fuel technologies.



# 3 Experimental

## 3.1 Materials

The starting material used for the preparation of heterogeneous acid catalysts was the natural zeolite clinoptilolite, sample clinofit<sup>®</sup> Si Premium, purchased by Vitarig Biomedsystems GmbH. Ammonium nitrate NH<sub>4</sub>NO<sub>3</sub> (Apolda, M=80,05 g/mol, > 99,9 % purity) was used for the NH<sub>4</sub><sup>+</sup> ion exchange of the. The hydrochloric HCl (~37%) and sulfuric acid H<sub>2</sub>SO<sub>4</sub> (>95%), HNO<sub>3</sub> (~65%) were provided by Fisher chemical. Dichloromethane CH<sub>2</sub>Cl<sub>2</sub> (99.8%) was analyst EMSURE<sup>®</sup>. Glycerol was provided by Sigma Aldrich (water content: <0.5%). The properties and origin of used alcohols are summarized in Table 5.

**Table 5:** Properties of alcohols.

Alcohol	Molar mass (g/mol)	Boiling point (°C)	Density (g/cm <sup>3</sup> )	Company	Purity
<i>t</i> -butanol	74.12	86	0.7812	Fisher/Acros	~99.5%
2-methylbutan-2-ol	88.15	103	0.8089	Merck KGaA	>99%
methanol	32.04	64.7	0.7914	Fisher/Acros	>99%
ethanol	46.07	78.325	0.78939	Merck OHG	>99%
<i>n</i> -propanol	60.1	97.4	0.8035	Merck OHG	>99%
<i>i</i> -propanol	-	82.4	0.78505	Merck OHG	>99%
<i>n</i> -butanol	74.12	117.26	0.8099	Apolda	~99%
<i>i</i> -butanol	-	108	0.802	Fisher/Acros	>99%
<i>sec</i> -butanol	-	99.5	0.8065	Fluka	>99%
<i>n</i> -pentanol	88.15	137.8	0.8148	Honeywell	>99%
2-pentanol	88.15	119.2	0.812	Merck	>98%
cyclohexanol	100.16	161.1	0.9624	Merck	>99%
1,3-butandiol	90.12	207	1.004	Sigma Aldrich	>99%

## 3.2 Catalyst preparation

The HCLIN200, HCLIN300, HCLIN400, HCLIN500, and HCIN600 zeolite catalysts (CLIN-clinoptilolite) were prepared by following two steps: First, the starting clinoptilolite was ion-exchanged with different concentrated  $\text{NH}_4\text{NO}_3$  solutions. The removed sample was washed with deionized water. In the second step, the dried ammonium exchanged sample was calcined.

### **Preparation of the ammonium form $\text{NH}_4\text{CLIN}$**

In detail, during ion exchange, the Vitaring Clinoptilolite was continuously stirred in an aqueous 0.2M  $\text{NH}_4\text{NO}_3$  solution two times at 80 °C for 2 hours each. Firstly, 250 mL of deionized water was heated up at 80 °C. Then 10 g of clinoptilolite powder was added, followed by the addition of 4g  $\text{NH}_4\text{NO}_3$ . Thereafter, the solution was continuously stirred at 80 °C for 2 hours in a glass beaker. The baker was covered with a glass (watch glass) to avoid the evaporation of water in order to maintain the concentration of the ion exchange solution constant. Then solid powder was allowed to settle down. The upper liquid was removed and refilled with another new 0.2M  $\text{NH}_4\text{NO}_3$  solution for the second ion exchange. Finally, the obtained samples were washed with deionized water several times, and then were dried overnight at elevated temperature. The obtained ammonium exchanged clinoptilolite was named  $\text{NH}_4\text{CLIN}$  because the original framework cations  $\text{Ca}^{2+}$ ,  $\text{Na}^+$ ,  $\text{K}^+$ , located in the pores, i.e. windows and cages, were gradually replaced by the  $\text{NH}_4^+$  ions.

### **Preparation of the acid H-form HCLIN**

To obtain the acid forms,  $\text{NH}_4\text{CLIN}$  samples were calcined in air at different temperatures for short times (1 minute and 30 minutes). In this process, the  $\text{NH}_4\text{CLIN}$  was heated up from room temperature to the desired temperature of 200 °C, 300 °C, 400 °C, 500 °C, and 600 °C, respectively, in an oven with the heat rate of 10 °C/min. The obtained acidic natural clinoptilolite zeolite catalysts were named HCLIN200, HCLIN300, HCLIN400, HCLIN500, and HCIN600, respectively, in accordance with the calcination temperature. They were stored in a desiccator until use for the reaction.

### **Preparation of acidic HCl-treated clinoptilolite HCLIN-HCl**

Besides via thermal treatment of the ammonium exchanged form, the acid clinoptilolite can be directly prepared by ion exchange with  $H^+$  ions (protons) with an aqueous solution of HCl acid:

The starting clinoptilolite was stirred in an aqueous 0.1 M to 0.5 M HCl solution for ion exchange of clinoptilolite cations by  $H^+$  ions at 80 °C for 2 hours. The obtained HCLIN-HCl was washed several times with deionized water, dried, and claimed at different temperatures. This way HCLIN-HCl200, HCLIN-HCl300, HCLIN-HCl400, HCLIN-HCl500 catalysts were obtained after heating of HCLIN-HCl samples at these temperatures for 30 minutes.

To check the influence of concentration of  $NH_4NO_3$  solution on the activity of the prepared catalysts, catalysts were prepared with different of  $NH_4^+$  concentrated solutions. The ion exchange was performed in an autoclave in order to avoid any of loss by evaporation during the ion exchange procedure for 4 hours at 80 °C.

## **3.3 Characterization**

The following methods were used for chemical analysis and characterization of the catalysts: XRD, AAS, EDX, SEM, TEM, FTIR, nitrogen adsorption and desorption, TGA, and ammoniac TPD.

### **X-ray diffraction (XRD)**

A powder X-ray diffractometer STADI-P (STOE) using monochromatic Ni-filtered  $CuK_{\alpha 1}$  radiation  $\lambda = 1.5406 \text{ \AA}$  was used to check the crystallinity of samples. The XRD pattern was recorded in the diffraction angle range of  $2\theta$ , 5-85° with a resolution of 0.02° (180 secs per step). The 40 kV high voltage and 40 mA current were generated by a Seifert high voltage generator (ID 3003). The equipment was controlled and the raw data were handled with the software STOE WinX<sup>POW</sup> (version 2.25, 2009). The used sample was milled in an agate mortar in order to homogenize the sample. All samples were measured by flat preparation in poly acetate foils. The sample was spun around its center during the measurement.

### **Atomic absorption spectrometry (AAS)**

The chemical composition of samples was determined by using an AAS spectrometer contrAA800D (Fa. Analytik Jena), For chemical analysis, *ca.* 20mg of the clinoptilolite

sample were suspended in a mixture of concentrated hydrochloric acid 6 mL HCl (36 wt%), 2 mL nitric acid HNO<sub>3</sub> (65 wt%) and, 2mL hydrofluoric acid HF (40 wt%) provided by Fisher chemicals and VWR chemicals in analytical grade. For digestion of the clinoptilolite, the mixture was transferred into Teflon autoclaves and treated in a microwave oven in two steps: 15 min at 155 °C followed by heating to 200 °C for 30 min and a final cooling step of 15 min at 50 °C. Ion exchange solutions were acidified with conc. HCl before measurement. Atomic absorption spectroscopic detection is carried out with a CCD-array detector in the spectral range from 190 to 900 nm using a Xenon short-arc Lamp and Burner system operating with an Air/Acetylene mixture at 2150-2400 °C.

### **C, H, N, S combustion analysis**

The percentage of H and N was determined using a LECO TruSpec Micro CHN/CHNS/O equipment for combustion analysis. 1 to 10 mg of sample were used. The combustion temperature was 1000 °C. The IR-detector was used for the determination of hydrogen content. A Thermal Conductivity Detector (TCD) was used for the determination of nitrogen.

### **Scanning electron microscopy and energy dispersive X-ray analysis (SEM and EDX)**

A S4800 field emission scanning electron microscope (FE-SEM, Hitachi, Japan) at an accelerating voltage of 5 kV was used to investigate the surface and morphology (size and shape) of the modified clinoptilolite. The magnification obtained with the SEM can be varied over a range of about six orders of magnitude from about 10 to 3,000,000 times.

The elemental composition of samples was analyzed by a field emission scanning electron microscope (SEM, MERLIN<sup>®</sup> VP Compact, Co. Zeiss, Oberkochen) equipped with an energy dispersive X-ray (EDX) detector (XFlash 6/30, Co. Bruker, Berlin). Representative areas of the samples were analyzed and the elemental distribution was mapped on basis of the EDX-spectral data by QUANTAX ESPRIT Microanalysis software (version 2.0). The samples were mounted on SEM-carrier with adhesive conductive carbon tape (co. PLANO, Wetzlar) and coated with carbon under vacuum (EM SCD 500, Co. Leica, Bensheim). SEM-images were taken from the selected regions. Measurement conditions like an applied detector, accelerating voltage, working distance are involved in the corresponding Figures.

### **Transmission electron microscopy (TEM)**

A small amount of Powder was mounted on copper grids (300 mesh, holey carbon film; QUANTIFOIL<sup>®</sup> S7/2, Jena). Excess material was removed by a gentle airflow.

Those prepared samples were analyzed by a transmission electron microscope (TEM, EM 902A, Zeiss, Oberkochen, Germany) equipped with a Tungsten cathode. Representative areas of the samples were analyzed with 80kV accelerating voltage. Imaging was obtained with a CCD camera (CCD-sensor THX 7888A, 14 $\mu$ m x 14 $\mu$ m pixel size, 1024 x 1024 pixel per mm<sup>2</sup>, Co. Proscan, Scheuring, Germany). Image processing was done by iTEM software (Olympus soft imaging solutions GmbH, Münster, Germany).

### **Fourier transform infrared spectroscopy (FTIR)**

A FT-IR spectrometer (Nicolet 380 from Bruker Alpha 2) with a platinum ATR (Attenuated Total Reflection) device in the spectral range of 400-4000 cm<sup>-1</sup> was used for the measurement of the mid-infrared spectra covering the lattice (framework) vibrations of zeolites. Samples were prepared without adding any matrix in a very thin film in a non-absorbing carrier normally that light transmittance through. The band intensities expressed in transmittance (%).

### **Nitrogen Adsorption and desorption**

“Sorptomat 2” Porotec, Thermo Scientific device was used for the measurement of nitrogen adsorption and desorption isotherm of the materials. The measurements were performed at liquid nitrogen temperature -196 °C condition. Before measurement, each sample was pretreated at a temperature of 200 °C under vacuum conditions. The weight of the sample was in the range 0.1- 0.2 grams. The isotherms were analyzed using the BET (Brunauer-Emmett-Teller) in the interval  $0.05 \leq p/p_0 \leq 0.4$  and BJH (Barrett-Joyner-Halenda) methods model applied to the desorption branch from  $p/p_0$  0.3 to 0.95 in order to determine the specific surface area and specific pore volumes.

### **Thermal analysis (TGA-DSC)**

The Setaram Labsys device 1600 combining differential Scanning calorimetry DSC and thermogravimetry was used to measure the mass loss and the heat flow (endothermic or exothermic) occurring during the temperature increase of the samples. The used sample weights were *ca.* 10-20 mg for each measurement. The samples were heated in air at a rate of

10 K/min. The “2000 Setpoint” software was used for measurements. The maximum temperature was 650 °C. A “Ram TGA alumina crucible” (origin: China, material: 99.5% alumina) was used. It can be reused by cleaning with water, acetone, and Aqua regia or king’s water optimally in a molar ratio of 1:3 a mixture of nitric acid and hydrochloric acid. (2 mL HCl 37%,  $d = 1.18$ , MW = 36.4 and 2 mL HNO<sub>3</sub> 65%  $d = 1.37$ ) to finish cleaning by calcination at 900 °C in 1 hour.

### **Temperature programmed desorption (TPD- NH<sub>3</sub>)**

A Thermo Scientific TPDRO 1100 series device was used to study the thermal desorption of ammonia and of ammonia released by the thermal decomposition of ammonium cations loaded on the zeolite. Before testing, samples were pretreated in flowing helium at 110 °C to remove loosely bound ammonia and water. TGA curves were recorded at a heating rate of K/min in a flow of 20 mL/min of helium. The TCD was for measurement of the heat curve, i.e. the uptake or release of heat by the thermal desorption materials ammonia and water, the thermal decomposition of organics, or structural changes in the material. To avoid water effects, the water was removed in a trap before reaching the detector.

## **3.4 Catalysis**

### **3.4.1 Apparatus and equipment**

For catalytic testing under reflux, laboratory glassware (Fig. 9) equipment was used. An ethanol thermometer was used to control the temperature inside of the reaction mixture. Syringes were used for sampling aliquots of the reaction mixture. A high-pressure reactor with 150 mL volume capacity (5500 Parr autoclave) with controller Parr 4848 was used to carry out the etherification reaction at elevated temperature under autogenous pressure (Fig. 10). The reaction mixtures were stirred and heated with a heatable laboratory magnetic stirrer. A Nabertherm oven with the Program Controller S27 was used for the thermal treatment of samples in the air. The centrifuge 5804 R (Eppendorf company) was used to separate the catalyst from the reaction mixture. A Rotary evaporator Laborota 4000 (Heidolph company) was used to separate the volatile compounds from the mixture used for fuel parameter analysis (element content ICP OES method, heating value DIN 51900-1, 3, density

at 15 °C with DIN EN ISO 12185, kinematic viscosity with DIN EN 16896). The reaction mixtures were stirred and heated with a heat able laboratory magnetic stirrer.

### 3.4.2 Catalytic testing

#### **Etherification**

For example, 10g glycerol and 32,6g *tert*-butanol (Gly/TBA ratio=1/4) was added into the Teflon beaker inside the autoclave then 0.5 g catalyst (5 wt% regarding glycerol) was added before installing (Fig. 10). The reaction mixture was heated to a temperature of 110 °C under stirring. The reaction temperature was reached after approximately 1h and 10 minutes. Aliquots of 1.5 mL were taken from the reaction mixture using a sampling valve of the autoclave after 30 min., then 1, 2, 4, and 6 h of reaction, respectively. In order to avoid unreacted solution inside the sample pipe, first, about 2 mL solution was released before keeping the solution for analysis. For reflux experiments at 86 °C, glass equipment was used. It consisted of a 3-necked bulb equipped with a condenser, a thermometer, and opening for aliquot samples.

#### **Catalyst reuse and cycling**

After the reaction, the catalyst was separated from the reaction mixture by centrifugation for catalyst cycling experiments. Water and ethanol were successively used 3 times to wash the catalyst. The catalyst was dried at 110 °C overnight, before repeated use in the etherification of glycerol with *t*-butanol using a new reaction mixture.



**Figure 9.** Etherification of glycerol in a reflux system.



**Figure 10.** High-pressure autoclave reactor.

*The reaction parameters were varied as follows:*

1. Gly/*t*-butanol ratio: 1/4, 1/5, and 1/8
2. Catalyst content: 2.5, 5, 7.5, and 10 % of glycerol mass, Gly/TBA = 1/4
3. Reaction time: 1min, 30 min 1h, 2h, 4h, 6h, 8h, 20h, and 24h.
4. Reaction temperature: 85 °C, 90 °C, 110 °C, 140 °C, and 160 °C.
5. Different alcohols: methanol, ethanol, *n*-propanol, *iso*-propanol, *n*-butanol, *n*-pentanol, *t*-butanol, 2-methyl-2-pentanol at 140 °C.

*Additionally, the catalyst activation and ion exchange conditions were varied:*

6. Calcination temperature of an ammonium exchanged NH<sub>4</sub>CLIN catalyst precursor: 200, 300, 400, 500, and 600 °C, related to Brønsted acidity and porosity
7. Calcination time: 1 min., 1 h, and 2h of synthesized catalyst HCLIN300, related to Brønsted acid sites.
8. Concentration of the ion exchange NH<sub>4</sub>NO<sub>3</sub> solution, related to catalyst acidity.
9. Acid treatment: 0.1- 0.5 HCl solutions were used to protonate the starting CLIN.



### 3.4.3 Analysis

The chemical composition of reaction mixtures sampled after different reaction times was analyzed using a GC/FID device. A 10 m long 0.20 $\mu$ m DB-Wax Gas Chromatography column with an open diameter of 0.1 mm was used to separate components. A GC-FID flame ionization detector was used, Aliquots of 1 $\mu$ L were injected and the analysis was performed with the heating program 40/5-6-180/10-8-240/5. The flow split rate was 1:50, the inlet temperature was 240 °C, peaks were automatically integrated, and transformed to the corresponding GC spectra. The GC peaks were analyzed by MS for the identification of the molecules.

The glycerol conversion, yields of glycerol ether, and the selectivity to different ether were calculated as follows.

*Conversion of Glycerol:*

$$X\% = \frac{A_{\text{initial Gly}} - A_{\text{unreacted Gly}}}{A_{\text{initial Gly}}} \times 100\%$$

The conversion is calculated by the change of the peak areas of the glycerol in the starting reaction mixture and after the reaction.

*Selectivity to mono, di, and tri ethers (M, D, and T)*

$$S_M\% = \frac{A_{M1} + A_{M2}}{A_{M1} + A_{M2} + A_{D1} + A_{D2} + A_T} \times 100\%$$

$$S_D\% = \frac{A_{D1} + A_{D2}}{A_{M1} + A_{M2} + A_{D1} + A_{D2} + A_T} \times 100\% \quad S_T\% = \frac{A_T}{A_{M1} + A_{M2} + A_{D1} + A_{D2} + A_T} \times 100\%$$

Where as  $A_{M1}$ ,  $A_{M2}$ ,  $A_{D1}$ ,  $A_{D2}$ ,  $A_T$  are peak area of M1, M2, D1, D2, and T (mono-, di- and tri-*tert*-butyl glycerol ether), in chromatograms of the reaction mixture.

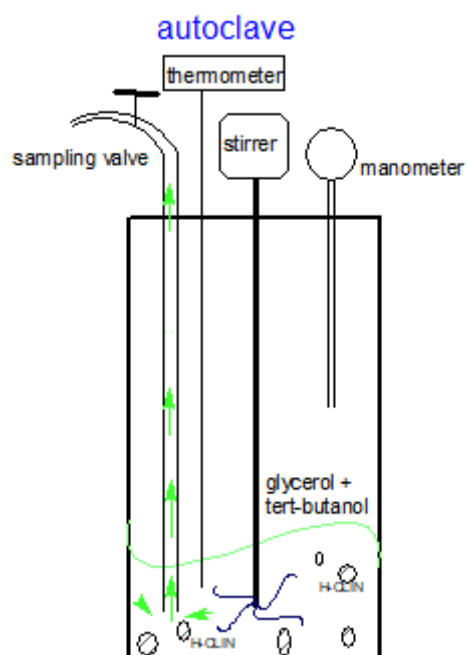


**Figure 11.** Construction of the autoclave reactor: High-pressure reactor with 150 mL volume capacity (5500 Parr autoclave) with controller Parr 4848 used in catalyst testing.

## 4 Results and discussion

### 4.1 Characterization

The starting natural clinoptilolite, ammonium exchanged clinoptilolite, and different acidic samples were characterized regarding their structure, crystallinity, morphology, porosity, and acid properties by XRD, SEM/TEM, FTIR lattice vibration spectra, nitrogen adsorption and desorption, TG-DSC and TPO measurements.

#### 4.1.1 X-ray diffraction analysis XRD

The obtained samples CLIN,  $\text{NH}_4\text{CLIN}$ , and HCLNs, which were activated in an oven at different temperatures namely 250, 300, 400, 450, 500, and 600 °C, were measured in order to investigate the crystallinity of modified clinoptilolite (Fig. 12).

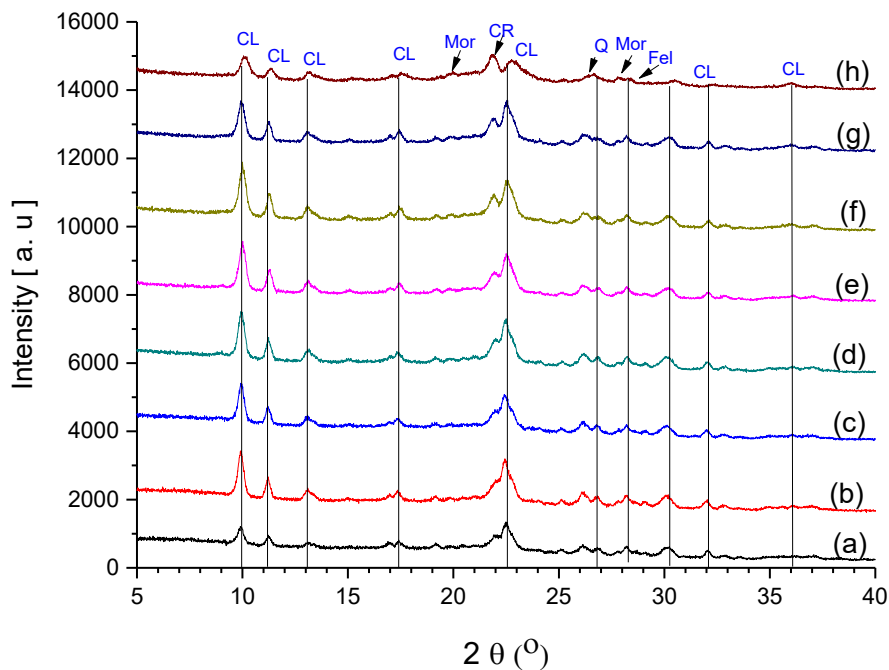


**Figure 12.** Powder XRD patterns of a) starting clinoptilolite CLIN, b) ammonium exchanged  $\text{NH}_4\text{CLIN}$ , and the acidic forms: c) HCLIN250, d) HCLIN300, e) HCLIN400, f) HCLIN450, g) HCLIN500, h) HCLIN600 calcined at corresponding temperatures (250 °C to 600 °C): "CL"- the typical peak of CLIN pattern, "CR"-Cristobalite, "Mor"- Mordenite, "Q"-Quartz, "Fel"-Feldspar.<sup>[64]</sup>

The X-ray diffraction patterns of the eight samples show that all samples contain clinoptilolite. Besides the clinoptilolite, the samples contain minor amounts of quartz, cristobalite, and alspars as an impurity. The calcination temperature was increased up to 600 °C to study the thermal stability. In effect, the background increases beyond heating to 400 °C indicating some loss in the crystallinity. Additionally, the intensity of the XRD reflection of cristobalite at  $2\theta = 21.8^\circ$  peak increases compared to the intensity of the neighboring clinoptilolite reflection (Table 6). Normally, the clinoptilolite structure starts to collapse above 500 °C.<sup>[65]</sup> In effect, calcination at 600 °C leads to partial destruction and amorphization of the clinoptilolite framework as indicated by the loss of intensity of the reflections and the marked increase of the background. In addition, the formation of the aluminosilicate laratorite was observed at 500 °C.<sup>[66]</sup>

As shown in Figure 6 and Table 4, the crystallinity increases with NH<sub>4</sub>CLIN after washing an ion exchange with ammonium nitrate solution at elevated temperature. This is likely due to the removal of amorphous impurities due to the treatment in the aqueous solution.

**Table 6:** Observed XRD reflections and peak intensities of natural clinoptilolite sample CLIN, ammonium-exchanged clinoptilolite NH<sub>4</sub>CLIN and acidic forms HCLIN obtained after calcination at 250°C to 600°C. Reflection angle  $2\theta$  (°): peak I to IX are (CL) 9.9°, (CL) 11.2°, (CL) 13.1°, (CL) 17.4°, (CR) 21.9°, (CL) 22.5°, (CL) 26.1°, (CL) 30.2°, (CL) 31.1° (CL- clinoptilolite, CR- cristobalite).

Samples	Intensity [a.u.] of the XRD reflections located at $2\theta$ [°] of clinoptilolite								
	9.9°	11.2°	13.1°	17.4°	21.9°	22.5°	26.1°	30.2°	31.1°
CLIN	1211	960	759	815	967	1345	677	627	514
NH <sub>4</sub> CLIN	1984	1225	898	834	1140	1751	776	669	554
HCLIN250	1883	1213	950	852	1052	1536	771	655	525
HCLIN300	2003	1243	883	834	1174	1795	763	621	530
HCLIN400	1934	1094	801	723	1050	1571	612	554	550
HCLIN500	1695	1087	789	857	1178	1707	729	624	486
HCLIN600	1211	852	739	727	1247	1106	704	521	385

Crystallite size was determined by the Scherrer equation:

$$D = \frac{K\lambda}{\beta \cos\theta}$$

Scherrer equation was published in 1918.

Where:  $D$  is the crystallite size nm,  $K = 0.9$  is a constant,  $\lambda = 0.15406$  nm wavelength of the x-ray radiation,  $\beta = \text{FWHM}$  is the full width at half maximum FWHM of the most intense diffraction peak 020 of CLIN,  $\theta =$  peak position radians.

**Table 7:** Crystallite sizes of clinoptilolite, ammonium exchanged clinoptilolite  $\text{NH}_4\text{CLIN}$  and its acidic forms HCLIN obtained after calcination at different temperatures (250 °C to 600 °C) determined by the Scherrer formulae from the width of the XRD reflection at  $\text{ca. } 2\theta = 9.9^\circ$ .

Sample	Reflection $2\theta^\circ$	FWHM $2\theta^\circ$	Crystallite size [nm]
CLIN	9.9	0.29	27.5
$\text{NH}_4\text{CLIN}$	9.91	0.33	24.2
HCLIN250	9.92	0.301	26.5
HCLIN300	9.93	0.305	26.1
HCLIN400	10.01	0.356	22.4
HCLIN500	9.93	0.39	20.4
HCLIN600	10.05	0.447	17.8

Table 7 and Figure 13 show that the size of sample crystals decrease when the calcination temperature of the sample increases. From HCLIN300 to HCLIN600 the crystallite size decreases from *ca.* 26 to 18 nm. These values are close to the size of the primary aggregate nanoparticle found in TEM *ca.* 50 nm.

In conclusion, the natural zeolite samples are composed mostly of clinoptilolite and show high thermal stability until close to 600 °C.

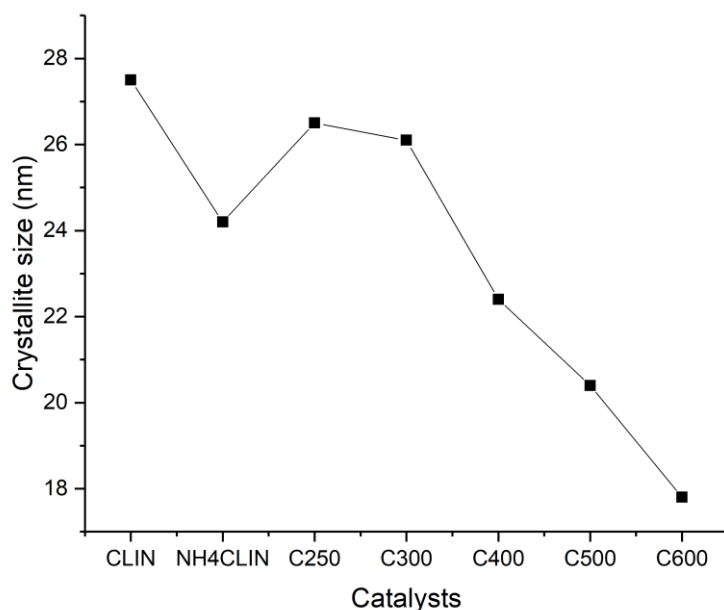


**Figure 13.** Influence of the calcination temperature on the crystallite size of clinoptilolite. Starting material CLIN, ammonium form  $\text{NH}_4\text{CLIN}$  (ion-exchange with 0.2M solution  $\text{NH}_4\text{NO}_3$ , 80 °C, 2h two times), calcination temperatures C250, C300, C400, C500, C600, samples named as HCLIN250, HCLIN300, HCLIN400, HCLIN500, HCLIN600.

#### 4.1.2 Chemical analysis AAS

The chemical composition of clinoptilolite samples was determined by atomic absorption spectroscopy AAS.

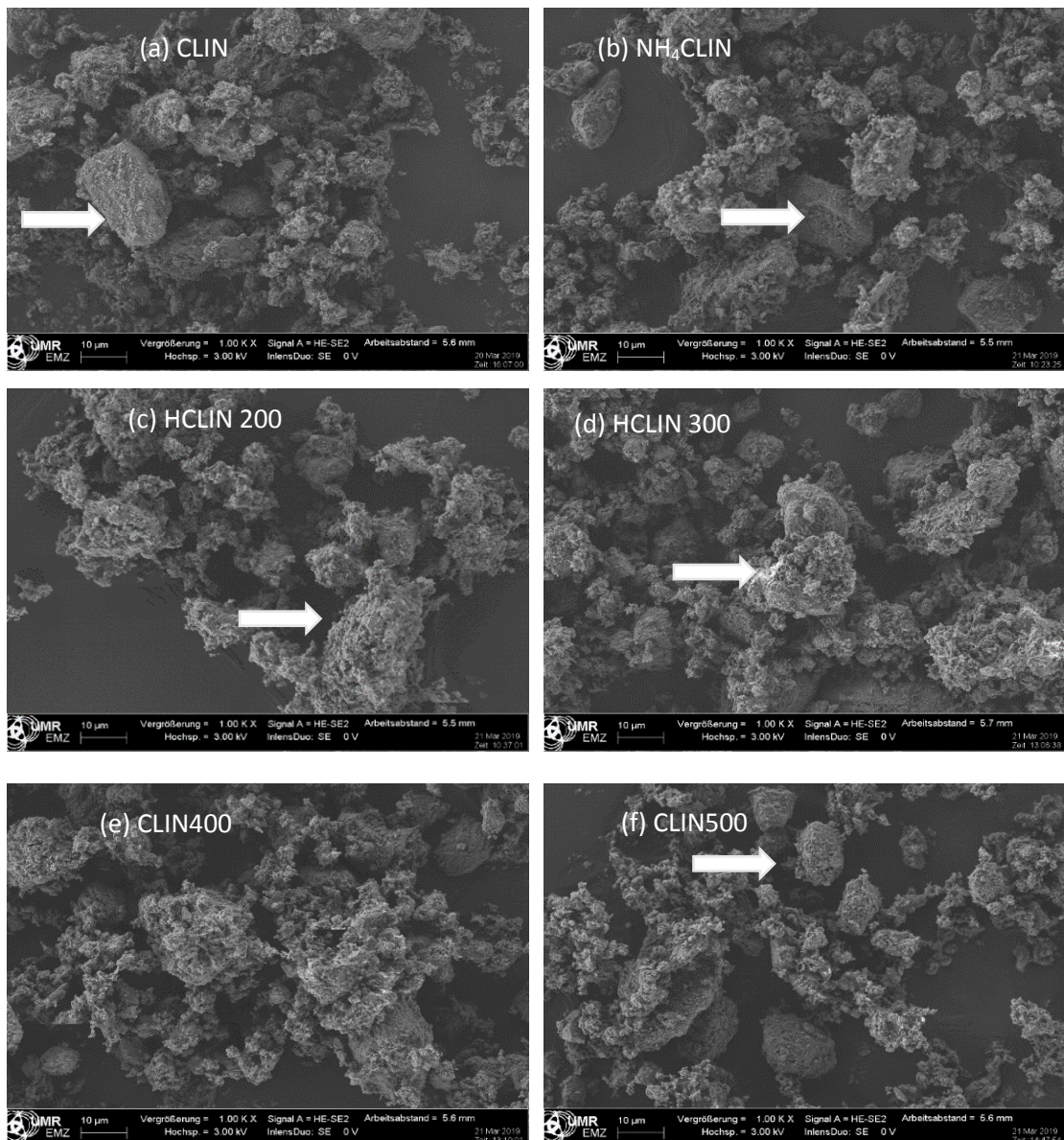
**Table 8:** Chemical composition (wt%) of elements Ca, K, Mg, Na, N, and H of four samples: Starting material CLIN, ammonium form  $\text{NH}_4\text{CLIN}$ , calcined samples at 300 °C HCLIN300, and 500 °C named as HCLIN500.

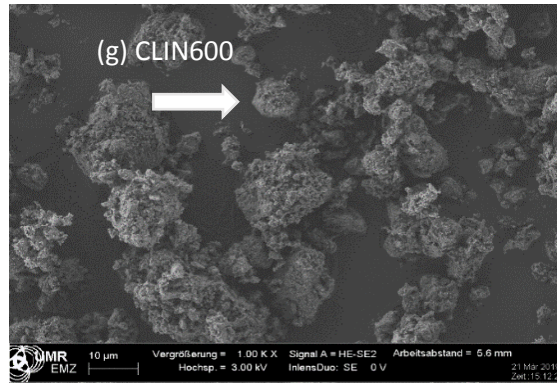
Samples/ Mass (%)	CLIN	$\text{NH}_4\text{CLIN}$	HCLIN300	HCLIN500
Ca	2.05	0.5	0.58	0.4
K	2.7	1.3	1.3	1.2
Mg	0.36	0.2	0.21	0.3
Na	0.77	0.56	0.53	0.3
Si	26.2	28.6	28.7	28.5
Al	6.7	7.1	7.05	7
N	-	1.7	0.9	-

The cations, which balance the negative charge introduced by tetrahedral framework aluminum, are mainly  $\text{Ca}^{2+}$  and  $\text{K}^+$ , which amounts to 2 wt% and 2.7 wt%. Besides, the CLIN sample contains some magnesium and sodium ions (Table 8). These results fit with the

properties of starting commercial material linoptilolite. A ternary ion exchange with ammonium with 0.2 M solution of  $\text{NH}_4\text{NO}_3$  at 80 °C in two hours, two times, the content  $\text{Ca}^{2+}$  and the other cations are released. Mainly aluminum and potassium ions are replaced by ammonium ions. The cation content released is 75% for  $\text{Ca}^{2+}$ , 50% for  $\text{K}^+$ , and 30% for  $\text{Na}^+$  (Table 8). Usually, the interaction of the cations with the negative charge framework increases with the cation charge and decreasing cation radius. Therefore, small and higher charge cations like  $\text{Ca}^{2+}$  (1.06 Å) are more difficult to exchange. The observed high exchange degree with linoptilolite points to a location of hydrated  $\text{Ca}^{2+}$  ions in the large cages where the interaction with the framework is lower than in the oxygen rings. The ammonium content reaches ca. 2.5 wt% after ion exchange as a result from the loss of cations.

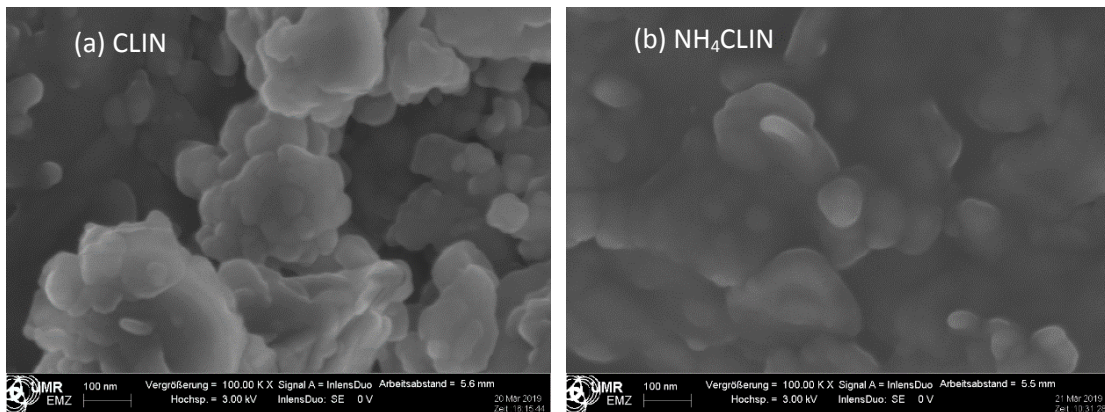
#### 4.1.3 Scanning electron microscopy (SEM)





**Figure 14.** SEM images of (a) CLIN, (b) NH<sub>4</sub>CLIN, (c) HCLIN200, (d) HCLIN300, (e) HCLIN400, (f) HCLIN500, (g) HCLIN600 with 1 k of magnification.

The SEM images (Fig. 14) at 1000 of magnification show that the surfaces of the CLIN and the NH<sub>4</sub>CLIN are similar. The stable and hard particle still remains and exists in the powder. The block like particle, agglomerates disintegrate into smaller particle. They also resemble aggregates. The appearance of the aggregated particle changes with thermal treatment temperature. The surfaces become more porous and look like nests or holes of µm size. The reason could be the rapid evaporation of loosely bound water and ammonium ions, which act as a “micro explosion” and causes internal stress and partial local collapses. The particles were separated. When the temperature increases to 500 or 600 °C, the surface was changed again. More small particles were formed by disintegration of larger ones.





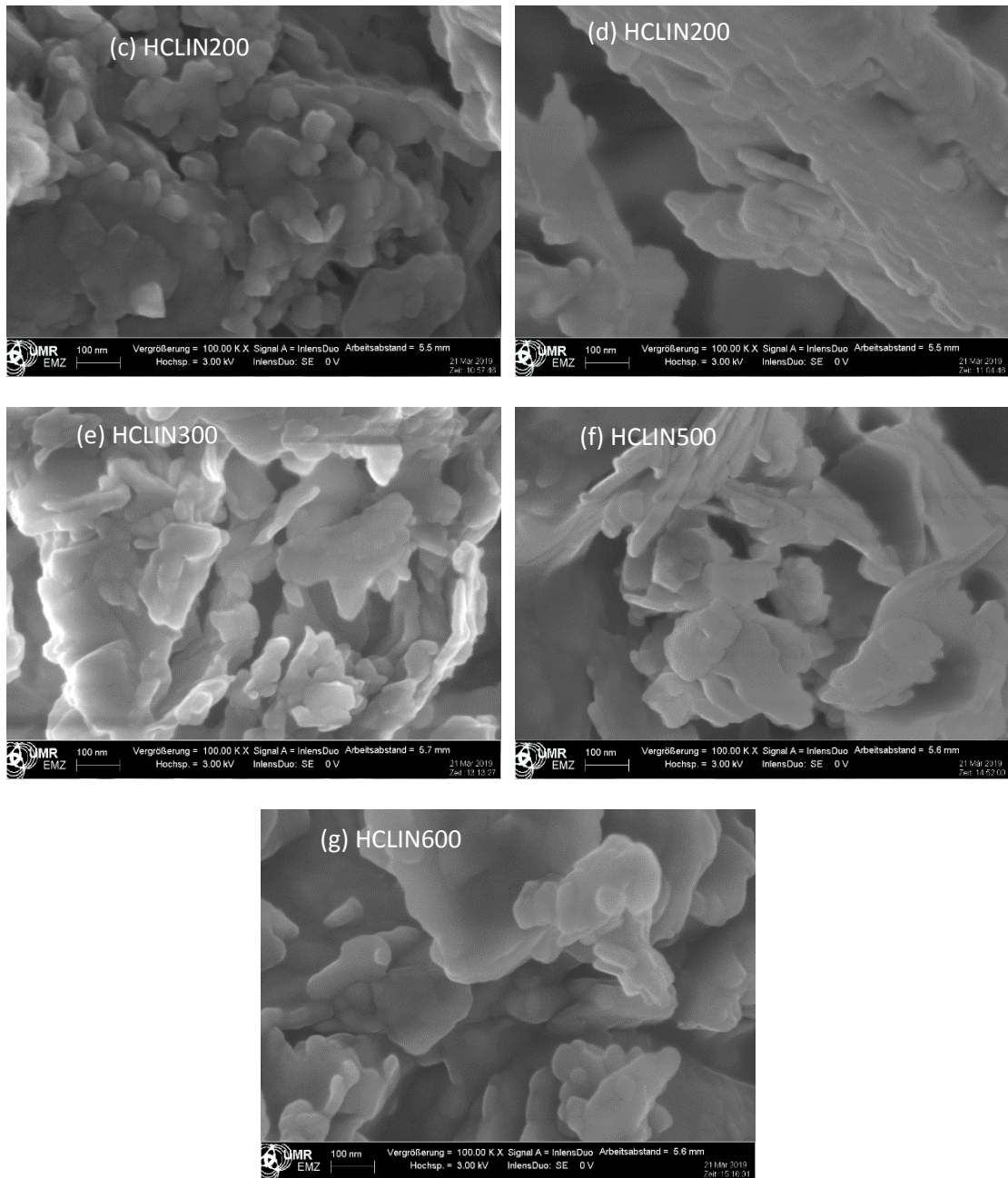


**Figure 15.** High resolution SEM images of (a) CLIN, (b)  $\text{NH}_4\text{CLIN}$ , (c)-(d) HCLIN200, (e) HCLIN300, (f) HCLIN500, (g) HCLIN600 with 100 k of magnification.

The high magnification SEM images (100 k) confirm the aggregate structure of the material (Fig. 15). Indeed, the  $\mu\text{m}$ -sized particle is composed of nanoparticles. It looks like they are stacked together in the samples CLIN,  $\text{NH}_4\text{CLIN}$ , and HCLIN200. The HCLIN300 showed more holes and more flowery particle shapes. At this temperature starts the fast decomposition of ammonium ions and the desorption of internal water, on the lighter wall of material. In addition, at the temperature 500 and 600 °C, we can see many layers were

reordered and stack together. The thermal treatment changes markedly the morphology of sample particles.

#### 4.1.4 Transmission electron microscopy (TEM)

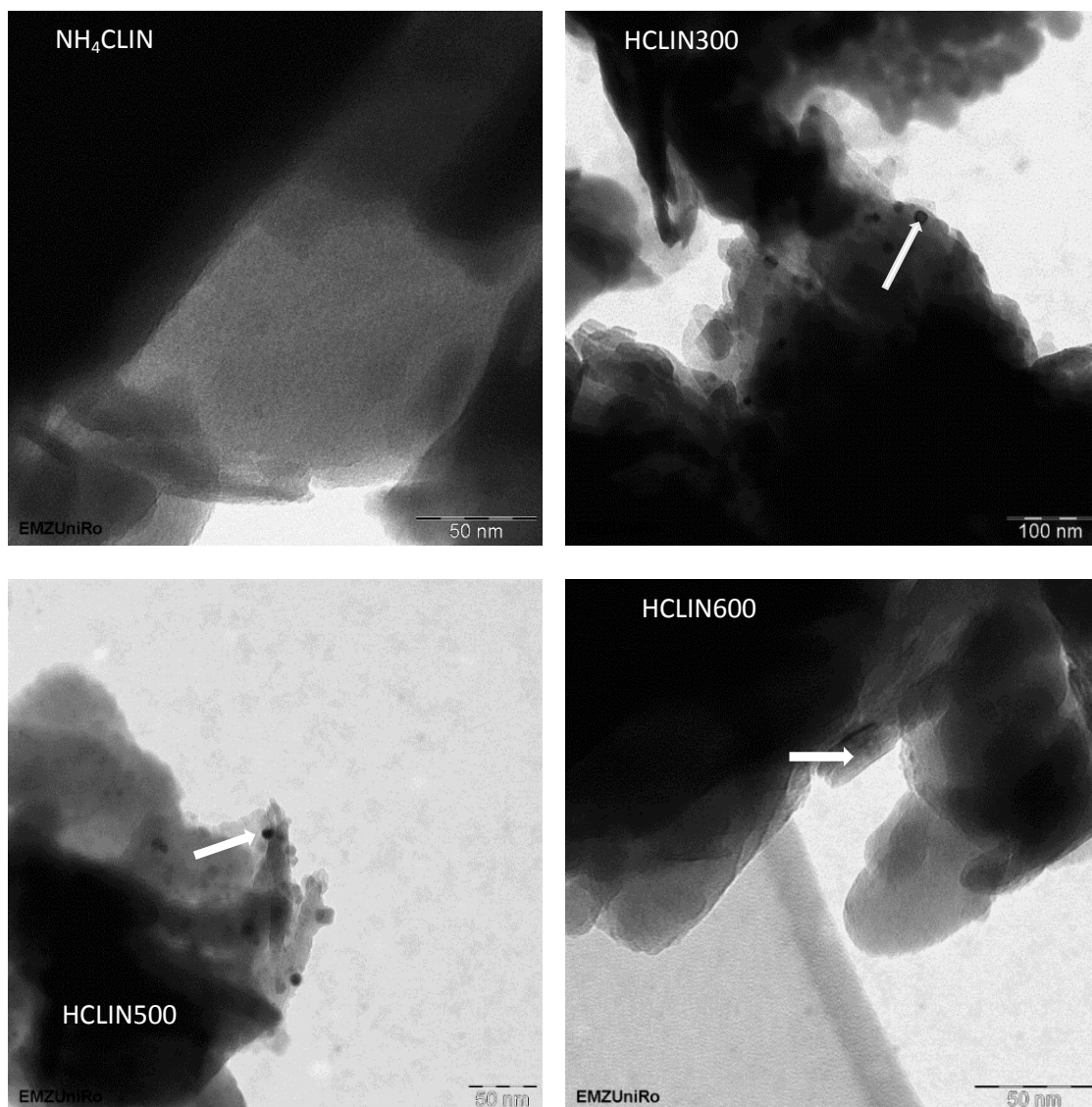


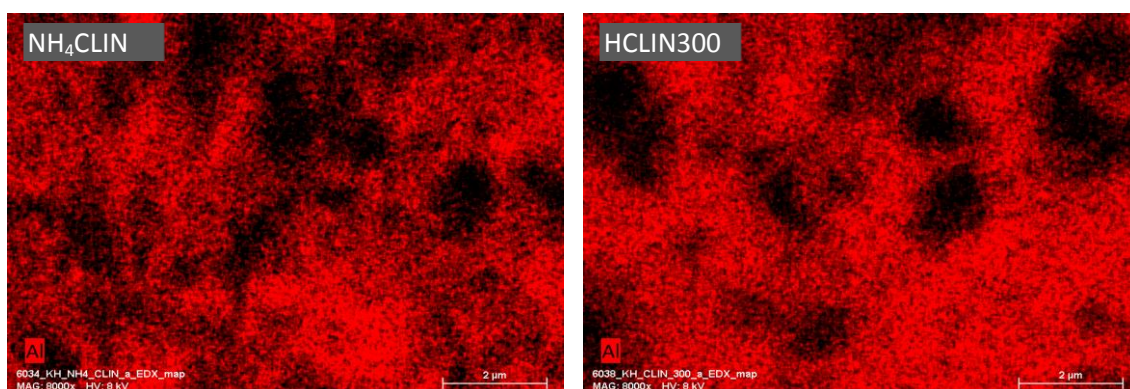
**Figure 16.** TEM images of 4 samples NH<sub>4</sub>CLIN, HCLIN300, HCLIN500, HCLIN600 sample at 50-100 nm scales.

In Figure 16, many nanoparticles appear, the size of the particles was estimated about 10 nm in HCLIN500 and at about 20 nm in HCLIN300. The particles remain after 300 and 500 calcination temperature. The outside cycle of the particle becomes closer and their density seems to increase when their size is decreased. In TEM images of the HCLIN600 sample, the round particles were not appeared like in HCLIN300 and HCLIN500. Instead, the plate-like of zeolite was easier observed.

The TEM results gave us an interesting image of ammonium zeolite materials calcined at different temperatures, whereas the small particles were formed and transformed during the calcination.

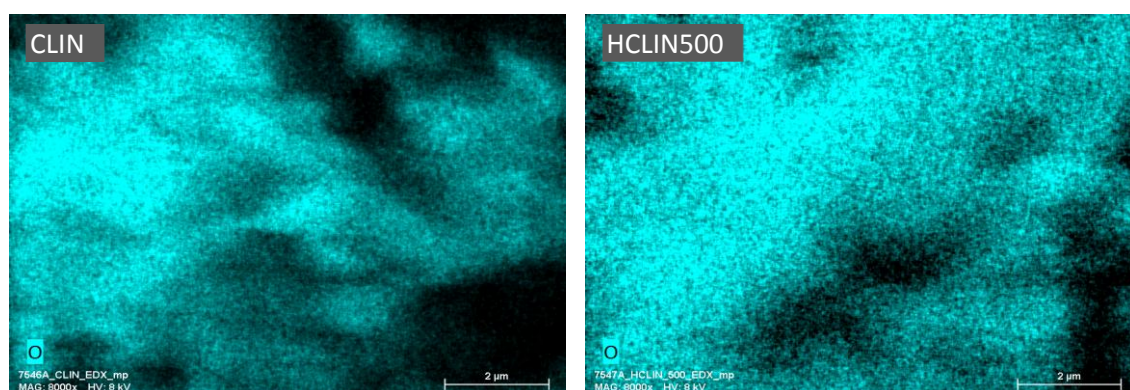
From 300 °C calcination samples, we can see many round particles inside the surface of materials. They are some impurities or some oxide particles. The sign of the particles was disappeared because of heat; they could be smelt and were removed. The layers can be seen.

#### 4.1.5 Energy dispersive x-ray analysis (EDX)



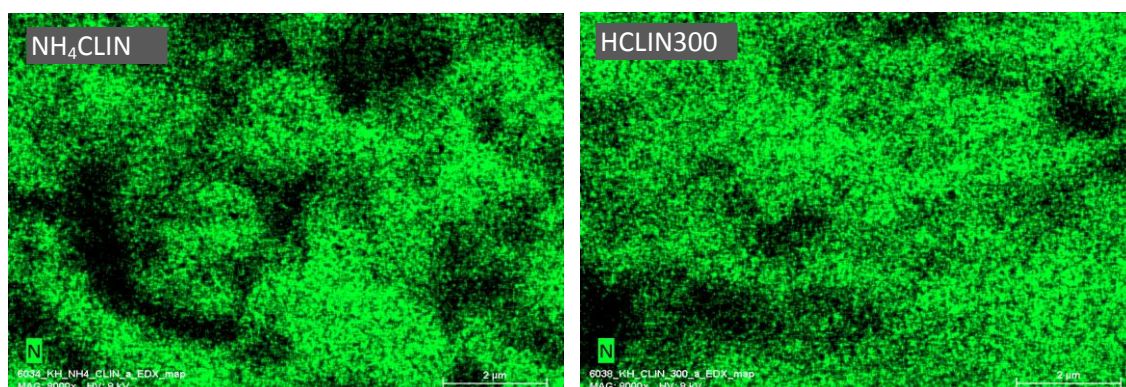
**Figure 17.** Energy dispersive X-ray (EDX) mapping analysis for aluminum element distribution in two samples NH<sub>4</sub>CLIN (right) and HCLIN300 (left).

Figure 17 shows the aluminum mapping found with NH<sub>4</sub>CLIN and HCLIN300. It does not change after ammonium ion exchange and calcination, because the framework is not affected under these conditions.



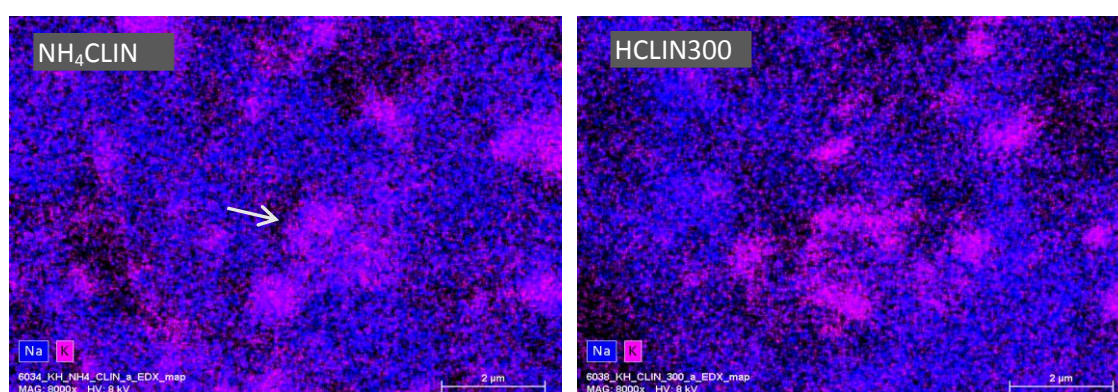
**Figure 18.** Energy dispersive X-ray (EDX) mapping analysis of oxygen element distribution in two sample CLIN (left), HCLIN500 (right).

The oxygen mapping with CLIN and HCLIN500 samples are presented in Fig. 18. The blue colored dots are homogeneously distributed over both the samples. This is in line with the expectation because the oxygen is a part of the aluminosilicate framework.



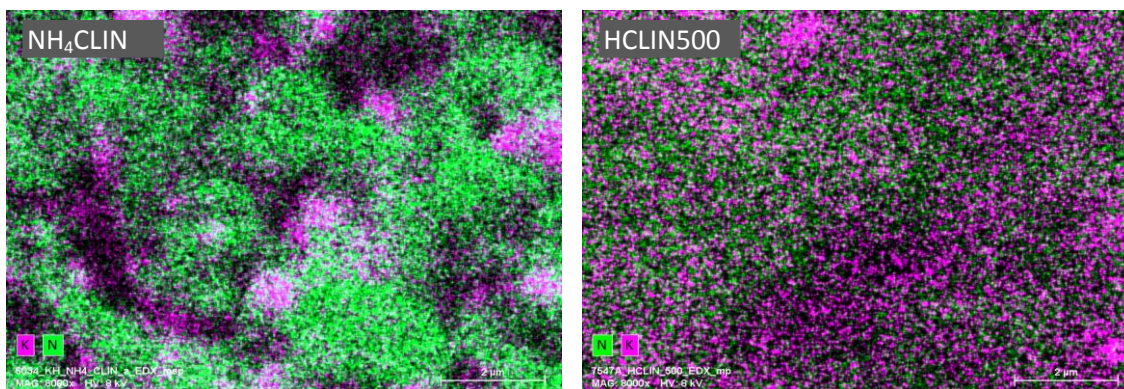
**Figure 19.** Element mapping based on energy dispersive X-ray (EDX) analysis of N distribution of two samples NH<sub>4</sub>HCLIN and HCLIN300

As shown in Figure 19 the N distribution in HCLIN300 was spread smoother than in NH<sub>4</sub>CLIN. It means that only some ammonium ions are decomposed. after calcination 300°C. But almost NH<sub>4</sub><sup>+</sup> ions still remain in the framework of the zeolite.



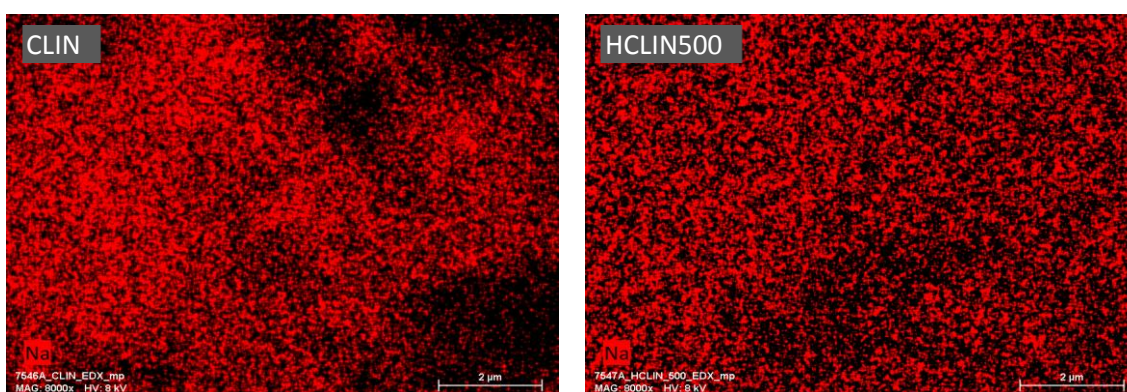
**Figure 20.** Energy dispersive X-ray (EDX) element mapping analysis of the K (pink) and Na (blue) distribution for two samples HCLIN300 (right) and NH<sub>4</sub>CLIN (left): blue colored dots represent Na and pink colored dots belong to K.

Figure 20 shows the sodium (blue dots) and potassium (pink dots) element mappings obtained with NH<sub>4</sub>CLIN and HCLIN300. The sodium ions are homogeneously distributed in the samples whereas the potassium ions form an island clearly distinguished from the sodium dots. This picture is maintained also after partial decomposition of the ammonium ions at 300 °C. This finding is confirmed by the mappings shown in Figure 21 (below).



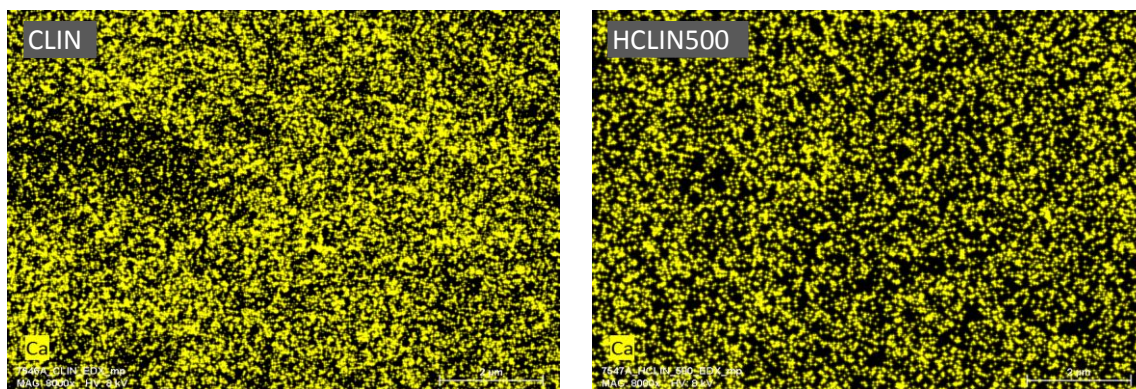
**Figure 21.** Energy dispersive X-ray (EDX) mapping analysis for nitrogen (green), and potassium (pink) element distribution in two sample NH<sub>4</sub>CLIN (left), HCLIN500 (right).

Figure 21 shows the nitrogen as ammonium form (green dots) and potassium (pink dots) mapping images obtained from NH<sub>4</sub>CLIN and HCLIN500 samples. The intensity of the nitrogen dots decreases markedly after heating to 500 °C. This is in line with the observed decomposition of the ammonium ions after calcination at 500 °C as observed with FTIR, TGA and TPDA, and shown below. Interestingly, the potassium ions are non-homogeneously distributed in the image resemble “islands” in the image resemble with NH<sub>4</sub>CLIN. With HCLIN500, potassium dots are observed within all sample parts, however, with low density. The non-homogeneous distribution is maintained. It seems, that with NH<sub>4</sub>CLIN the pink potassium dots are covered by the green nitrogen ones. This could mean potassium is partly located in inner particle sites, whereas ammonium ions prefer in part the outer sphere.



**Figure 22.** Energy dispersive X-ray (EDX) mapping analysis for sodium element distribution in two samples CLIN (left), HCLIN500 (right).

Figure 22 shows the Na ion mapping (red dots) for the starting CLIN and HCLIN500. The Na is homogeneously distributed in both the samples. Only the intensity of the mapping image is lower due to the loss of sodium to the ammonium ion exchange. These results are similar to the ammonium (nitrogen) mapping and Ca mapping images.



**Figure 23.** Energy dispersive X-ray (EDX) mapping analysis for calcium element in two samples CLIN (left), HCLIN500 (right).

Figure 23 shows the Ca ion mapping for the starting CLIN and after ammonium ion exchange and calcination at 500 °C. The  $\text{Ca}^{2+}$  ions (yellow dots) are homogeneously distributed throughout both of the samples. However, the yellow dots are less dense indicating a lower calcium content with HCLIN500 caused by the ammonium ion exchange. This finding is in line with the chemical analysis.

#### 4.1.6 Nitrogen adsorption and desorption measurements

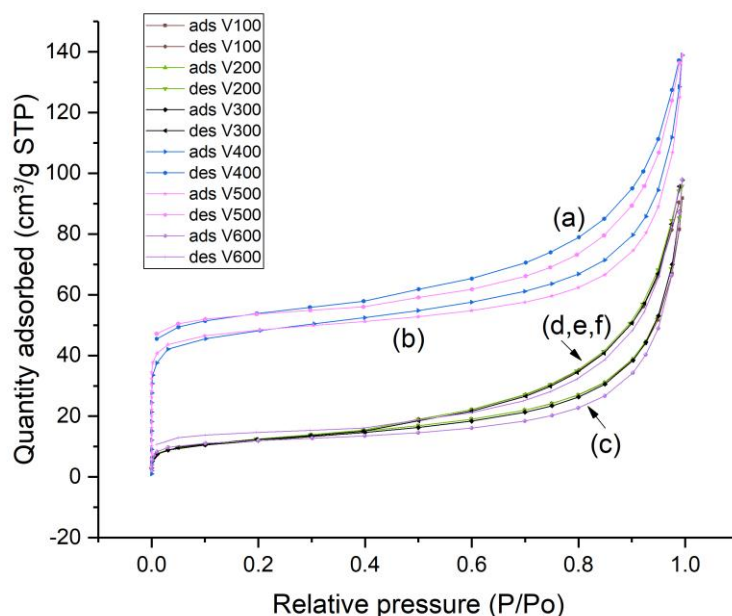


**Figure 24.** Nitrogen adsorption/desorption isotherms of a) HCLIN400, b) HCLIN500, c) HCLIN600, d)  $\text{NH}_4\text{CLIN100}$ , e)  $\text{NH}_4\text{CLIN200}$ , f) HCLIN300.

In Figure 24 are shown the nitrogen adsorption and desorption isotherms of several clinoptilolite catalysts. The isotherms are a combination of the type I micropores and type II macropores isotherms according to the IUPAC nomenclature (Fig. 25 Table 9). The nitrogen uptake at a very low relative pressure of  $p/p_0$  of 0 to 0.05 is due to the adsorption in the micropores of the zeolite framework. Uptakes at higher pressures are due to the filling of mesoporous. Adsorption at high relative pressures of  $p/p_0 > 0.6$  is due to adsorption in the interparticle macropores. Obviously, the highest microporosity and BET specific surface areas are found with HCLIN400, and HCLIN500, ca. 195 and 151  $m^2/g$ . In this case, the ammonium ions located in and blocking the micropores are decomposed by the thermal treatment. This way the internal micropore system is opened. The pore system of samples calcined at a lower temperature is still blocked. Therefore, the samples NH<sub>4</sub>CLIN100, NH<sub>4</sub>CLIN200, and HCLIN300 show only a low increase of the adsorption isotherm at low relative pressure. The same holds with the sample calcined at 600 °C, although this temperature is sufficient for the decomposition of pore-blocking ammonium ions (Table 10). However, the framework destruction indicated by the XRD measurements leads obviously also to a loss and/or the blocking of the micropores in the clinoptilolite crystals. The microporosity is strongly decreased but the macroporosity interparticle pores is maintained. This is also confirmed by the SEM and TEM images.

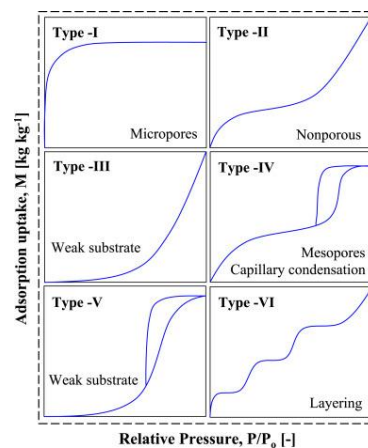


**Figure 25.** The IUPAC classification of adsorption isotherms of different porous systems showing both the adsorption and desorption pathways. Note the differences observed between internal micropores and inter particle macropores (type I and type II isotherms).<sup>[79]</sup>

**Table 9:** Classification of pores by the pore size.

Pores	Pore size [nm]
Micro pores	< 2
Meso pores	2~50
Macro pores	> 50

**Table 10:** Specific surface areas and specific micropore volumes of ammonium exchanged and thermally activated HCLINs

Sample	BET Surface Area m <sup>2</sup> /g	Micropore Area (m <sup>2</sup> /g)	External Surface Area (m <sup>2</sup> /g)	Micropore volume cm <sup>3</sup> /g	Macropore Volume cm <sup>3</sup> /g
<b>HCLIN200</b>	25.9		26.7	0.004	0.04
<b>HCLIN300</b>	42.7	5.7	37	0.002	0.02
<b>HCLIN400</b>	194.9	162.4	32.5	0.067	0.131
<b>HCLIN500</b>	150.8	120.4	30.4	0.053	0.112
<b>HCLIN600</b>	33	9.0	24	0.005	0.05

#### 4.1.7 Fourier transform infrared spectroscopy FTIR

The starting clinoptilolite, the ammonium-exchanged form, and obtained clinoptilolite catalysts HCLIN were investigated by FTIR spectroscopy in order to follow independently the composition of the ammonium ions by the increase of the intensity of the ammonium mode. Infrared spectroscopy IR allows also use to determine roughly the ratio of aluminum in the framework. The lattice vibrations of the Si-O-Al framework appear in the mid-IR in the spectral range of 400-1200 cm<sup>-1</sup>. The vibration band at ca. 1250-950 cm<sup>-1</sup> is assigned to antisymmetric T-O-T stretching vibrations. Symmetric stretching vibrations appear at 720-650 cm<sup>-1</sup>; T-O bending bands appear at 420-500 cm<sup>-1</sup>. Structure sensitive vibrations of secondary building units as the zeolite double-ring units DRV are observed at 650-500 cm<sup>-1</sup>. Deformation vibrations of adsorbed water molecules occur at ca. 1630 cm<sup>-1</sup>.



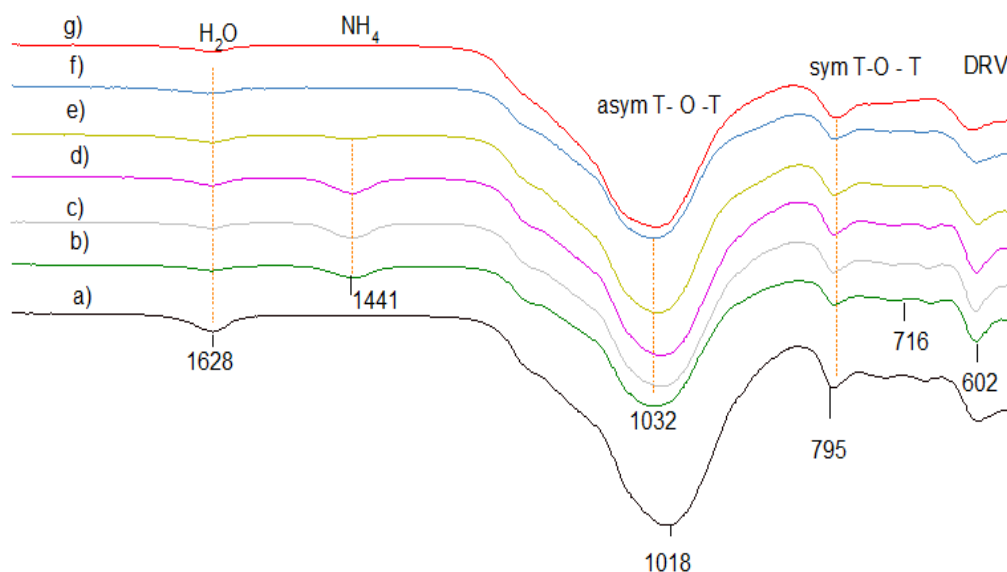


**Figure 26.** FTIR lattice vibration spectra of clinoptilolite CLIN after different treatment: a) starting material CLIN, b) ammonium exchanged  $\text{NH}_4\text{CLIN}$ , and c) calcined HCLIN200, d) HCLIN300, e) HCLIN400, f) HCLIN500, g) HCLIN600.

The FTIR spectra of the starting clinoptilolite CLIN, ammonium exchanged  $\text{NH}_4\text{CLIN}$  and thermally activated HCLINs are shown in Fig. 26. The asym.T-O-T vibration at  $1018\text{ cm}^{-1}$  in the spectrum of the starting clinoptilolite is shifted to a higher wavenumber from  $1018$  to  $1032\text{ cm}^{-1}$  Figure 26, Table 11 after exchange of the zeolite cations by ammonium ions and desorption of loosely bound water at  $200\text{ }^\circ\text{C}$ .

**Table 11:** Wavenumbers of typical zeolite lattice vibrations and vibrations of functional groups of clinoptilolite CLIN, ammonium exchanged  $\text{NH}_4\text{CLIN}$ , and different calcined HCLIN samples.

Samples/ Vibration ( $\text{cm}^{-1}$ )	$\text{NH}_4^+$ vibration	$\text{OH}^-$ vibration	T-O-T (T=Si/Al) asym- stretching	T-O-T sym- Stretching	Double ring vibration
CLIN		1628	1018	795	599.8
$\text{NH}_4\text{CLIN}$	1441	1628	1032	792	602
HCLIN200	1441	1627	1024	793	600
HCLIN300	1441	1632	1024	793	602
HCLIN400	1441	1632	1029	793	598
HCLIN500		1635	1034	793	602
HCLIN600		1627	1031	790	605

This shift relates to the different interaction of the ammonium ions with the framework compared to Na, K, Ca, and Mg ions and the role of water. The framework shrinkages cause a decrease of the T-O bond lengths in the T-O-T bridges T=Si, Al tetrahedral atoms. Additionally, a new vibration band at  $1441\text{ cm}^{-1}$  appears in the FTIR spectrum of  $\text{NH}_4\text{CLIN}$ . It is assigned to the deformation vibration of the exchanged ammonium ions. The intensity of this band decreases with raising calcination temperature slowly. A strong decrease, i.e. decomposition of ammonium ions is observed after raising the temperature to  $400\text{ }^\circ\text{C}$ . The ammonium ion adsorption band nearly disappears after heating to  $500\text{ }^\circ\text{C}$ .

The FTIR results confirm that the major part of ammonium ions is decomposed by heating the samples to  $400\text{-}500\text{ }^\circ\text{C}$ . Thereby ammonia gas is released. The ammonium ions located in the pore windows are decomposed and replaced by  $\text{H}^+$  protons. The pores are opened as observed by the nitrogen adsorption and desorption experiments.

#### 4.1.8 Thermogravimetric analysis TGA

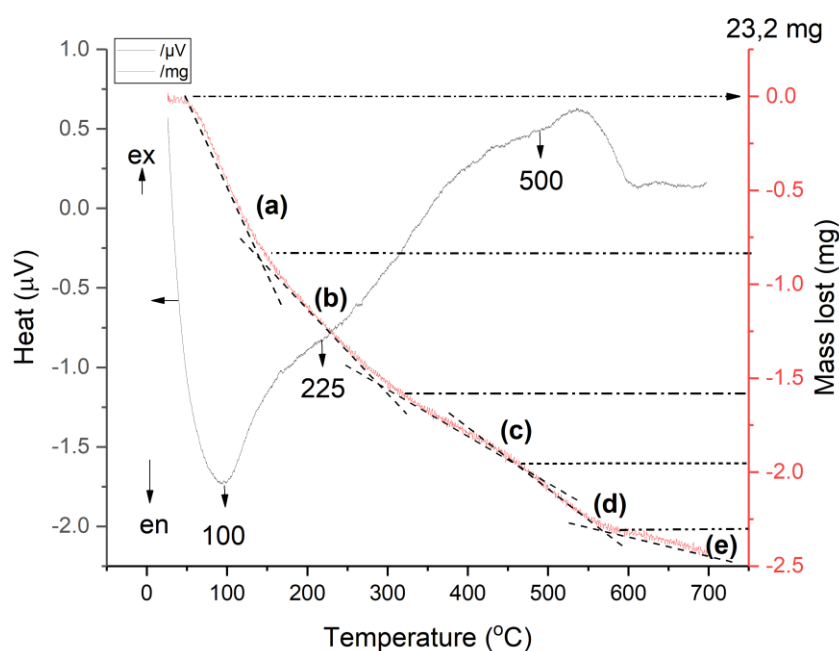


**Figure 27.** Combined TG-DSC curves of an ammonium exchanged  $\text{NH}_4\text{CLIN}$  with 5 weight loss steps. a) from 50 to  $150\text{ }^\circ\text{C}$ , b) from 150 to  $280\text{ }^\circ\text{C}$ , c) from 280 to  $450\text{ }^\circ\text{C}$ , d) from 450 to  $570\text{ }^\circ\text{C}$ , e) above  $600\text{ }^\circ\text{C}$ .

The combined TG-DSC curves of  $\text{NH}_4\text{CLIN}$  are shown in Figure 27. A markedly endothermic weight loss is observed from  $50$  to  $150\text{ }^\circ\text{C}$  assigned to water removal by heating the sample to *ca.*  $200\text{ }^\circ\text{C}$ . It is assigned to the loss of weakly bound water molecules as

indicate by the low temperature of the peak maximum of 100 °C in the DSC curve. A 150 °C step from 150-280 °C strongly bound water, e.g. bound to cations is desorbed from the zeolite pores giving rise to an endothermic shoulder in the DSC curve with a plateau at 225 °C. Step 3 starting from 280 °C to 450 °C is assigned to the decomposition of ammonium and also some dehydration or dehydroxylation. Step 4 the decrease of the weight loss curve between ca. 450 -570 °C is assigned to the decomposition of strongly bound ammonium ions with corresponding desorption of ammonia from stronger Brønsted sites created after decomposition of the ammonium ions. It is also an exothermic process. Further enhancement of the temperature causes dehydroxylation. At high finalination temperature, partial destruction of the clinoptilolite lattice occurs. Step 5 above 600 °C is assigned to dehydroxylation of the framework, which is in part connected with structural destruction, amorphization as indicated by XRD.

The weight loss of ammonia: less than 3.2 wt% per step. Because step contains also of some strongly bound water, the amount of ammonium is ca. 2.4 wt%. The maximum possible ammonium content achievable after complete ammonium ion-exchange of the clinoptilolite is ca. 4 wt%. Hence, the real ion exchange degree is <60%. This is also confirmed by the TPD values, which amounts to a maximum ammonium content of 1.76 wt%.

The total lost weight of NH<sub>3</sub> as in order from approximate 300 °C to 550 °C is 3% of clinoptilolite from TGA Fig. 27. In the theoretical formula of clinoptilolite is Na<sub>2</sub>, K<sub>2</sub>, Ca<sub>3</sub>Al<sub>6</sub>Si<sub>30</sub>O<sub>72</sub>·24H<sub>2</sub>O if 100% of cations was replaced by NH<sub>4</sub><sup>+</sup> the formula will become NH<sub>4</sub><sup>+</sup><sub>6</sub>Al<sub>6</sub>Si<sub>30</sub>O<sub>72</sub>·24H<sub>2</sub>O M=2694 the percentage of NH<sub>4</sub><sup>+</sup> will be approximately 108/2694\*100 ≈ 4%.

#### 4.1.9 Temperature-programmed desorption of ammonia TPD

The acidity of different activated HCLIN catalyst was studied by temperature-programmed desorption of ammonia. The maximum available acidity, concentration of BS, was determined by the thermal decomposition of the ammonium-exchanged clinoptilolite by heating to 700 °C (Fig. 28). The decomposition of the ammonium ions starts at ca. 230 °C.

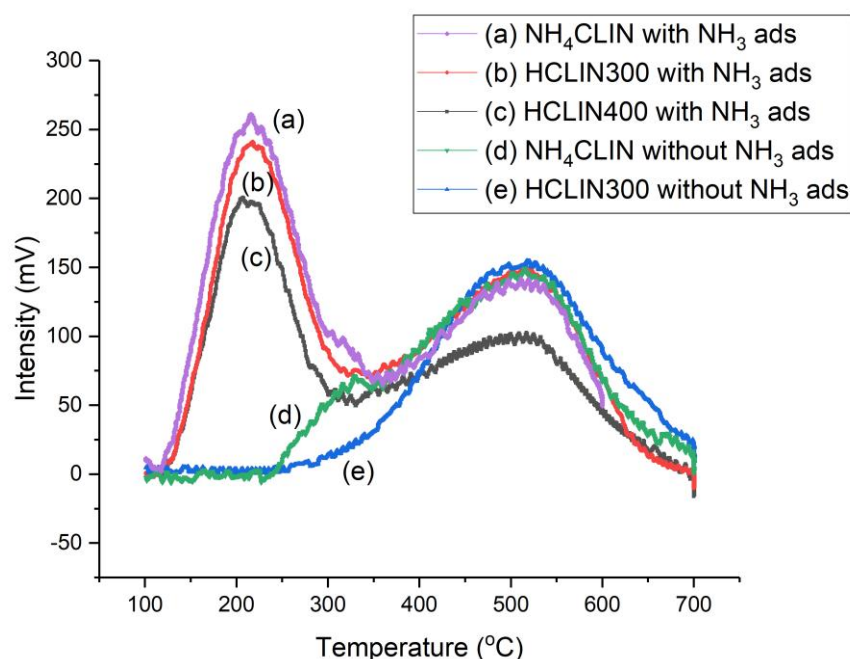


**Figure 28.** Temperature programmed ammonia desorption curves of  $\text{NH}_4\text{CLIN}$  (exchange condition: 0.2M  $\text{NH}_4\text{NO}_3$  at 80 °C for 2 hours two times; calcination at 300 °C and 400 °C in 30 minute) with  $\text{NH}_3$  flow treatment for  $\text{NH}_4\text{HCLIN}$  (a), HCLIN300 (b), HCLIN400 (c) (Pre-treatment of samples at 180 °C,  $\text{NH}_3$  gas loading at 100 °C). Without  $\text{NH}_3$  loading  $\text{NH}_4\text{CLIN}$  (d) and HCLIN300 (e).

In the first step until 320 °C, ammonia is desorbed from weak BS. Thereafter, ammonia desorption continues and reaches a maximum at *ca.* 520 °C followed by a decrease and tailing until 700 °C. The desorption of ammonia at higher temperatures is assigned to medium 400 °C and strong 520 °C acid sites. Correspondingly, the observed peak maximum indicates the presence of very strong BS in HCLIN catalysts. With HCLIN300 Fig. 28e mainly weaker acid sites are likely to compare Table 12. These BS are stable. Resorption of ammonia over these sites again Fig. 28 as well as in the  $\text{NH}_4\text{CLIN}$  sample Fig. 28a. The total amount of desorbed ammonia with the ammonia-loaded sample is increased compared to the ammonium-exchange sample, because ammonia adsorption occurs not only on the BS but also at weaker interacting adsorption sites in the pores. The temperature maximum of the low-temperature desorption is *ca.* 200 °C. Both desorption parts at low and high temperatures overlap. The low amount of ammonia desorbed from  $\text{NH}_4\text{HCLIN}$  until 300 °C is in line with a low specific surface area of this catalyst. The micropores are still blocked by the ammonium ions. In contrast, ammonia desorption occurs with heating to 400 °C, sample HCLIN400, is higher. The maximum acidity could be 1.0 mmol/g with HCLIN500 Table 12. Micropores are opened which leads to high nitrogen

uptake of these samples at low relative pressure which is assigned to the adsorption in the micropores, i.e. a large specific surface area is created.

**Table 12:** Amounts of ammonia released from NH<sub>4</sub>CLIN, and from remaining ammonium ions of thermal activated catalysts HCLIN300, HCLIN400, and HCLIN500, and calculated acidity measured by TPD of ammonia.

Sample	Total released NH <sub>3</sub> (μmol/g)	Estimated NH <sub>3</sub> (mass%)	Formed BS (μmol/g)	Conv. degree of NH <sub>4</sub> <sup>+</sup> to BS (%)
NH <sub>4</sub> CLIN	1405	2.4	0	0
HCLIN300	1155	1.96	250	17
HCLIN400	1002	1.7	403	28
HCLIN500	396	0.67	1009	72

The re-exchange of some BS H<sup>+</sup> ions by treatment with aqueous ammonium acetate solution shows that with HCLIN 300 complete re-exchange occurs (Fig. 28). However, with HCLIN400 and HCLIN500, the re-exchange to the NH<sub>4</sub>CLIN form is not complete. Only 90 and 65% of ammonium sites could be re-established with HCLIN400 and HCLIN500, respectively (Fig. 28 and 29). This difference is assigned to a loss of ion exchange sites, i.e. BS, at the framework aluminum by dehydroxylation of bridging Al-OH-Si during the dealumination process. The dehydroxylation increases with rising temperature (compare Scheme 6 above).

#### 4.1.10 Summary

The starting natural clinoptilolite CLIN is crystalline, with a crystallite size of ca. 27 nm. It contains ca. 90% of clinoptilolite beside of some crystobalite, quartz, field spars, and mordenite as shown by XRD. The clinoptilolite shows a high thermal stability of up to 600 °C.

The AAS analysis shows that the sample contains mostly potassium and calcium cations beside of some sodium and magnesium ions. Up to ca. 60% of the interstitial cations can be replaced by ammonium ions via ion exchange in aqueous 0.2 M solution of ammonium nitrate to give the NH<sub>4</sub>CLIN form. The framework composition (aluminum and silicon) was not changed by the ion exchange procedure.

The material consists of strongly aggregated nanoparticles of flat elongated plate like shape as shown by SEM and TEM images. The size of the nanoparticle varies between *ca.* 20-100 nm. With thermal treatment, the morphology of sample particles changes from a closed flat surface of sample CLIN and NH<sub>4</sub>CLIN to more rough surfaces and more holes are created at higher calcined samples. The porosity facilitates the mass transfer and, hence, the access of the active sites in the micro pores.

Nitrogen adsorption and desorption measurements show that the starting material is highly macro porous. This finding is in line with the SEM/TEM images. They show a rough surface and the presence of large holes in the agglomerated particles. The micropore system is blocked by the interstitial exchangeable zeolitic cations. The micro pore system is opened after the exchange of the cations by ammonium ions, followed by the thermal decomposition of the ammonium ions. Thereby ammonia is released leaving protons (H<sup>+</sup>) at the former cation sites forming the bridging Brønsted acid sites BS (Si-O(H)-Al). The obtained acid catalyst is called HCLIN.

The micropore system is opened after calcination beyond 300 °C. Maximum micro porosity is achieved after heating the material to 400 °C (specific surface area: 195m<sup>2</sup>/g and specific micro pore volume: 0.067cm<sup>3</sup>/g). Further increase of the calcination temperature to 500 °C–600 °C causes a decline of the micro porosity. Even the material is thermally stable. Some structural loss occurs already after calcination at 500 °C, followed by structural damage at 600°C.

The HCLIN catalyst is strongly acidic. Temperature-programmed desorption measurements show that the desorption of ammonia by NH<sub>4</sub><sup>+</sup> decomposition from NH<sub>4</sub>CLIN occurs in the temperature range of 250-500 °C. The catalyst contains weak, medium-strong and strong BS. Ammonium re-exchange experiments show a decrease of the ion exchange capacity after heating the catalyst at high temperature indicating some structural loss. This finding is in line with the observed decrease in the micro porosity after calcination at high temperature.

Investigation at low temperature gave more information of weak BS acid site and the effect of porosity and the location of the strong and medium BS inside of micropore or material channel. The ion exchange process could bring maximum NH<sub>4</sub> located inside the pore and channel of the clinoptilolite framework where NH<sub>3</sub> gas could not be retained as seen in NH<sub>3</sub>-TPD results of the samples. Calcination at too high temperature was the cause of acidity loss (Fig. 29). This finding will be clarified in the following catalysis part.

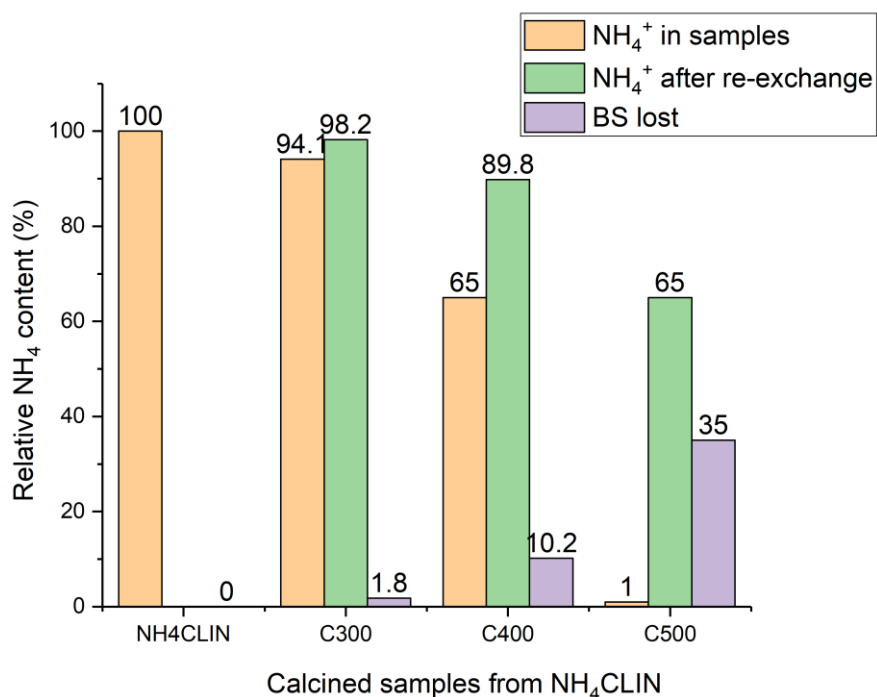


**Figure 29.** Decrease of the ammonium ion content of HCLIN compared to NH<sub>4</sub>CLIN after thermal activation at 300 °C to 500 °C, recreation by ammonium re-exchange, and the corresponding loss of BS by thermal dehydroxylation obtained from FTIR measurements.

## 4.2 Catalysis

This work aims to study the etherification of glycerol with *tert*-butanol over the heterogeneous acidic natural zeolite catalyst clinoptilolite HCLIN to the corresponding mono-, di- and tri-ether. The di- and tri-ether are the more wished products. However, glycerol is a very reactive molecule. It tends to form a resin by dehydration and polymerization products already during thermal heating. The latter are absorbed by the zeolite catalyst leading to blocking of the pores and active acidic Brønsted sites. Therefore, an assessment of catalyst preparation and testing was carried out to identify reasonable use of conditions of catalyst activation and testing or a detailed study of the catalytic performance of HCLIN catalysts.

### 4.2.1 Assessment of catalyst preparation and testing

The influence of the activation temperature, activation time, and ammonium ion exchange conditions on the catalytic conversion and porosity of HCLIN was tested in an order to identify reliable catalyst testing conditions assessment.

#### 4.2.1.1 Influence of the activation temperature

In a first step, the influence of the activation temperature on the conversion of glycerol over different alkaline HCLINs at a temperature of 110 °C was studied (Fig. 30). The amount of catalyst was 5% of the glycerol reactant mass. As starting material ammonium exchange linoptilolite NH<sub>4</sub>CLIN was activated at 230, 320, 420, 520 and 620 °C, respectively, for 30 minutes. During the activation, the ammonium ions are decomposed to the so-called active Brønsted acid H-form HCLIN. Thereby ammonia is released. The NH<sub>4</sub>CLIN sample calcined at 200 °C was not catalytically active (Fig. 31). Ammonium ions were not decomposed at this temperature. The samples thermally treated above 200 °C were catalytically active. The conversion of glycerol to glycerol *tert*-butyl ether increases during the course of reaction with the different activated catalysts. Surprisingly, the catalyst calcined at a low temperature of 320 °C shows the highest conversion activity although the concentration of active sites is low. Even the catalyst activated at 230 °C is active. The decomposition of ammonium ions to active protons H<sup>+</sup> just starts at this low temperature. *Ca.* 55% conversion is achieved after 6 h of reaction with this catalyst. With rising the activation temperature to 620 °C, the conversion drops markedly to *ca.* 3%. HCLIN600 is nearly inactive. Besides the mono-ether, only small amounts of di-ether are formed (<3%).

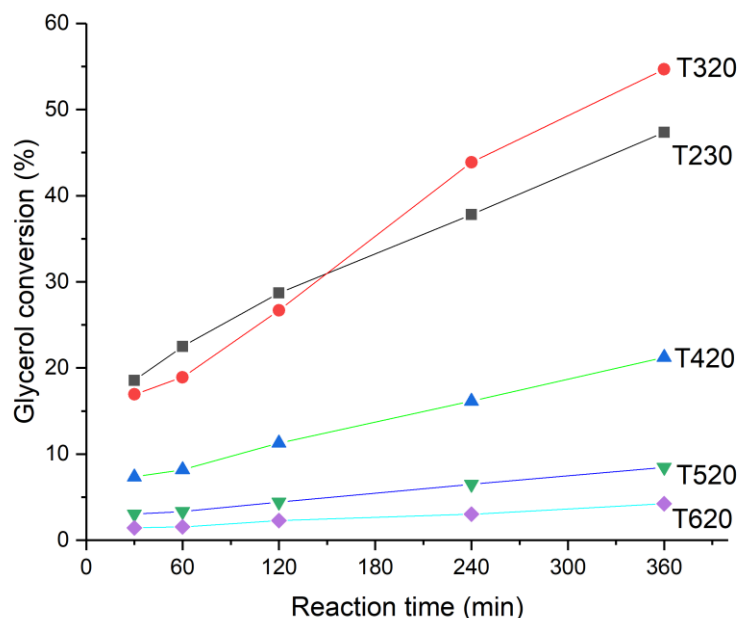


**Figure 30.** Influence of the activation temperature on the conversion of glycerol over HCLIN catalysts: NH<sub>4</sub>CLIN200, HCLIN300, HCLIN600 calcined for 30 min at 230, 320, 420, 520, and 620 °C. Reaction conditions: 110 °C in autoclave, Gly/TBA = 1/4, i.e. 5% catalyst per mass of glycerol. NH<sub>4</sub>CLIN prepared with two times exchange with 0.2 M NH<sub>4</sub>NO<sub>3</sub> solution 80 °C for 2 hours each).



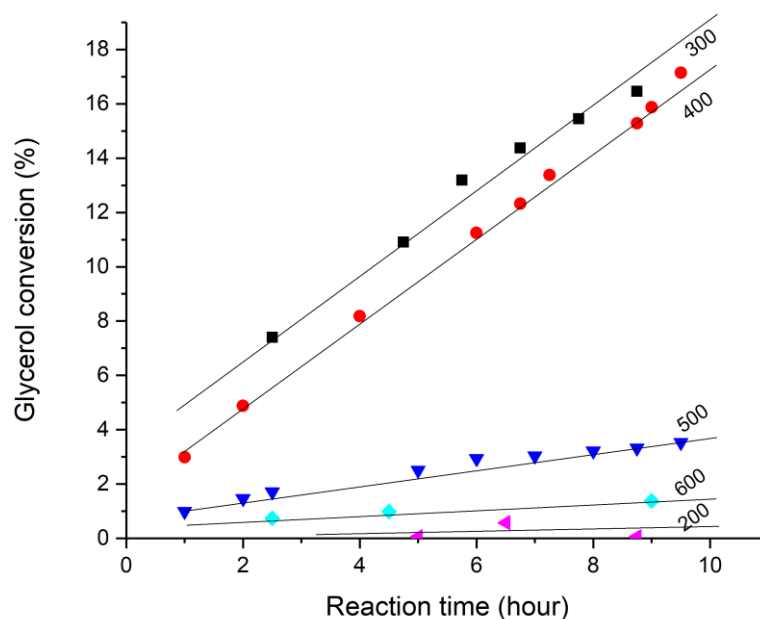


**Figure 31.** Glycerol conversion vs. calcination temperature: HCLIN200, HCLIN300, HCLIN600 catalysts, calcined in 1 min at 200, 300, 400, 500, and 600 °C (achieved oven temperatures). Reaction condition: 86 °C under reflux, Gly/TBA = 1/4, catalyst/Gly mass = 7.5 %. Catalyst preparation was used  $\text{NH}_4\text{NO}_3$  0.5M.

In the second set of experiments, the reaction temperature was decreased from 110 °C to 86 °C to enable to work simply under reflux conditions. Only mono-ether was formed under these mild reaction conditions under normal pressure and at a low temperature of 86 °C, the oiling point of *t*-butanol TBA. For compensation of the lower temperature, the catalyst loading was increased from 5 to 7.5 mass per glycerol (Fig. 31). Again, the catalyst calcined at a low temperature of 300 °C shows the highest activity, closely followed by the catalyst calcined at 400 °C. Although the catalyst loading was increased, the decrease of the reaction temperature led to a marked increase in the conversion to ca. 13% after 6 h of reaction. The conversions increase nearly linearly even after a long reaction time of ca. 9-10 h. The latter points to high stability of the active catalysts. The catalyst activity increases markedly with raising calcination temperature. Catalysts calcined at 500 and 600 °C show very low activity. The glycerol conversion was lower than 4% after 6 h of reaction. Interestingly, the conversion of glycerol starts rapidly after rising the pre-treatment temperature from 200 to 230 °C. Generally, the conversions increase nearly linearly with the reaction time. This confirms the stability of the catalyst during the catalytic reaction.

The results show that the linoptilolite catalyst achieves the highest performance when the starting ammonium form of linoptilolite is only shortly calcined for one minute at

Comparatively low activation temperature. Therefore, the catalyst HCLIN300 activated at 300 °C shows the highest activity. NH<sub>4</sub>CLIN fired at 200 °C shows no activity. The activity increases with rising temperature to 600 °C.

#### 4.2.1.2 Influence of the activation temperature on the BET specific surface area

The activation temperature also influences the specific surface area (Table 13). The specific surface areas of the modified ammonium clinoptilolite NH<sub>4</sub>CLIN belong mainly to their internal micropore system, while the contribution of the external surface is lower and is similar to the starting CLIN, NH<sub>4</sub>CLIN, and HCLINs catalysts. Interestingly, the specific surface area increases only slightly with HCLIN300. HCLIN400 and HCLIN500 show the high specific surface area as expected.

**Table 13:** Specific surface area of clinoptilolite catalysts calcined at different temperatures: 200, 300, 400, 500, 600 °C.

Samples/ BET treatment	HCLIN200	HCLIN300	HCLIN400	HCLIN500	HCLIN600
BET Surface area (cm <sup>2</sup> /g)	35.8	42.7	194.9	150.8	33

#### 4.2.1.3 Influence of ammonium ion exchange conditions

Aqueous ammonium nitrate solution was used for the ammonium ion exchange of the starting clinoptilolite. The ammonium ion exchange was carried out with different concentrations of ammonium nitrate solutions and different reaction times (Table 14). The obtained ammonium exchange samples were activated at 300 °C. The activation conditions for the preparation of the HCLIN catalysts were also varied. An the catalytic activity in the conversion of glycerol with TBA was tested (Fig. 32). Best results were obtained for a catalyst exchange twice with a 0.2 M ammonium nitrate solution at 80 °C for 2 h and activated again at 300-320 °C for 1 min.

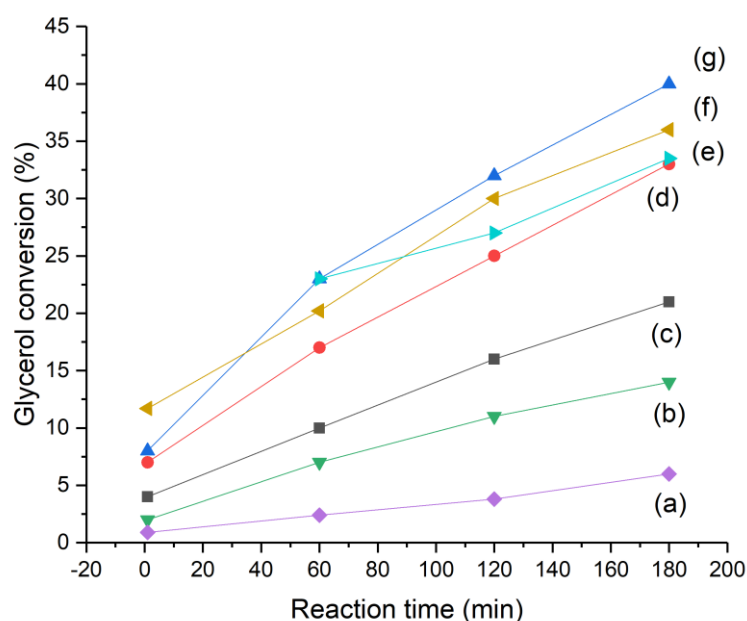


**Figure 32.** Glycerol conversion Vs reaction time  $t$  over HCLIN300 catalysts, calcined  $320\text{ }^{\circ}\text{C}$  in 1 min. Condition:  $110\text{ }^{\circ}\text{C}$  in autoclave, reaction time: 1 min, 1 h, 2 h, and 3 h, Gly/TBA = 1/4, catalyst/Gly mass = 5 %. Ion exchange with different concentration of  $\text{NH}_4\text{NO}_3$  solution a) 0.05 M, b) 0.1 M, c) 0.4 M, d) 0.2 M, and two times ion exchange with 0.2 M solution e), f) calcination at  $300\text{ }^{\circ}\text{C}$  in 1 min, 30 min, and g) at  $320\text{ }^{\circ}\text{C}$  1 min.

The activity conversion of HCLIN catalysts increases with the ammonium ion exchange at concentrations below 0.2 M. This increase is closely related to the concentration of active sites created under these ion exchange conditions. Concentrations lower than 0.2 M are not useful because of the loss of activity by lower BS concentration. On the other hand, ammonium ion concentrations larger than 0.4 M do not increase the catalyst activity, the number of active sites. Finally, the use of 200 mL of 0.2 to 0.5 M ammonium nitrate exchange solutions with a loading of 10 g of linoptilolite is useful with respect to catalyst activity and sustainable saving means. The ion exchange process is more efficient if we use a concentration of 0.2 M instead of *ca.* 0.5 M and renew two times the solution or ion exchange.

**Table 14:** Conditions of catalyst preparation by ion exchange and calcination, amount of starting material in  $\text{NH}_4\text{NO}_3$  concentration solution, the temperature of ion exchange, calcination condition.

Reaction solution	Clinoptilolite/ $\text{NH}_4^+$ concentration	Exchange T° and time	Catalyst activation
0.5 M	2g/50mL 0.5M	80 °C, 1h	200-600 °C, 1 min
0.4, 0.2, 0.1, 0.05 M	2g/50 mL of 1.6, 0.8, 0.4, 0.2g $\text{NH}_4\text{NO}_3$ ,	autoclave 4h, 80 °C	320 °C, 1min
0.2 M	10g/250mL 0.2M	80 °C, 2h/2 times	300, 350, 400-600 °C, 1 min
0.2 M	10g/250mL 0.2M	80 °C, 2h/2 times	200-600 °C 30 min

#### 4.2.1.4 Conclusion of assessment

The acidified natural zeolite clinoptilolite HCLIN is catalytically active in the etherification of glycerol with tertiary butanol and shows improved selectivity to di-ether at selected catalyst activation and reaction conditions. The di-ether is the wished product for use as a diesel fuel additive.

Interestingly, the highest conversion is observed with the soft thermally activated weak acidic HCLIN300, where the micropore system is still closed and, conclusively, the reaction takes place at or near the catalyst surface.

In contrast, the conversion is declined with medium and strong acidic HCLIN400 and HCLIN500 although the pore system is opened and the high specific surface area should favor the conversion. Obviously, strong acid sites lead to the formation of “coke” by glycerol decomposition, which poisons the catalytic active sites.

Therefore, the catalytic performance of HCLIN is very sensitive to the catalyst preparation, i.e. the material workup and ammonium ion exchange conditions, and thermal activation procedure as heating rate, calcination temperature, and time.

Although the catalyst is thermally stable, some loss of BS is observed after calcination at temperatures beyond 400 °C. About 35% of BS is lost by dehydroxylation at 500 °C. HCLIN contains the medium strong, strong, and very strong acid sites.

Reaction conditions as the reaction temperature, reaction time, and catalyst loading markedly influence the catalytic performance. The water released during the course of the reaction by the condensation of alcohols is a limiting factor. Consequently, the hydrophobicity of the system should play an important role. Indeed, alcohols containing tertiary alkyl groups show superior conversion and selectivity.

The HCLIN catalyst is reusable after washing with water and alcohol.

## 4.2.2 Catalytic performance

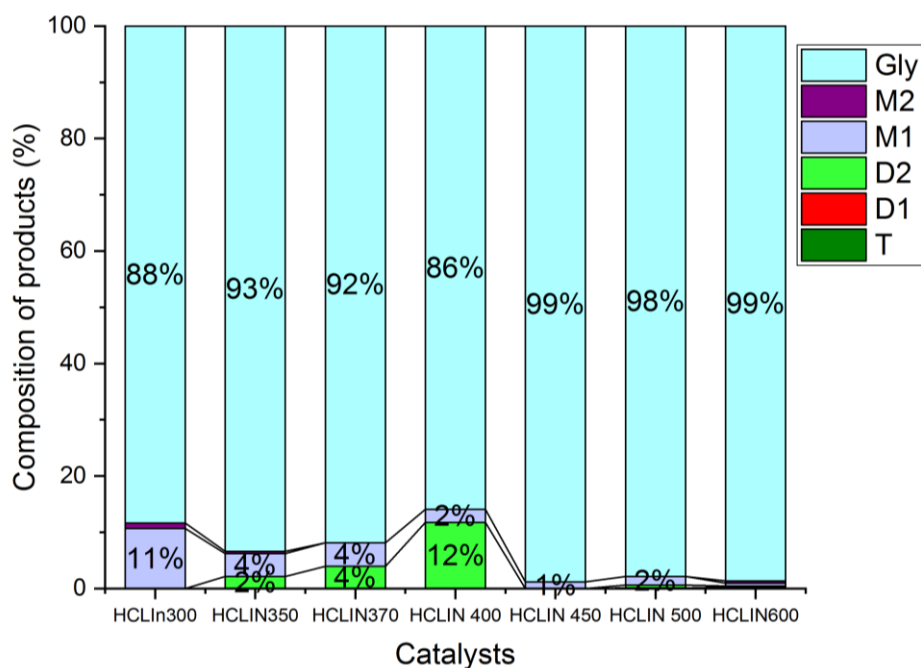
The catalytic performance was investigated in detail using HCLIN catalysts prepared from an  $\text{NH}_4^+$  exchanged clinoptilolite, which was two times exchanged for 2 hours with a 0.2 M ammonium nitrate solution at 80 °C. The influence of activation temperature of the catalyst as well as of various reaction parameters was investigated. For comparison, the etherification was also tested with other primary, secondary and tertiary alcohols.

The starting standard conditions of reactions were: starting materials glycerol and *tert*-butanol, reaction temperature 110 °C, the ratio of reactant Gly/TBA= ¼ by mass, autogenous pressure in the autoclave, 5 %wt catalyst loading per mass of glycerol, catalyst HCLIN300 which shows the highest activity.

### 4.2.2.1 Influence of catalyst activation on the activity and selectivity

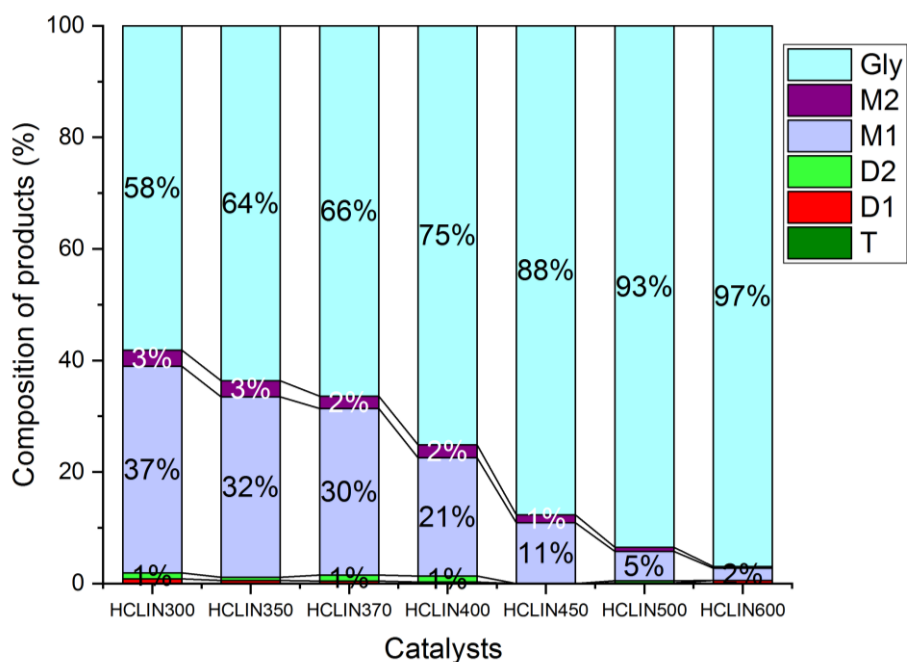
#### ➤ *Influence of the activation temperature*

Figure 33 shows the influence of the activation temperature of the catalyst on the conversion of glycerol to mono- and *tert*-butyl ether M and D after 1 min. of reaction. Usually, a strong increase in the conversion is expected with the rising activation temperature of the catalyst due to the liberation of BS by the decomposition of the exchange ammonium ions and the corresponding opening of the internal pore system, i.e. the increase of the specific surface area. Table 13 above. The activity of BS increases with the activation temperature too. Surprisingly, a high conversion of ca. 11 is already observed at a low activation temperature of 300 °C with HCLIN300 after a short reaction time of 1 minute. Mostly the mono-ether M1 is formed. Further stepwise increase of the activation temperature to 400 °C leads only to a small increase of the conversion to 14. However, the selectivity to the *tert*-ether is markedly increased to ca. 85. The formation of the *tert*-ether D2 increases gradually with the activation temperature starting from 300 °C to 350 °C, 370 °C and 400 °C from 0 to 12. Obviously, mono-ether is formed already with low activity. The formation of the *tert*-ether requires a higher activity site density and probably stronger BS. HCLIN400 provides more activity and medium-strong BS.



**Figure 33.** Influence of the catalyst activation temperature on the glycerol conversion to M1, M2, D1, D2 ethers over different catalysts. Reaction condition: 110 °C, 1 min just after reaching the reaction temperature in the autoclave), Gly/TBA =1/4, catalyst/Gly mass = 5 %, reaction time: Using catalyst is HCLIN300 short time activated for 1 min at 300 °C.

Interestingly, catalysts activate at a higher temperature as HCLIN450, HCLIN500 and HCLIN600 are less active and show only a low conversion of <3% after 1 minute of reaction.



**Figure 34.** Influence of the catalyst activation temperature on the glycerol conversion to M1, M2, D1, D2 ethers after 4h of reaction over different catalysts HCLIN300 to HCLIN600 (short-time activation of 1min). Reaction condition: 110 °C, in autoclave, Gly/TBA =1/4, catalyst/Gly mass = 5 % in reaction time: 4h.

The in in gs o s e r v e at the onset o r e a t i o n are somewhat h a n g e with the o u r s e o t h e r e a t i o n . T h e a i t y o H C L I N 3 0 0 is m a r k e l y l o w e r 0.25 mmol/g t h a n t h a t o H C L I N 4 0 0 0.468 mol/g a n d H C L I N 5 0 0 0.76 mmol/g . A t t h e s a m e t i m e , t h e s p e i i s u r a e a r e a is i n r e a s e f r o m c a . 36 m<sup>2</sup>/g H C L I N t o c a . 195 m<sup>2</sup>/g a n d 151 m<sup>2</sup>/g , r e s p e t i v e l y . T h e r e o r e , a n i n r e a s e o t h e c o n v e r s i o n w i t h r i s i n g t e m p e r a t u r e w o u l d e x p e c t e . B u t , i n e e , t h e o p p o s i t e i s o s e r v e . H C L I N 3 0 0 s h o w s t h e h i g h e s t a t i v i t y / o n v e r s i o n w h i c h i n c r e a s e s m a r k e l y w i t h r i s i n g a t i v a t i o n t e m p e r a t u r e s . I t i s c o n l u d e t h a t t h e s t r o n g a i s i t e s o r m e a t h i g h e r a t i v a t i o n t e m p e r a t u r e s a v o r t h e f o r m a t i o n o f g l y e r o l e c o m p o s i t i o n p r o d u c t s w h i c h b l o c k t h e a t i v e s i t e s . A s h a r p d e c l i n e o f t h e c a t a l y t i c a t i v i t y o s e r v e , s p e c i a l l y w i t h h e a t i n g e y o n 400 °C . T h e m a j o r p a r t o f t h e p o r e s y s t e m i s s t i l l l o c k e d w i t h H C L I N 3 0 0 . O n l y c a . 15 % o f t h e a m m o n i u m i o n s a r e e x c h a n g e d . T h e r e o r e , i t i s c o n l u d e t h a t t h e e t h e r i f i c a t i o n o f g l y e r o l w i t h t e r t - b u t a n o l p r o c e e d s a t o r n e a r t h e c r y s t a l s u r f a c e o f t h e l i n o p t i l o l i t e a n d r e q u i r e s o n l y w e a k B S . T h e s t r u c t u r e o f t h e H C L I N c a t a l y s t i s s t r o n g l y e s t r o y e a t e r a l i n a t i o n a t 600 °C w i t h a c o r r e s p o n d i n g l o s s o f t h e c a t a l y t i c a t i v i t y . I n c o n t r a s t t o t h e s h o r t r e a c t i o n t i m e o f 1 m i n , a l m o s t n e a r m o n o - e t h e r i s o r m e d ( F i g . 34 ) . T h i s i s d u e t o t h e f o r m a t i o n o f w a t e r d u r i n g t h e c o u r s e o f t h e e t h e r i f i c a t i o n . T h e w a t e r i s p r e f e r e n t i a l l y a s o r b e d a t t h e z e o l i t e c a t a l y s t s u r f a c e . I t c o m p e t e s w i t h t h e T B A a n d a v o r s t h e a d d i t i o n a l r e a c t i o n o f d i - e t h e r t o m o n o - e t h e r . T h i s p o i n t s t o a L a n g m u i r - H i n s h e l w o o d m e c h a n i s m , w h e r e t h e r e a c t i o n p a r t n e r i s a s o r b e d a t t h e c a t a l y s t s u r f a c e .

A d d i t i o n a l l y , s o m e l o s s o f a i t y b y o x y d a t i o n i s o s e r v e d . T h e a l i n a t i o n o f t h e c a t a l y s t a t a t e m p e r a t u r e o f 500 °C c a u s e s a l o s s o f a i s i t e s b y c a . 35 % a s s h o w n b y F T I R m e a s u r e m e n t s o f H C L I N 5 0 0 a f t e r r e - e x c h a n g e o f t h e p r o t o n s b y t r e a t m e n t w i t h a m m o n i u m a c e t a t e s o l u t i o n ( T a b l e 15 ) . T h e c h a n g e o f t h e a m m o n i u m c o n t e n t w a s a l l o w e d b y t h e c h a n g e o f t h e i n t e n s i t y o f t h e a m m o n i u m v i b r a t i o n a n d c o m p a r e d t o t h e i n t e n s i t y o f t h e a n t i s y m m e t r i c T O T l a t t i c e v i b r a t i o n a n d . T h e l a t t e r w a s u s e d a s i n t e r n a l s t a n d a r d ( F i g . 35 ) . W i t h o u t l o s s o f s i t e s , t h e a m m o n i u m c o n t e n t o f t h e s t a r t i n g N H<sub>4</sub>C L I N s h o u l d b e r e / e s t a b l i s h e d a f t e r r e - e x c h a n g e o f t h e a m m o n i u m . H o w e v e r , t h e a c t u a l c o n t e n t i s m a r k e l y l o w e r w i t h t h e a l i n e d s a m p l e s . T h e c a t a l y t i c a t i v i t y i s i n c r e a s e d ; t h e c o n v e r s i o n s o f G l y a r e l o w s h o w n i n F i g u r e 34 .

**Table 15:** Influence of the calcination temperature of HCLIN catalysts on the degree of ammonium re-exchange determined by IR spectroscopy from the change of the intensity of ammonium  $\text{NH}_4^+$  deformation band. The intensity of the asym TOT vibration band used as internal standard.

Samples	TOT <sub>Asym</sub> intensity (a.u.)	$\text{NH}_4^+$ intensity (a.u.)	$\text{NH}_4^+$ / TOT <sub>Asym</sub> intensity ratio	Degree of $\text{NH}_4^+$ re-exchange (%)
HCLIN500	7.2	0	0	0
Re-HCLIN500	7.2	0.478	0.0664	65.2
HCLIN400	7.22	0.478	0.0662	65
Re-HCLIN400	8.01	0.732	0.0914	89.8
HCLIN300	7.64	0.732	0.0958	94.1
Re-HCLIN300	8.21	0.821	0.1	98.2
$\text{NH}_4\text{CLIN}$	9.31	0.948	0,1018	100

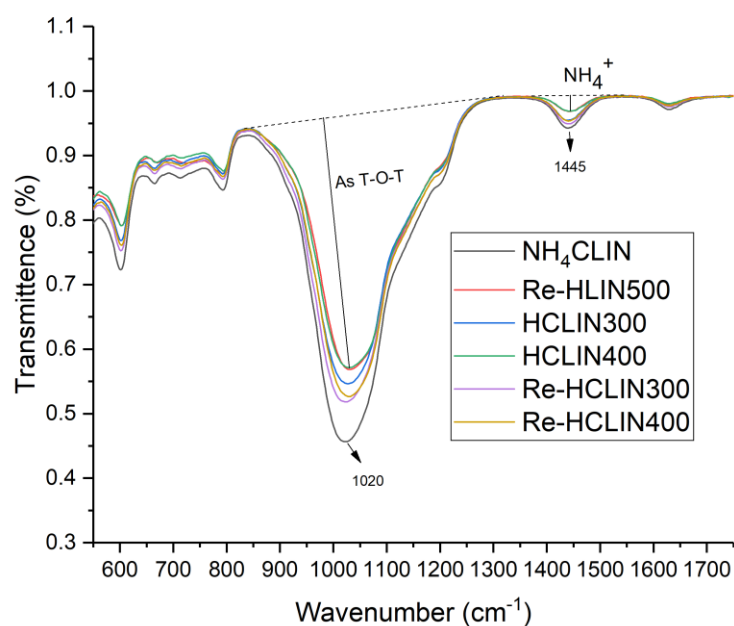


**Figure 35.** IR spectra of ammonium exchanged  $\text{NH}_4\text{CLIN}$ , HCLINs obtained after calcination at 300, 400, and 500 °C and corresponding ammonium re-exchanged samples Re-HCLIN. The deformation vibration band at 1440  $\text{cm}^{-1}$  corresponds to the vibration of the ammonium ion  $\text{NH}_4^+$ .



➤ Influence of the calcination time

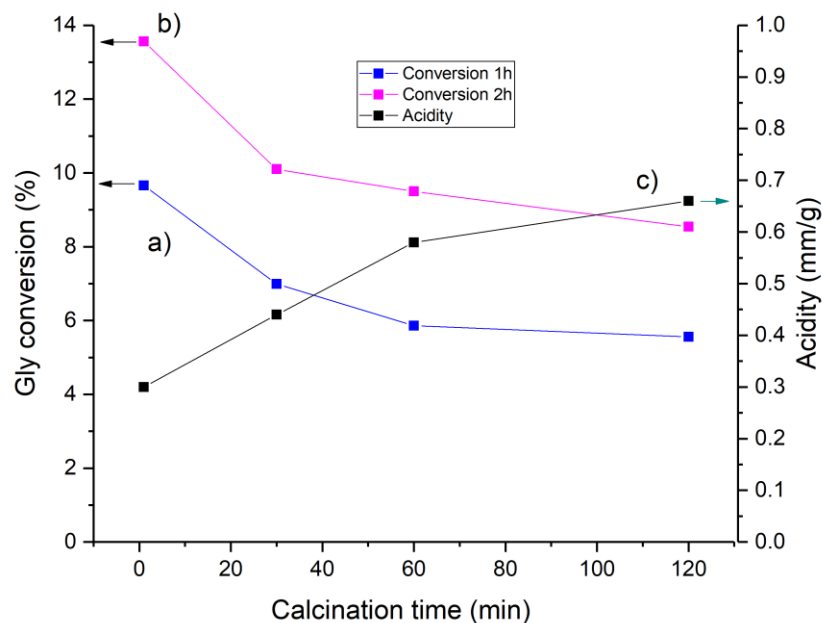


**Figure 36.** Influence of the calcination time of HCLIN300 catalyst on the conversion of glycerol with TBA after a) 60 min and b) 120 min of etherification reaction, c) influence on acidity of catalyst (Table 16). Reaction condition: Gly/TBA = 1/4, catalyst/Gly mass = 5 %, 110 °C in autoclave).

**Table 16:** Influence of calcination time to the decomposition of ammonium ion to BS during the formation of HCLIN300 by activation of NH<sub>4</sub>CLIN at 300 °C.

Calcination time (at 300 °C)	asymT-O-T/NH <sub>4</sub> <sup>+</sup> intensity (a.u.)	NH <sub>4</sub> <sup>+</sup> /asym T-O-T intensity ratio	NH <sub>4</sub> <sup>+</sup> content (%)
0 min <sup>*)</sup>	9.105/0.838	0.092	100
1 min	8.9/0.57	0.06412	69.7
30 min	8.92/0.461	0.05165	56
1h	9.123/0.351	0.03847	41.8
2h	8.234/0.258	0.03133	34

<sup>\*)</sup> starting NH<sub>4</sub>CLIN,

The activity of catalysts is also affected by the calcination time as shown in Figure 36. The highest activity of HCLIN300 catalysts, i.e. conversion, is achieved just after reaching the required activation temperature and activation time *ca.* 1 minute. The calcination time is counted after reaching the wished calcination temperature. Prolonged calcination causes a decrease in the glycerol conversion. After 1h of reaction, the conversion decreases from *ca.* 10 to 5 after prolongation of the activation time to 120 min (Fig. 36a). After 2h of reaction, the

conversion increase from *ca.* 15 to 80 (Fig. 36-). At the same time, the activity, related with the amount of exchanged  $\text{NH}_4^+$  ions, increases from *ca.* 0.27 to *ca.* 0.67 mmol/g. Generally, the activity, i.e. conversion on the catalyst, increases with prolonged reaction time. The results show that the clinoptilolite catalyst achieves the highest performance when the starting ammonium form of clinoptilolite is only shortly calcined for one minute at the designated activation temperature.

The catalyst HCLIN300 activated at 300 °C for short time shows the highest activity. The pure ammonium exchange  $\text{NH}_4\text{CLIN}$ , fired at 200 °C, shows no activity. The activity increases with rising temperature to 600 °C.

#### 4.2.2.2 Influence of reaction conditions on the activity and selectivity

##### ➤ Influence of the reaction time

The influence of the reaction time on the conversion and the formation of mono- and di-ethers is shown in Figure 37 in terms of product yields and remaining not converted glycerol. The course of the reaction was followed over a period of 24 hours using the most active catalyst HCLIN300 activated at 300 °C. The reaction temperature was 110 °C. After a rapid increase of the conversion in the first 6 hours, the reaction proceeds slower. An increase of non-converted glycerol from *a.* 45 to 27 is observed after 24h of the reaction. This confirms the stability of the catalyst during the course of reaction. The mono-ether is the main reaction product. *ca.* 51 and 63 mono-ether are formed after 6h and 24h of reaction, respectively. The formation of di-ether and some tri-ether is markedly lower and increases from *ca.* 3 to *ca.* 10 after 24h. Mono- and di-ethers are formed successively. The catalysts HCLIN400 and HCLIN500, which exhibit higher activity and porosity, do not overcome the conversion obtained with the less active and less porous catalyst HCLIN300. Obviously, the pores and active sites of these catalysts are blocked by glycerol decomposition and reaction products formed at strong acid sites. Catalysis takes place at the outer surface of the catalyst particles.

In conclusion, the catalysts are stable over a long time of reaction. Prolonged reaction time of 24h favors markedly the increase of the conversion to *ca.* 73 and the yield of mono- and di-ethers *ca.* 63 and 10, respectively, with HCLIN. Therefore, the reaction time is a significant parameter.

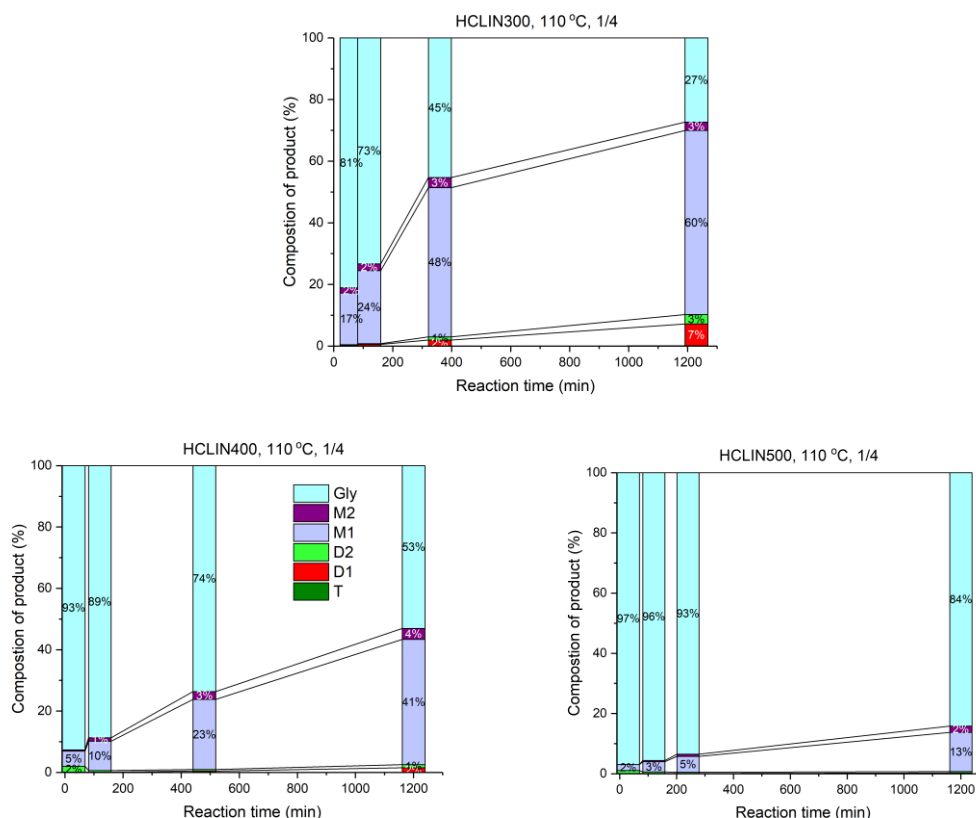


**Figure 37.** Glycerol conversion vs. reaction time over HCLIN300, catalyst 30 min calcination) - change of the composition of the reaction solution. Condition: 110 °C in autoclave, Gly/TBA =1/4, catalyst 5 % per mass of glycerol, after reaction time: 30 min, 2h, 6h 20h, HCLIN400 30min, 2h, 8h, 24h), HCLIN500 30min, 2h, 6h, 24h).

➤ *Influence of the Gly to TBA ratio*

The influence of the Gly/TBA ratio on the conversion and the formation of mono and di-ether is shown in Figure 38. The decrease of the glycerol to *tert*-butanol ratio, i.e. the enhancement of the TBA content from the standard condition 1/4 to 1/5 and 1/8 have only minor influence on the conversion of glycerol. The remaining glycerol content changes from *ca.* 45, 49 and 46 after 6h, from 27 to 28 and 22 after 24h of reaction, respectively. Correspondingly, the yield of the mono- and di-ether varies from *ca.* 73 to 72 and 78 after 24h, respectively. The selectivity to di- and tri-ether is *ca.* 13 after 24 hours.

In summary, the influence of the Gly/TBA molar ratio is comparatively low. The conversions of glycerol reach 72 to 78 after 24h of reaction. The yield of mono-ether reaches 63 to 68%. The yield of di- and tri-ether reaches *ca.* 10%. The M1 to M2 mass ratio is a. 60/3 to 65/3, and the D1/D2 ratio is about 2, after 24 h of the reaction.

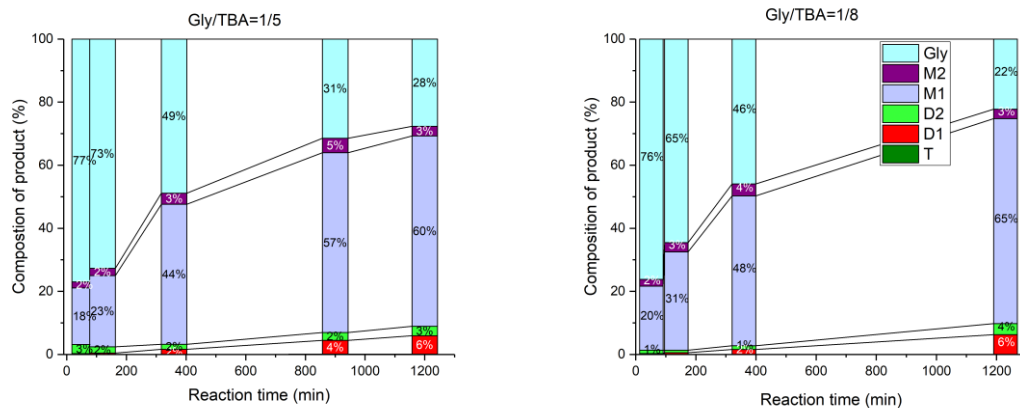


**Figure 38.** Influence of the Gly/TBA ratio on the content of M1, M2, D1, D2, T, Gly of the reaction solution with time: 1min, 2h, 6h 20h 30 min, 2h, 6h, 20h. Gly/TBA ratio=1/5 (left) and 1/8 (right), reaction temperature: 110 °C

➤ *Influence of reaction temperature*

The influence of the reaction temperature on the conversion of glycerol and the formation of mono- and di-ether over HCLIN300 is shown in Figure 39. The reaction temperature was increased from 110 °C to 140 and 160 °C, respectively. With rising temperature to 140 °C, a strong increase of the conversion to *ca.* 78% is observed after 4h of reaction. Further rise of the temperature to 160 °C leads only to a further moderate increase of 5% to *ca.* 83% conversion. At the same time, the selectivity to di-ether increases from *ca.* 4% to 34% at 160 °C. The formation of tri-ether is always very low and reaches only *ca.* 1.7% at 160 °C. The highest increase in conversion is observed between 110 °C and 140 °C *ca.* 78%. Higher temperature favors the formation of the di-ether, which might require higher activation energy. Additionally, the amount of disturbing/competing adsorbed water at the catalyst might be lowered. In summary, the reaction temperature has an important influence on the conversion of glycerol as well as the selectivity to mono-, di-, and tri-ether.

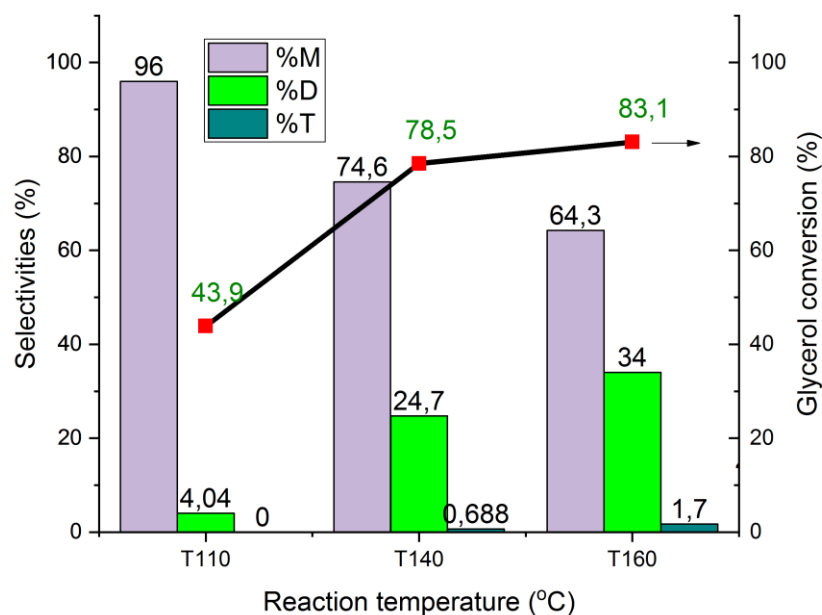


**Figure 39.** Influence of the reaction temperature on the conversion of glycerol to M1, M2, D1, D2 ethers and on the selectivity over different catalysts. Conditions: in an autoclave, Gly/TBA =1/4, catalyst content 5% per mass Gly, HCLIN300, reaction time 4h, reaction temperature 110 °C 140 and 160 °C.

➤ *Effect of catalyst loading for HCLIN300*

The influence of the catalyst loading on the conversion of glycerol and the selectivity to mono-, di- and tri-ether is shown in Figure 40. The catalyst loading was varied between 2.5 and 10. The decrease of the loading by 50% from 5 to 2.5 leads to a markedly increase in the conversion from ca. 69 to 59. In contrast, the doubling of the loading causes only an increase of the conversion by 10%, i.e. the conversion was increased slightly to ca. 76. However, the selectivity to di-ether was increased markedly from ca. 13.7 to 20.7%.

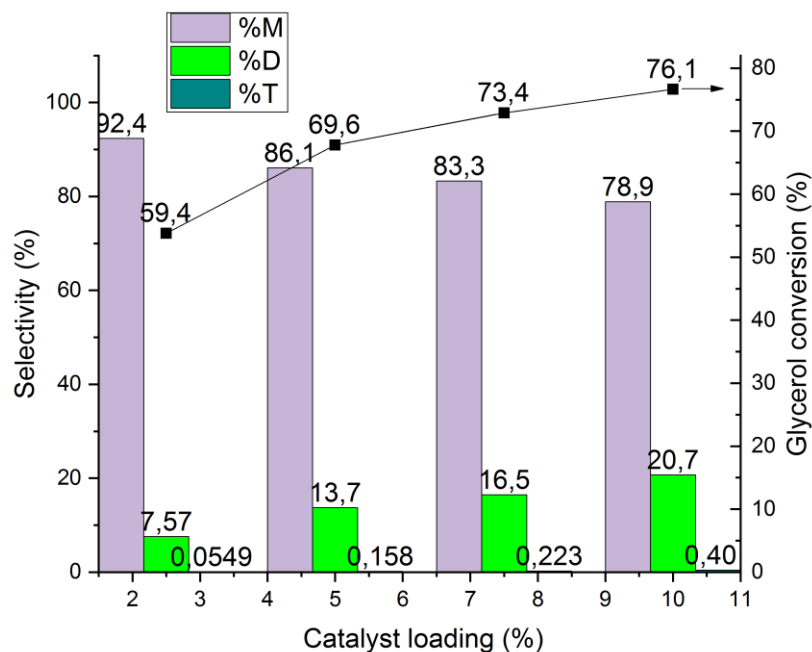


**Figure 40.** Influence of the catalyst loading on glycerol conversion to mono-ether M, di-ethers D, and tri-ether T (rare to see <1%) over HCLIN300. Catalyst loading: 2.5, 5, 7.5, 10 % per mass of glycerol. Reaction conditions: 110 °C, 4h reaction time, in an autoclave, Gly/TBA=1/4. The catalyst obtained by 30 min calcination HCLIN300.

In sum, the increase of the catalyst loading from ca. 2.5 to 10, led to an increase of the conversion of glycerol to mono- and di-ethers by ca. 25% only from 59.4 to 76.1%. Whereas the selectivity to di-ethers increased by a factor of 3 from ca. 7.57 to 20.7% mainly at the expense of mono-ethers. The increase in amount of molecular sieve catalyst and increase in the amount of solvent water adsorbed in internal pores in the reaction mixture and a more “dry” catalyst is present. Both should favor the formation of di-ether.

The catalyst loading has an important impact on the selectivity to di-ether, which is markedly improved from ca. 7 to 21% by increasing the catalyst loading from 2.5 to 10% with respect to the glycerol content.

#### 4.2.2.3 Catalyst reuse

Re-usability and stability of the catalyst

The re-usability of the catalyst was tested with the most active catalyst HCLIN300. For this, the used catalyst was washed with water or ethanol.

The reusability of the catalyst was performed three times to prove the advantages of heterogeneous linoptilolite catalyst or reuse. The solid catalyst was separately sedimentation or centrifugation. The supernatant phase was decanted. The reused catalyst

was washed with deionized water, ethanol and dried in an oven at 110 °C overnight. The conversion of glycerol in dependence on the reaction time or the starting catalyst and reuse catalysts are shown in Figure 41. The results show that the catalyst can be reused. The catalyst was three times reused and shows a high conversion after 2 hours of reaction. An activity loss in terms of conversion of ca. 23% is observed only, ca. 77% of activity in terms of conversion remains. Ca. 97% of activity remains after the first run in two hours of reaction. Both 30 and 5% catalyst loading of HCLIN300 were used in the following experiments (Fig. 42a and b). With low catalyst loading, the differences and losses are larger.

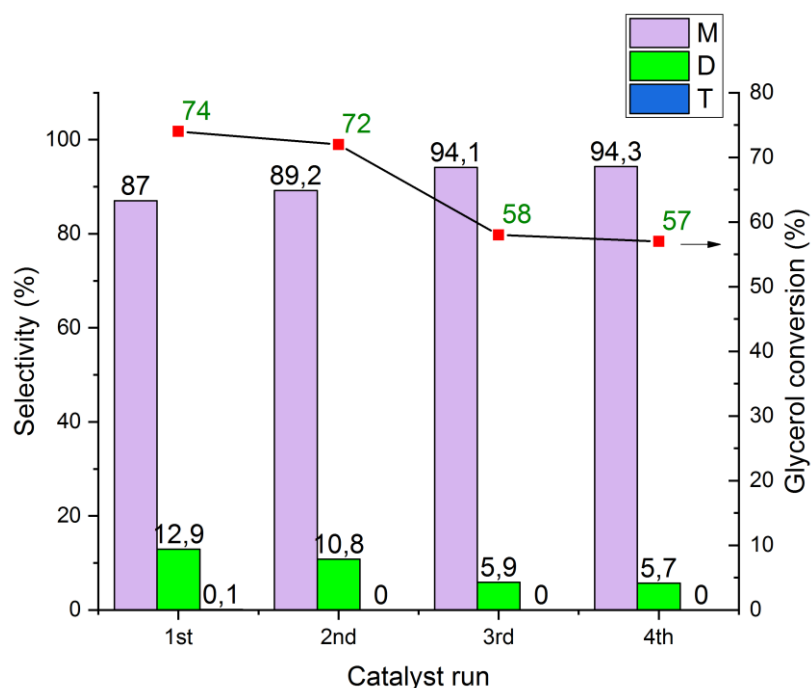


**Figure 41.** Influence of the re-use of HCLIN300 on the selectivity to mono-, di, and tri-ether (M, D, T) in the etherification of glycerol and *t*-butanol. Catalyst: HCLIN300 (NH<sub>4</sub>CLIN ion-exchanged solution 0.2 M, 30 min calcination), reaction condition: 110 °C in autoclave for 2h, Gly/TBA =1/4, catalyst/Gly mass ratio = 0.3.

Besides the loss of activity, an increase in the selectivity to mono-ethers due to the expense of di-ether was observed (Fig. 41). The latter could be due to the increase in present water in the catalyst after washing.

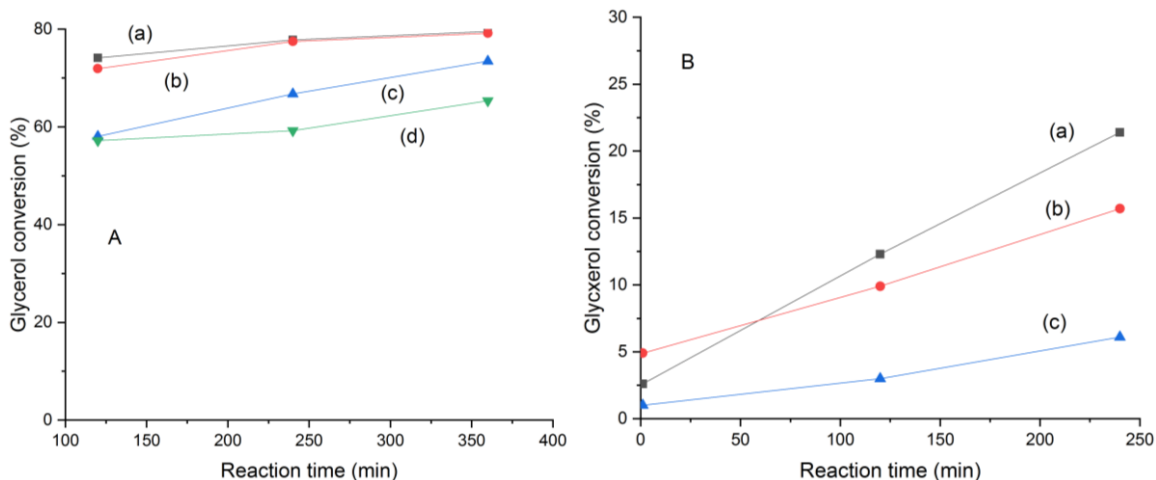


**Figure 42.** The conversion of glycerol reaction using HCLIN300 with a catalyst loading of A) 30% and B) 5% with respect to the glycerol content: a) NH<sub>4</sub>CLIN - ion-exchanged with 0.2M NH<sub>4</sub>NO<sub>3</sub> solution, 30 min. calcination), b) first, c) second, and d) third reuse. Reaction condition: 110 °C in autoclave 2h, Gly/TBA=1/4.

Therefore, the effect of the catalyst washing with water and ethanol was analyzed by thermogravimetric analysis. In effect, the water washed reuse catalyst contains markedly more loosely bound water. Obviously, water is a key factor limiting the formation of di- or tri-ether. Figure 43 shows the TG and DSC curves obtained with the use as well as with water and ethanol washed samples. Washing with ethanol leads to enhance removal of loosely bound water as seen by the decrease of the DSC peak at 100 °C and the corresponding weight loss in the TG curve. Simple washing of the catalyst is sufficient for the reactivation of the catalyst.

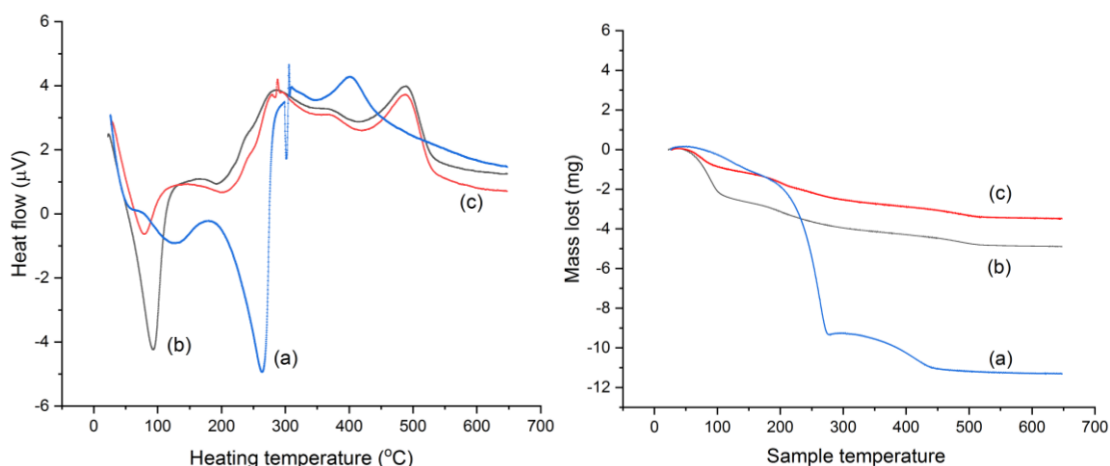


**Figure 43.** DSC (left) and TG curve (right) of the used catalyst and the reactivated catalyst: a) Used catalyst HCLIN300 without washing (—), b) separated catalyst washed with water (—), c) separated catalyst washed with ethanol (—).

In detail, the obtained TG/DSC curves of the used catalyst and the washed catalysts are shown in Figure 43 the TG curve of the used catalyst shows three-weight loss steps (Fig. 43 right). The first weight loss between ca. 100-150 °C is assigned to the desorption of



loosely bound water. The second large weight decrease between 180 to 270 °C is assigned to the removal of glycerol and some reaction products. Both are strongly endothermic (compare Fig. 43 left). The following exothermic weight loss between ca. 350-430 °C is assigned to the decomposition of stronger bound glycerol and other reaction products. After washing with water, the total weight loss is decreased from 11 wt% to ca. 5 wt%. The amount of water desorbed at 100-150 °C is increased to 2.5%. The second weight loss between 180 to 270 °C of glycerol is markedly decreased and the weight loss between 350-430 °C is absent. These findings are supported by the decrease of the corresponding endothermic peaks in the DSC curve (Fig. 43 left). Obviously, the remaining glycerol is effectively removed by workup by washing with water. An additional high-temperature weight loss is now observed between ca. 450-530 °C. It is an exothermic DSC peak at ca. 490 °C and assigned to thermal decomposition/omposition of remaining ammonium ions. This loss is not observed with the used catalyst because the ammonium is burned off with the glycerol and its reaction products. The appearance of the TG/DSC curves obtained with the ethanol washed catalyst is similar. However, the remaining water content and the corresponding DSC peak intensity is markedly lower.

In summary, the results show the HCLIN300 catalyst can be reused. The workup of the catalyst by washing with water and ethanol is efficient. The advantage of washing with ethanol is the removal of adsorbed water. Therefore, samples were washed 2 times, first with water followed by washing with ethanol were used. The decrease of the selectivity to di-ether with the washed and reused catalysts shows again the limiting factor of water in the etherification reaction.

#### 4.2.2.4 Summary of catalytic performance

The acid natural zeolite clinoptilolite HCLIN is catalytically active in the etherification of glycerol with tertiary butanol and shows improved selectivity to di-ether at selected catalyst activation and reaction conditions. The di-ether and tri-ether are the wished products for use as a synthetic fuel additive. The HCLIN catalyst can be reused and cycled with low loss in activity.

Interestingly, the highest conversion is observed with the soft thermally activated weak acidic HCLIN300, where the micropore system is still closed and, conclusively, the reaction takes place at or near the catalyst surface.

In contrast, the conversion is declined with medium and strong acidic HCLIN400 and HCLIN500 although the pore system is opened and the high specific surface area should favor the conversion. Obviously, strong acid sites lead to the formation of “coke” by glycerol decomposition, which poisons the catalytic active sites. Many strong acid sites are not accessible.

Therefore, the catalytic performance of HCLIN is very sensitive to the catalyst preparation, i.e. the material workup and ammonium ion exchange conditions, and thermal activation procedure as heating rate, calcination temperature, and time.

Although the catalyst is thermally stable, some loss of BS is observed after calcination at temperatures beyond 400 °C. About 35% of BS is lost by dehydroxylation at 500 °C. These HCLIN contain most strong and very strong acid sites, which are related to their location such as external or internal pores.

Reaction conditions as the reaction temperature, reaction time, and catalyst loading markedly influence the catalytic performance. The water released during the course of the reaction by the condensation of alcohols is a limiting factor. Consequently, the hydrophobicity of the system should play an important role. Indeed, alcohols containing tertiary alkyl groups show superior conversion and selectivity.

The comparison with the acidic organic resin and the other shows that the catalytic performance of HCLIN in the etherification reaction compares to the highest active zeolite BEA catalyst with respect to the conversion of glycerol and the selectivity to the wished di-ether fuel additive. In contrast to the mono-ether, the di-ether is miscible with diesel fuel.

**Table 17:** Comparison of the catalytic performance of the natural zeolite catalyst HCLIN with synthetic zeolite catalysts and the acidic organic resin A-15.

<b>Catalysts</b>	<b>C<sub>Gly</sub>%</b>	<b>S<sub>M</sub>%</b>	<b>S<sub>D</sub>%</b>
<b>A-15</b>	96	70	25
<b>H-BEA</b>	90	45	45
<b>HZSM-5</b>	20	99	1
<b>MOR</b>	9	97	3
<b>FAU</b>	33	82	18
<b>HCLIN</b>	80	72	28

## 4.3 Different alcohols

The influence of the alkyl chain length and branched alcohols on the conversion of glycerol to the corresponding ether was tested using different C<sub>1</sub> to C<sub>5</sub> alcohols. The tests were carried out with the most active catalyst HCLIN300 using optimal reaction temperature of 140 °C. At least ethanol and butanol are obtained by fermentation of sustainable natural feedstock. The results show that the HCLIN300 catalyst can catalyze the etherification of these alcohols with glycerol. Usually, the stabilization of the formed intermediate carbocation increases with the chain lengths of the alkyl groups and their branching. In effect, the observed conversions with linear and branched alcohols are low (Fig. 44). Among these, *n*-butanol and secondary pentanol form more di-ether, 5- and 7- after two hours of reaction.

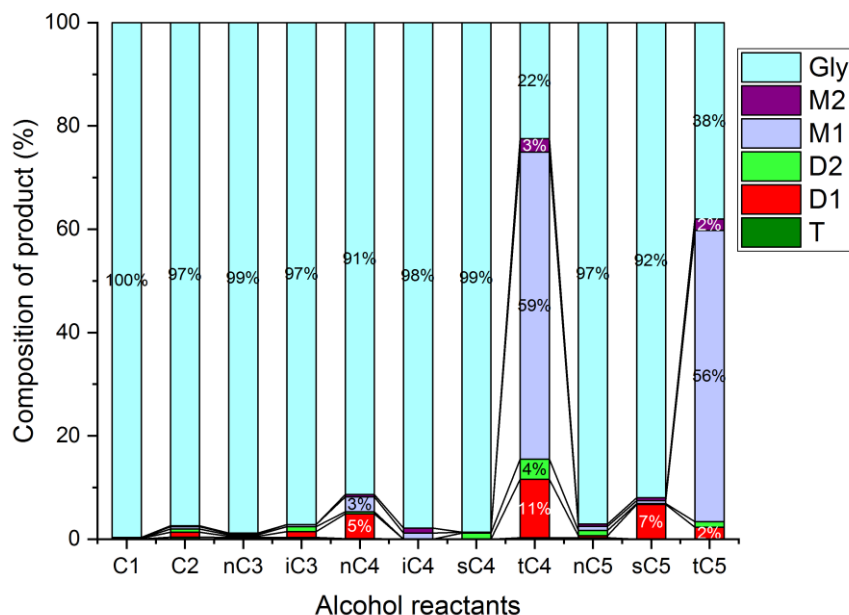


**Figure 44.** Comparison of the conversion achieved of different alcohol reactants (C1-C5) in the etherification with glycerol over HCLIN300. The difference of their isomers *n*, *iso*, *sec*, *tert* (noticed as n, i, s, t) was compared. All the samples were taken after 2 hours of reaction at 140 °C, 5% catalyst loading, and ratio with glycerol 1:4, in an autoclave.

In contrast, high conversions of glycerol to ether are observed with the branched *t*-butanol and 2-methyl-2-butanol (*t*-amyl) alcohol, as shown in Figure 45. A reason for the high conversion could be the better stabilization of the formed carbocation by tertiary alkyl groups. Additionally, shielding of the reaction site at the catalyst by an “umbrella” of hydrophobic tertiary alkyl groups from water, which is higher with the *t*-amyl group, is expected to favor

the reaction. Remarkable high formation of di- ether is found with 2-methyl-2-butanol (Fig. 45). These interesting results should be verified by further experiments. The di-ether (D) and tri-ether (T) are the more wished products for use as a fuel additive. They are better miscible with the diesel than the mono-ether (M). Among the different alcohols reacting with glycerol, *t*-butanol and *t*-pentanol have the highest activity. However, *t*-butanol has higher conversion comparing with *t*-pentanol because of its carbocation stability. Besides the steric hindrance of the reactants to the OH group position of Gly, the selectivity of ether is defined: selectivity of M1 and D1 ether is higher than M2, D2. These reactants look like a hydrophobic umbrella with three hydrocarbons to protect the ether group from water to avoid the back reaction.

The results show that hydrophobicity is an important factor. The water disturbs the etherification reaction. It competes with the glycerol in the reaction with the intermediate carbocation. In addition, it favors the back reaction of the mono-ether or di-ether.

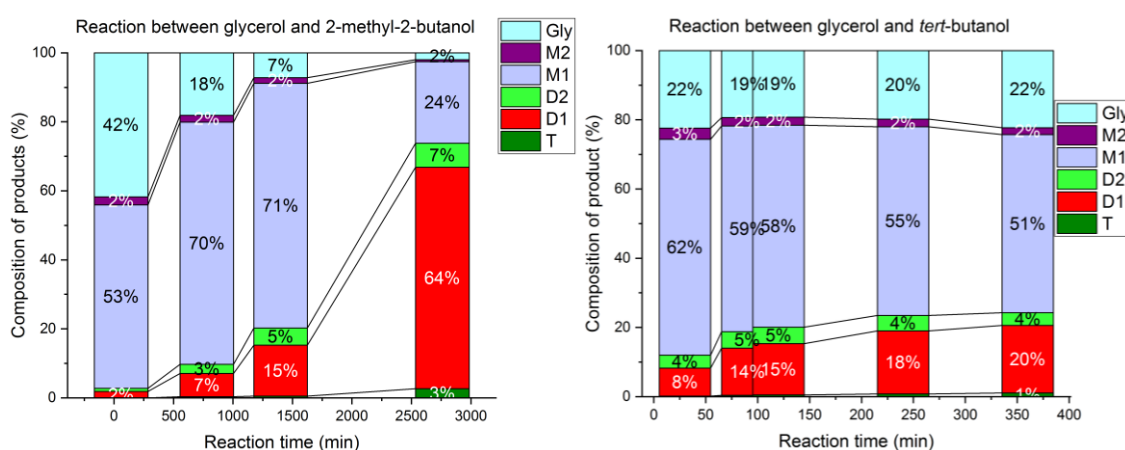


**Figure 45.** Composition of M1, M2, D1, D2, T, Gly of the products in the etherification reaction of glycerol with *t*-amyl alcohol after different reaction times: 30 min, 2h, 6h, 1 day, 2 days. Reaction conditions: autoclave, autogenous pressure, 140 °C, 5wt% catalyst, 1:4 Gly/*t*-amyl ratio (left), With *t*-butanol after 30min, 1h30, 2h, 4h, and 6h of reaction. 1:4 Gly/*t*-butanol ratio (right).

The limiting role of water is initially overcome by the high selectivity to di-ether after short time of reaction, where no water is present. Water is overcome during the etherification reaction, the increase of the selectivity to di-ether with growing catalyst loading and rising reaction temperature to 140 °C, and the decrease of di-ether selectivity with reuse catalysts after washing.

### Properties of fuel additive

The obtained sustainable synthetic fuel the glycerol *t*-amyl di-ether etherification product is miscible with diesel fuel:

- Heating value [J/g]: 29362,
- Kinematic viscosity,  $\text{mm}^2/\text{s}$ : 17,774,
- Density,  $\text{g}/\text{m}^3$ :  $\text{g}/\text{m}^3$ : 0,9637.

In contrast to the mono-ether, which is not sufficiently soluble in diesel, the obtained glycerol di-ether product is a potential suitable fuel additive.

## 5 Conclusions

Natural zeolite clinoptilolite is a superior starting material for the preparation of green Brønsted acid heterogeneous catalysts HCLIN, in non-hazardous method via ammonium exchange and elimination of the obtained ammonium ion-exchange form  $\text{NH}_4\text{CLIN}$ .

In addition, the catalytic performance is comparable with the most active synthesized zeolite catalyst BEA. Herein, the catalytic performance with respect to the conversion of glycerol and the selectivity to the di-ether increases in the order: A-15 > HCLIN  $\approx$  H-BEA > FAU > ZSM-5 > MOR. Table 17.

Further, the catalytic activity of HCLIN catalysts is very sensitive to activation conditions, i.e. the activation temperature and time. HCLIN catalysts contain weak, medium-strong, and strong Brønsted acid sites depending on ammonia treatment between 250 °C and 550 °C. HCLIN catalysts are highly active in the etherification of glycerol with tertiary butanol. Besides mono-ether, also di-ether is formed. The latter are preferential products.

The acidity, specific surface area, and porosity increase markedly with rising the activation temperature to 400 °C and 500 °C, respectively. The micropore system becomes accessible after activation at a temperature beyond ca. 300 °C.

Interestingly, the catalyst with the lowest acidity and low specific surface area, which was obtained after short activation by elimination at 300 °C, shows the highest catalytic activity in terms of glycerol conversion. Obviously, the catalysis takes place at or near the external surface of the aggregate clinoptilolite crystals. The micropores are still nearly closed at this temperature.

With rising the activation temperature from 300 °C to 500 °C a severe loss of glycerol conversion is observed although the acidity and specific surface areas are high. This is likely due to catalyst poisoning by glycerol decomposition products formed at strong acid sites. The weak acid sites are deactivated at higher activation temperature.

In addition, the dehydroxylation reaction of Brønsted acid sites from HCLIN during the activation was observed at low temperature 300 °C with different activation time. The selectivity to the di-ether is high after short reaction time and at low conversion. At this stage, the system contains low amount of reaction water, which would facilitate the alkyl reaction to the mono-ether. It could also explain why the high adsorption ability of zeolite.

Generally, the selectivity of di-ether increases with growing reaction temperature, reaction time, and catalyst loading. Maximum selectivity of *tert*-butyl glycol di-ether is obtained at 140 to 160 °C of reaction, with *ca.* 25 to 34 wt % selectivity and *ca.* 20 to 28 % yield. This value is high comparing to other synthetic zeolites.

The comparison with the other short chain alcohol reactants shows that highest conversion of glycol and selectivity to di-ether is observed with *tert*-butanol and *tert*-pentanol. This is due to the stabilization of the intermediate oxonium ion and its shielding from reaction water by the large hydrophobic *tert*-alkyl groups as umbrella effect. With the short chain alcohols as methanol, ethanol, propanol only low conversion and selectivity is observed.

The water formed during the etherification is a limiting factor, especially for the formation of di-ether because it competes with *tert*-butanol in the etherification reaction. Therefore, hydrophobicity and water removal from the reaction mixture are decisive for further improvements of the catalytic system.

Therefore, the natural zeolite HCLIN catalyst is a superior catalyst or the replacement of environmental less benign mineral acids and bases in the etherification of glycol with *tert*-butanol.

The catalyst is highly available and can be reused. The oxonium di-ether can be used as sustainable synthetic fuel additive. It is soluble in bio diesel which is an important requirement for its application.

## 6 Reference

- [1] J. Pfeiffer, *Fossil Resources and Climate Change – The Green Paradox and Resource Market Power*, **2017**.
- [2] C. Graves, S. D. Ebbesen, M. Mogensen and K. S. Lackner, *Renew. Sustain. Energy Rev.*, **2011**, 15, 1–23.
- [3] M. W. Ackley, R. F. Giese and R. T. Yang, *Zeolites*, **1992**, 12, 780–788.
- [4] J. Wei, Q. Ge, R. Yao, Z. Wen, C. Fang, L. Guo, H. Xu and J. Sun, *Nat. Commun.*, **2017**, 8, 1–8.
- [5] W. Chanmanee, M. F. Islam, B. H. Dennis and F. M. MacDonnell, *Proc. Natl. Acad. Sci.*, **2016**, 113, 2579–2584.
- [6] M. Sato, *Spec. Publ. - Geochemical Soc.*, **1991**, 2, 271–283.
- [7] A. P. Nel, P. van Rensburg and M. G. Lambrechts, *South African J. Enol. Vitic.*, **2014**, 35, 304–320.
- [8] T. G. Laughlin, A. N. Bayne, J. F. Trempe, D. F. Savage and K. M. Davies, *Nature*, **2019**, 566, 411–414.
- [9] A. Melis, *Energy Environ. Sci.*, **2012**, 5, 5531–5539.
- [10] L. Shi and B. P. Tu, *Curr. Opin. Cell Biol.*, **2015**, 33, 125–131.
- [11] C. J. Bailey, B. Cain, B. G. Peters, N. York, C. W. Bonneau and T. W. Strickneubauer, **2006**, 27, 107–123.
- [12] O. S. Stamenković, A. V. Veličković and V. B. Veljković, *Fuel*, **2011**, 90, 3141–3155.
- [13] E. Lotero, Y. Liu, D. E. Lopez, K. Suwannakarn, D. A. Bruce and J. G. Goodwin, *Ind. Eng. Chem. Res.*, **2005**, 44, 5353–5363.
- [14] S. K. Hoekman, A. Broch, C. Robbins, E. Cenicerros and M. Natarajan, *Renew. Sustain. Energy Rev.*, **2012**, 16, 143–169.
- [15] D. Y. C. Leung, X. Wu and M. K. H. Leung, *Appl. Energy*, **2010**, 87, 1083–1095.



- [16] M. Rasmussen and S. D. Minteer, *J. Electrochem. Soc.*, **2014**, 161, H647–H655.
- [17] K. Klepáčová, D. Mrave , E. Hajekova an M. Bajus, *Pet. Coal*, **2003**, 45, 54–57.
- [18] F. Frusteri, F. Arena, G. Bonura, C. Cannilla, L. Spadaro and O. Di Blasi, *Appl. Catal. A Gen.*, **2009**, 367, 77–83.
- [19] A. Talebian-Kiakalaieh, N. A. S. Amin, N. Najaafi and S. Tarighi, *Front. Chem.*, **2018**, 6, 1–25.
- [20] F. Zaccheria, N. Scotti and N. Ravasio, *Catalysts*, **2019**, 9, 1–21.
- [21] S. Magar, S. Kamble, G. T. Mohanraj, S. K. Jana and C. Rode, *Energy and Fuels*, **2017**, 31, 1227–1277.
- [22] V. O. Samoilov, D. N. Ramazanov, A. I. Nekhaev, A. L. Maximov and L. N. Bagdasarov, *Fuel*, **2016**, 172, 310–319.
- [23] P. U. Okoye, A. Z. Abdullah and B. H. Hameed, *Fuel*, **2017**, 209, 538–544.
- [24] M. Aghbashlo, M. Tabatabaei, H. Rastegari, H. S. Ghaziaskar and T. Roodbar Shojaei, *Renew. Energy*, **2018**, 126, 242–253.
- [25] J. A. Melero, G. Vicente, G. Morales, M. Paniagua, J. M. Moreno, R. Roldán, A. Ezquerro and C. Pérez, *Appl. Catal. A Gen.*, **2008**, 346, 44–51.
- [26] B. P. Pinto, J. T. De Lyra, J. A. C. Nascimento and C. J. A. Mota, *Fuel*, **2016**, 168, 76–80.
- [27] A. Cornejo, I. Barrio, M. Campoy, J. Lázaro and B. Navarrete, *Renew. Sustain. Energy Rev.*, **2017**, 79, 1400–1413.
- [28] S. Magar, S. Kamble, G. T. Mohanraj, S. K. Jana and C. Rode, *Energy and Fuels*, **2017**, 31, 12272–12277.
- [29] C. Cannilla, G. Bonura, L. Frusteri and F. Frusteri, *Environ. Sci. Technol.*, **2014**, 48, 6019–6026.
- [30] C. Cannilla, G. Bonura, L. Frusteri and F. Frusteri, *Chem. Eng. J.*, **2015**, 282, 187–193.
- [31] S. Wang and Y. Peng, *Chem. Eng. J.*, **2010**, 156, 11–24.
- [32] V. B. Kazansky, *Catal. Today*, **1988**, 3, 367–372.
- [33] R. C. Deka, *Indian J. Chem. Technol.*, **1998**, 5, 109–123.
- [34] M. Ga kowski, K. Tara h, Kuterasiński, J. Po o iński, S. Jar zewski, P. Kuśtrowski

- and J. Datka, *Microporous Mesoporous Mater.*, **2018**, 263, 282–288.
- [35] N. Nuttens, D. Verboekend, A. Deneyer, J. Van Aelst and B. F. Sels, *ChemSusChem*, **2015**, 8, 1197–1205.
- [36] Y. Qiu, X. Hou, G. Liu, L. Wang and X. Zhang, *Microporous Mesoporous Mater.*, **2017**, 243, 176–185.
- [37] B. K. Gebbink, *Front Matter*, **2017**.
- [38] A. Corma, S. Zones and J. Cejka, Eds., *Zeolites and Catalysis*, Wiley, **2010**.
- [39] A. Radosavljevic-Mihajlović, V. Donur, A. Daković, J. Lemić and M. To mašević-Čanović, *J. Serbian Chem. Soc.*, **2004**, 69, 273–281.
- [40] M. Moshoeshoe, M. Silas Nadiye-Tabbiruka and V. Obuseng, *Am. J. Mater. Sci.*, **2017**, 2017, 196–221.
- [41] Y. Ji, H. Yang and W. Yan, *Catalysts*, **2017**, 7, 1–31.
- [42] J. Lu, Z. Zhao, C. Xu, A. Duan and P. Zhang, *J. Nat. Gas Chem.*, **2005**, 14, 213–220.
- [43] A. S. M. Junaid, M. Rahman, H. Yin, W. C. McCaffrey and S. M. Kuznicki, *Microporous Mesoporous Mater.*, **2011**, 144, 148–157.
- [44] M. Trckova, L. Matlova, L. Dvorska and I. Pavlik, *Vet. Med. (Praha)*, **2004**, 49, 389–399.
- [45] N. Mansouri, N. Rikhtegar, H. Ahmad Panahi, F. Atabi and B. K. Shahraki, *Environ. Prot. Eng.*, **2013**, 39, 139–152.
- [46] E. Chmielewska and E. Chmielewska, *Gen. Chem. Chem. Chem.*, **2019**, 5, 190001.
- [47] C. Miranda, J. Urresta, H. Cruchade, A. Tran, M. Benghalem, A. Astafan, P. Gaudin, T. J. Daou, A. Ramirez, Y. Pouilloux, A. Sachse and L. Pinard, *J. Catal.*, **2018**, 365, 249–260.
- [48] T. Ikeda, T. Nagase, N. Hiyoshi and Y. Oumi, *Microporous Mesoporous Mater.*, **2012**, 163, 42–50.
- [49] G. Kirov and L. Filizova, *Geochemistry, Mineral. Petrol.*, **2012**, 49, 65–82.
- [50] N. V. Vlasenko, Y. N. Kochkin, G. M. Telbiz, O. V. Shvets and P. E. Strizhak, *RSC Adv.*, **2019**, 9, 35957–35968.
- [51] B. Rabindran Jermy and A. Pandurangan, *J. Mol. Catal. A Chem.*, **2006**, 256, 184–192.

- [52] S. Li, A. Zheng, Y. Su, H. Zhang, L. Chen, J. Yang, C. Ye and F. Deng, *J. Am. Chem. Soc.*, **2007**, 129, 11161–11171.
- [53] C. Deng, J. Zhang, L. Dong, M. Huang, B. Li, G. Jin, J. Gao, F. Zhang, M. Fan, L. Zhang and Y. Gong, *Sci. Rep.*, **2016**, 6, 1–13.
- [54] M. Boronat and A. Corma, *ACS Catal.*, **2019**, 9, 1539–1548.
- [55] T. E. Warner, M. Galsgaard Klokke and U. G. Nielsen, *J. Chem. Educ.*, **2017**, 94, 781–785.
- [56] K. Miyake, Y. Hirota, K. Ono, Y. Uchida, M. Miyamoto and N. Nishiyama, *New J. Chem.*, **2017**, 41, 2235–2240.
- [57] D. R. S. Pedrolo, L. K. De Menezes Quines, G. De Souza and N. R. Marcilio, *J. Environ. Chem. Eng.*, **2017**, 5, 4788–4794.
- [58] E. A. Hildebrando, C. G. B. Andrade, C. A. F. da Rocha Junior, R. S. Angélica, F. R. Valenzuela-Diaz and R. de F. Neves, *Mater. Res.*, **2014**, 17, 174–179.
- [59] I. Kiricsi, C. Flego, G. Pazzuconi, W. Parker, R. Millini, C. Perego and G. Bellussi, **1994**, 4627–4634.
- [60] G. Busca, *Microporous Mesoporous Mater.*, **2017**, 254, 3–16.
- [61] S. Abbasian and M. Taghizadeh, *Int. J. Nanosci. Nanotechnol.*, **2014**, 10, 171–180.
- [62] P. M. Veiga, A. C. L. Gomes, C. O. Veloso and C. A. Henriques, *Appl. Catal. A Gen.*, **2017**, 548, 2–15.
- [63] R. Varala, V. Narayana, S. R. Kulakarni, M. Khan, A. Alwarthan and S. F. Adil, *Arab. J. Chem.*, **2016**, 9, 550–573.
- [64] J. Adinehvand, A. Shokuhi Rad and A. S. Tehrani, *Int. J. Environ. Sci. Technol.*, **2016**, 13, 2705–2712.
- [65] E. Vlad, C. S. Bildea and G. Bozga, *Sci. World J.*, **2012**, 2012, 1–6.
- [66] N. Ozbay, N. Oktar, G. Dogu and T. Dogu, *Ind. Eng. Chem. Res.*, **2012**, 51, 8788–8795.
- [67] C. Saengarun, A. Petsom and D. N. Tungasmita, *Sci. World J.*, **2017**, 1–11.
- [68] L. Chen, B. Nohair, D. Zhao and S. Kaliaguine, *ChemCatChem*, **2018**, 10, 1918–1925.
- [69] G. M. Lari, G. Pastore, M. Haus, Y. Ding, S. Papadokonstantakis, C. Mondelli and J.

- Pérez-Ramírez, *Energy Environ. Sci.*, **2018**, 1–18.
- [70] M. P. Pico, A. Romero, S. Rodríguez and A. Santos, *Ind. Eng. Chem. Res.*, **2012**, 51, 9500–9509.
- [71] C. M. Dominguez, A. Romero and A. Santos, *Catalysts*, **2019**, 9, 1–14.
- [72] S. S. Poly, M. A. R. Jamil, A. S. Touchy, S. Yasumura, S. M. A. H. Siddiki, T. Toyao, Z. Maeno and K. ichi Shimizu, *Mol. Catal.*, **2019**, 479, 110608.
- [73] L. Aguado-Deblas, R. Estevez, M. Russo, V. La Parola, F. M. Bautista and M. L. Testa, *Materials (Basel)*, **2020**, 13, 1–16.
- [74] M. Chamack, A. R. Mahjoub and A. Akbari, *Catal. Commun.*, **2018**, 110, 1–4.
- [75] V. L. C. Gonçalves, B. P. Pinto, J. C. Silva and C. J. A. Mota, *Catal. Today*, **2008**, 133–135, 673–677.
- [76] M. S. Khayoon and B. H. Hameed, *Appl. Catal. A Gen.*, **2012**, 433–434, 152–161.
- [77] M. S. Khayoon, S. Triwahyono, B. H. Hameed and A. A. Jalil, *Chem. Eng. J.*, **2014**, 243, 473–484.
- [78] A. Dziejzicka, B. Sulikowski and M. Ruggiero-Mikołajczyk, *Catal. Today*, **2016**, 259, 50–58.
- [79] M. Sultan, T. Miyazaki and S. Koyama, *Renew. Energy*, **2018**, 121, 441–450.

## 7 Appendix

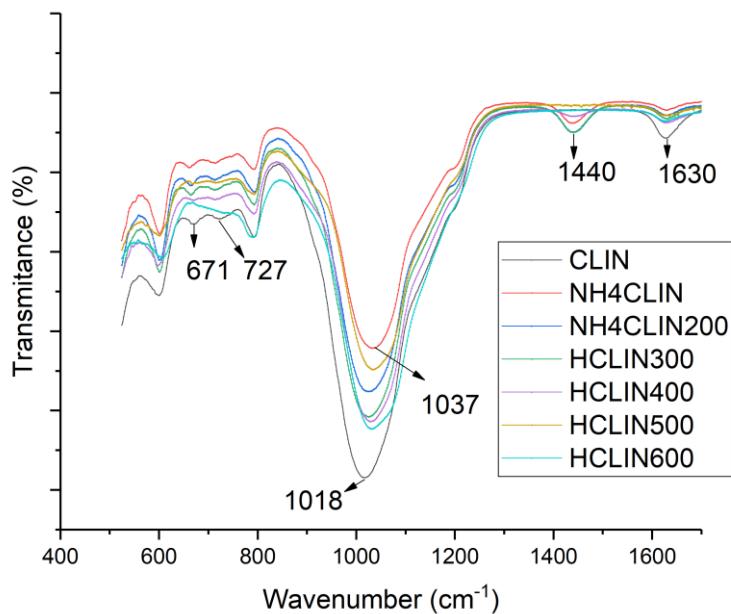


**Figure 46.** FTIR lattice vibration spectra of clinoptilolite CLIN after different treatment: a) starting material CLIN, b) ammonium exchanged NH<sub>4</sub>CLIN, and c) calcined HCLIN200, d) HCLIN300, e) HCLIN400, f) HCLIN500, g) HCLIN600.

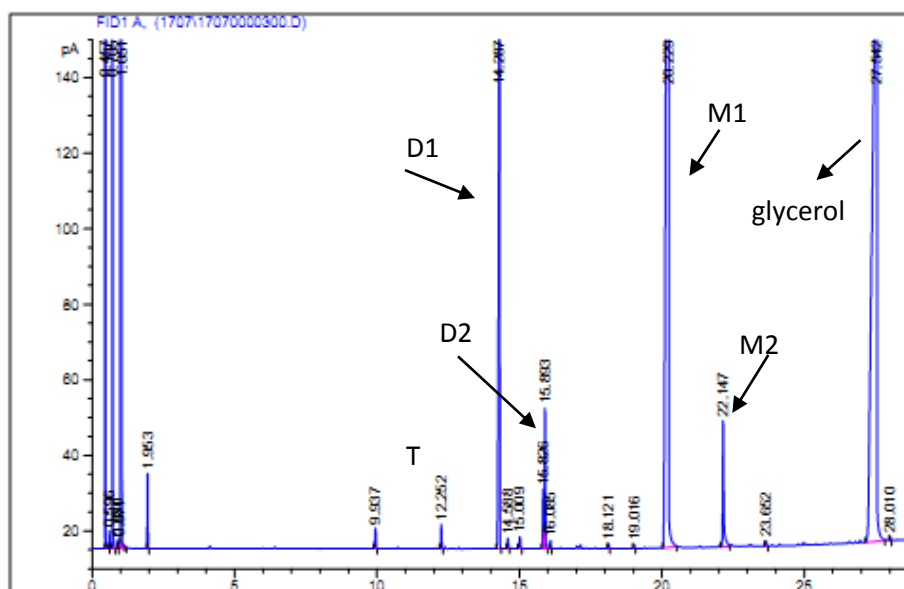
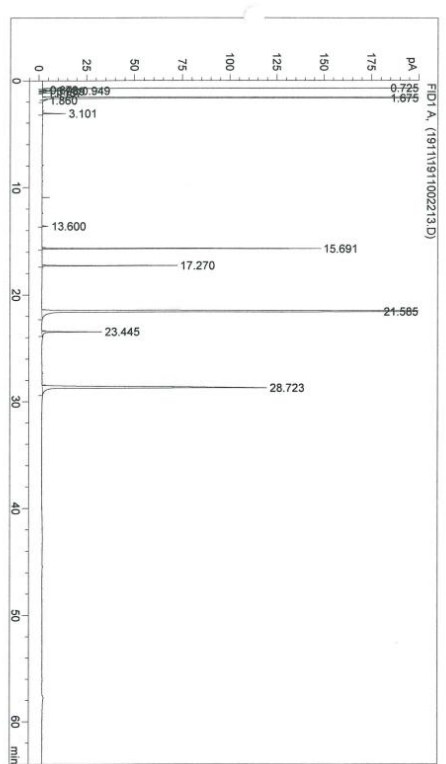


**Figure 47.** GC-FID result of samples of reaction between glycerol and *t*-butanol. The peaks of, T, D1, D2, M1, M2, and Gly were noted with their retention time.

=====  
 Acq. Operator :  
 Acq. Instrument : GC 9  
 Injection Date : 11/23/2019 4:52:52 AM  
 Seq. Line : 11  
 Location : Vial 11  
 Inj : 1  
 Inj Volume : 1 µl  
 Acq. Method : D:\HPCHEM\1\METHODS\DE-WAX-DEUTSCH.M  
 Last changed : 11/22/2019 2:59:56 PM  
 (modified after loading)  
 Analysis Method : D:\HPCHEM\1\METHODS\DE-WAX-DEUTSCH.M  
 Last changed : 11/25/2019 9:40:33 AM  
 (modified after loading)  
 Method Info : 10m DB-Wax 40/5-6-180/10-8-200/20



Area Percent Report

Sorted By : Signal  
 Multiplier : 1.0000  
 Dilution : 1.0000  
 Use Multiplier & Dilution Factor with ISTDs

Signal 1: FID1 A,

Peak #	RetTime [min]	Type	Width [min]	Area [pA*s]	Height [pA]	Area %
1	0.725	BB	0.0103	617.52063	1021.67804	3.77390
2	0.873	BV	0.0137	1.92869	2.32395	0.01179
3	0.949	VV	0.0146	15.99950	19.11906	0.09778
4	0.989	VV	0.0167	5.93406	5.84114	0.03627
5	1.118	VV	0.0213	1.37793	1.02591	0.00842
6	1.157	VB	0.0194	5.43038	4.33510	0.03319
7	1.675	BV	0.0477	1.12107e4	3046.96094	68.51299
8	1.860	VB	0.0370	4.67871	1.78664	0.02859

# CURRICULUM VITAE



1. Full Name and Title: PhD student Do Trung Hieu
2. Date of Birth: 27/01/1990
3. Nationality: Vietnamese
4. Institution: Inorganic Chemistry, Faculty of Chemistry, Rostock University.
5. Contact Details  
Email : hieu.chemistry2701@gmail.com

Website: <https://www.schulz.chemie.uni-rostock.de/arbeitsgruppe/>

## Research interests

---

- Catalytic organic synthesis,
- Studying of mesoporous materials: mesoporous silica-zirconia, application of zeolites and SBA-15 products for industries, environmental,
- Solid super-acid use as a safely catalyst in n-hexane isomerization, etherification of *tert*-butanol with glycerol, biodiesel production,
- Modified natural zeolite as green catalyst.

## Skills

---

- Good at soft skills: teamwork, communication, time management;
- Good at computer skills: Microsoft Office and internet applications;
- Fundamentals of HPLC, LC-MS, GC, GC-MS, UV-VIS, XRD, TGA, BET, TPD MiniSIM
- Training at Petroleum Chemistry Research Laboratory, HaNoi University of science, NMR;
- Laboratory experiments

## Strengths

---

- Able to work under high pressure, work independently or as part of a team;
- Able to quickly accustom myself to new tasks;
- Hard-working, careful, open-minded, enthusiastic;
- Have a sense of responsibility and passion for the job.

Language: English Certification Ielts 6.0- C1 (CEFR), A1 Germany

## **EDUCATION**

- B.Sc.: In Petroleum of Chemistry, Hanoi University of Science, Vietnam National University, English program - Advanced Class of Chemistry (2008- 2013)
- M.Sc.: In Molecular chemistry - Medicinal chemistry, University of Rennes 1, France, 2014
- Training course in Institute of Radiochemistry and Radioecology University of Pannonia, Veszprém, Hungary, 2015
- PhD student in Rostock University, from 2018 until 22/6/2021

## **Awards**

- 2008 Oct: 2nd prize in High school Physic competitions of Hanam province

## **Reference**

1. Prof. Dr. Axel Schulz (Head of the Inorganic Department, University of Rostock)
2. Dr. Hendrik Kosslick (Inorganic Department, University of Rostock)
3. Prof. Dr. Le Thanh Son (Vice Director of the Hanoi University of Science (VNU))

Date of delivery: 30.03.2021

Date of defense: 22.06.2021